SLIP-LINE FIELD SOLUTION WITH DEAD ZONE FOR LARGE NEGATIVE RAKE CUTTING

by

MINASSE ABEBE

B.S., Addis Abeba University, 1972

A MASTER'S THESIS

submitted in partial fulfillment of the
requirements for the degree

MASTER OF SCIENCE

Department of Mechanical Engineering

Kansas State University
Manhattan, Kansas

1980

Approved by:

F. C. Appl

Major Professor

THIS BOOK
CONTAINS
NUMEROUS PAGES
WITH THE ORIGINAL
PRINTING BEING
SKEWED
DIFFERENTLY FROM
THE TOP OF THE
PAGE TO THE
BOTTOM.

THIS IS AS RECEIVED
FROM THE
CUSTOMER.

TABLE OF CONTENTS

TABLE OF CONTENTS - Continued

LIST OF TABLES

LIST OF FIGURES

LIST OF FIGURES - Continued

LIST OF FIGURES - Continued

NOMENCLATURE

α	Negative rake angle
D	Depth of cut
W	Width of cut
d	Chip thickness
U	Workpiece velocity
U_{PC}, U_{GH}, etc.	Velocities in the Hodograph
U^*_{EG}, U^*_{DC}, etc.	Velocity discontinuities in the Hodograph
Y'	Yield stress in pure uniaxial tension
k,K	Yield stress in pure shear
α-Line	Slip-line of the family denoted by the parameter ϕ
β-Line	Slip-line of the family denoted by the parameter $(\phi+\pi/2)$
$\eta, \eta_1, \eta_2, \eta_3$	Friction angles; the angles between slip-lines and interfaces
R	Radius of the centered fan field PED
d_o	Height of chip formation, length HL in Fig. 4.1
$\phi, \phi_{10}, \phi_{12}$	The counter-clockwise angle of an α-line from the positive x-axis
$\theta, \theta_6, \theta_8$	The counter-clockwise angle of an α-line from the positive x-axis
$\sigma_x, \sigma_y, \sigma_z, \sigma, \sigma_n$	Normal stresses
$\sigma_1, \sigma_2, \sigma_3$	Principal normal stresses
$\tau_{xy}, \tau_{yx}, \tau$	Shear stresses
p	Hydrostatic stresses

$P_1, P_2, \ldots$etc.]
$P_a, P_b, P_v, P_v', P_7'$] Compressive normal stresses

$s_1, s_2, \ldots$etc.]
s_a, s_b, s_v, s_v'] Shear stresses

$P_3{}^D, P_{13}{}^D, P_{BC}{}^D, P_{va}{}^D$ Dimensionless compressive normal stresses

$s_3{}^D, S_{13}{}^D, S_{BC}{}^D, S_{va}{}^D$ Dimensionless shear stresses

FH — Horizontal component of the cutting force

FV — Vertical component of the cutting force

VOH — Ratio of the vertical component of the cutting force to the horizontal component of the cutting force

FT — Component of the cutting force normal to the tool face

FN — Component of the cutting force parallel to the tool face

FTD, FHD, FVD — Dimensionless components of cutting force; parallel to the tool face, horizontal and vertical, respectively.

PMOK — Dimensionless mean pressure on the tool face

X, x — Coordinate direction parallel to the tool face

Y, y — Coordinate direction normal to the tool face

ΣFy — Summation of forces in Y-direction

ΣFx — Summation of forces in X-direction

ΣM_o — Summation of moment about 0 in Fig. 4.4

m — Adhesion coefficient

μ — Friction coefficient

AR — Real area of contact

β_1, β_2 — Parameters in the Equation for AR

ξ — Parameter in the Equation for $\left(\frac{\sigma n}{2k}\right)_{lim}$

V_x, V_y — Velocity Components in X and Y directions

1.0 INTRODUCTION

Machining is an important metal removal process in manufacturing. However, the mechanics of this process are not fully understood. In the past, theoretical studies of metal cutting with positive rake angle tools have been conducted. Various theories have been presented, e.g., Merchant [1], Lee and Shaffer [5] and Hill [6]. But, on the nature of the cutting process with large negative rake angles very little published literature is available. Even if high negative rakes for single point cutting tools are rarely used, it is necessary to understand the cutting mechanisms at such rakes. Negative rakes exist in cutting with grinding grits, at the nose radius of a single point tool and in drilling rocks with diamond drill bits.

Rubenstein et al. [11] conducted experiments with large negative rake tools and concluded that chip formation ceases at about -55 deg. rake in machining both aluminum and 70:30 brass. They also observed that at higher negative rake angles the workpiece material flows sideways instead of up the rake face.

Rowe and Wetton [13] applied the slip-line field theory to the problem of indenting by a symmetrical truncated wedge. Their theory predicts first the formation of a frontal bulge (prow) which later transforms to a chip. The formation of the prow was experimentally proved.

Komanduri [14] conducted experiments in machining with a wide range of negative rake tools. He observed that it is possible to

obtain chips with as high a negative rake as -75 deg. At -85 deg. rake no chip was formed but the tool rubbed the work material causing considerable side flow. He also concluded that the ratio of the thrust force to cutting force is greater than 1 for high negative rakes. His other observations were that the force parallel to the rake face becomes zero at -76 deg. rake, and that a prow formed ahead of the cutting edge.

Abdelmoneim and Scrutton [28] conducted experiments with rake angles ranging from -55 deg. to -80 deg. in machining non-ferrous materials. One experimental observation was that no chip formed when using tools of -80 deg. rake.

Yoshihiro Kita et al [27] studied the mechanism of metal removal with a conic abrasive tool. They observed a stagnant region ahead of the tool face during cutting. Besides they found a relationship between the stagnant region and chip formation. If the position of the stagnant tip is under the surface of the workpiece the chip can be formed; but if the position of the stagnant tip is above the surface of the workpiece no chip will be produced.

Challen and Oxley [31] used slip-line field analysis to explain the deformation of a soft asperity by a hard one, the hard one being a negative rake model. They derived equations for wear rates and coefficients of friction.

Hein [35] developed an approximate slip-line field for a negative rake angle cutting problem. His solution was an upper bound type. His conclusion was that slip-line field theory can be applied to problems of cutting with large negative rake angle tools.

Yoshihiro Kita et al. [36] studied experimentally the cutting mechanism with large negative rake tools. In their experiments they tried to simulate plane strain in cutting. They observed a stagnant region ahead of the tool face. The size of this region increases as the rake angle becomes more negative. In their conclusions they noted that the ratio of the vertical force to the horizontal force is greater than 1.

Most of the research done on negative rake angle cutting has been experimental. The objective of the study conducted here is to develop a theory of the mechanics of cutting with large negative rake angle tools. As a basis for this study, the slip-line method, which has been successfully used in solving problems related to other types of metal forming processes is used. In developing the slip-line field, the formation of the prow and the stagnant region ahead of the tool, which have been experimentally demonstrated are considered. Using this method, from the given rake angle, type of material and depth of cut, the theoretical forces are calculated and are compared with available experimental results.

2. THEORY OF PLANE STRAIN PLASTIC DEFORMATION [21, 32, 34]

2.1 Conditions and Assumptions

There are many cutting processes, like orthogonal machining in which the depth of cut is relatively small compared to the width of cut, so that permanent deformation occurs in plane strain. Plane plastic deformation implies that the displacements of elements in the plastically deforming region all occur in parallel planes, for instance the X - Y plane, and are independent of the Z co-ordinate.

The workpiece material is assumed to be homogeneous and isotropic. In any plane, Z=constant, the same stress-strain relationship is applicable; the components of stresses depend only on X and Y, and τ_{xz}, τ_{yz} are zero. Thus the Z-direction is a principal direction and σ_z is a principal stress.

The elastic strains which must occur before the material is sufficiently stressed to become plastic are ignored. In such cases it is reasonable to assume that the workmaterial has an infinite Young's modulus of elasticity.

In the plastically deforming region of the workpiece strain-hardening is neglected so that the material is assumed to flow at constant yield stress. This material is referred to as rigid-perfectly plastic. The strain-rate at each point in the deforming region is usually different. The effect this may have on the yield stress is therefore ignored. During deformation involving high values of strain, most of the external energy used is dissipated as heat. Temperature gradients that can arise may affect the material properties; but this effect is neglected.

The slip-line method, which is based on plane strain plastic deformation, requires several assumptions that may not agree with the physical phenomenon it attempts to describe. However, many problems of real importance have been solved [20] which show good agreement with

experiment and theory.

2.2 Basic Plane Strain Equations

It can be shown for plane strain deformation in the X - Y plane

$$\sigma_z = \frac{\sigma_x + \sigma_y}{2} = p \quad \text{and} \quad \tau_{xz} = \tau_{yz} = 0 \tag{2.1}$$

The maximum shear stress in the plane flow is expressed as

$$\tau_{max} = \frac{\sigma_1 - \sigma_3}{2} = K \tag{2.2}$$

or

$$\tau_{max} = \left[\left(\frac{1}{4}\right) (\sigma_x - \sigma_y)^2 + \tau_{xy}^2 \right]^{\frac{1}{2}} \tag{2.3}$$

The principal stresses are

$$\sigma_1 = p + K, \; \sigma_2 = \sigma_z = p, \quad \text{and} \; \sigma_3 = p - K \tag{2.4}$$

Assuming the von-Mises yield criterion, the yield occurs when the maximum shear attains the value

$$K = Y'/\sqrt{3} \text{ , where } Y' \text{ is the yield stress in tension.} \tag{2.5}$$

The differential equations of equilibrium of forces for plane strain deformation in the X - Y plane, neglecting body and inertia forces are

$$\frac{\partial \sigma_x}{\partial x} + \frac{\partial \tau_{yx}}{\partial y} = 0 \tag{2.6}$$

$$\frac{\partial \tau_{xy}}{\partial x} + \frac{\partial \sigma_y}{\partial y} = 0 \tag{2.7}$$

Equations (2.3), (2.6), and (2.7) represent three equations with three unknowns. If the boundary conditions are stated only in terms of stresses, the above equations are sufficient to define the stress distribution independent of strain. This type of problem is referred to as being statically determinate. However, if displacements or velocities are specified over part of the boundary, the stress-strain equations may have

to be employed, and the problem becomes more complicated.

For the plane strain case, writing the strain rates in terms of velocities, we have for the requirement of constant volume (incompressiblity)

$$\frac{\partial V_x}{\partial x} + \frac{\partial V_y}{\partial y} = 0 \qquad (2.8)$$

The Saint Venant - von Mises plasticity relations can be re-arranged to give

$$\frac{\sigma_x - \sigma_y}{2\tau_{xy}} = \frac{\partial V_x/\partial x - \partial V_y/\partial y}{\partial V_x/\partial y + \partial V_x/\partial x} \qquad (2.9)$$

This states that the direction of the surface of maximum tangential stress coincides with the direction of the surface which experiences the maximum rate of shear strain.

So we have five equations (2.3), (2.6), (2.7), (2.8), and (2.9) for the five unknowns σ_x, σ_y, τ_{xy}, V_x, and V_y. This type of problem is referred to as statically indeterminate since the equations for stresses and velocities that have to be solved simultaneously are extremely difficult.

The state of stress at some point C in a plastically deforming region may be represented by the Mohr stress circle diagram as shown in Fig. 2.1.

The stresses σ_x, σ_y, and τ_{xy} can be expressed in terms of the hydrostatic pressure, p, and the yield shear stress, K, as follows

$$\begin{aligned} \sigma_x &= -p - K \operatorname{Sin} 2\phi \\ \sigma_y &= -p + K \operatorname{Sin} 2\phi \\ \pm\tau_{xy} &= \pm K \operatorname{Cos} 2\phi \end{aligned} \qquad (2.10)$$

2.3 Plain Strain Slip-Line Field Theory

2.3.1 Slip-Lines

The maximum shear stresses, $\tau_{max} = \pm K$ act on surfaces which make

THIS BOOK CONTAINS NUMEROUS PAGES WITH DIAGRAMS THAT ARE CROOKED COMPARED TO THE REST OF THE INFORMATION ON THE PAGE.

THIS IS AS RECEIVED FROM CUSTOMER.

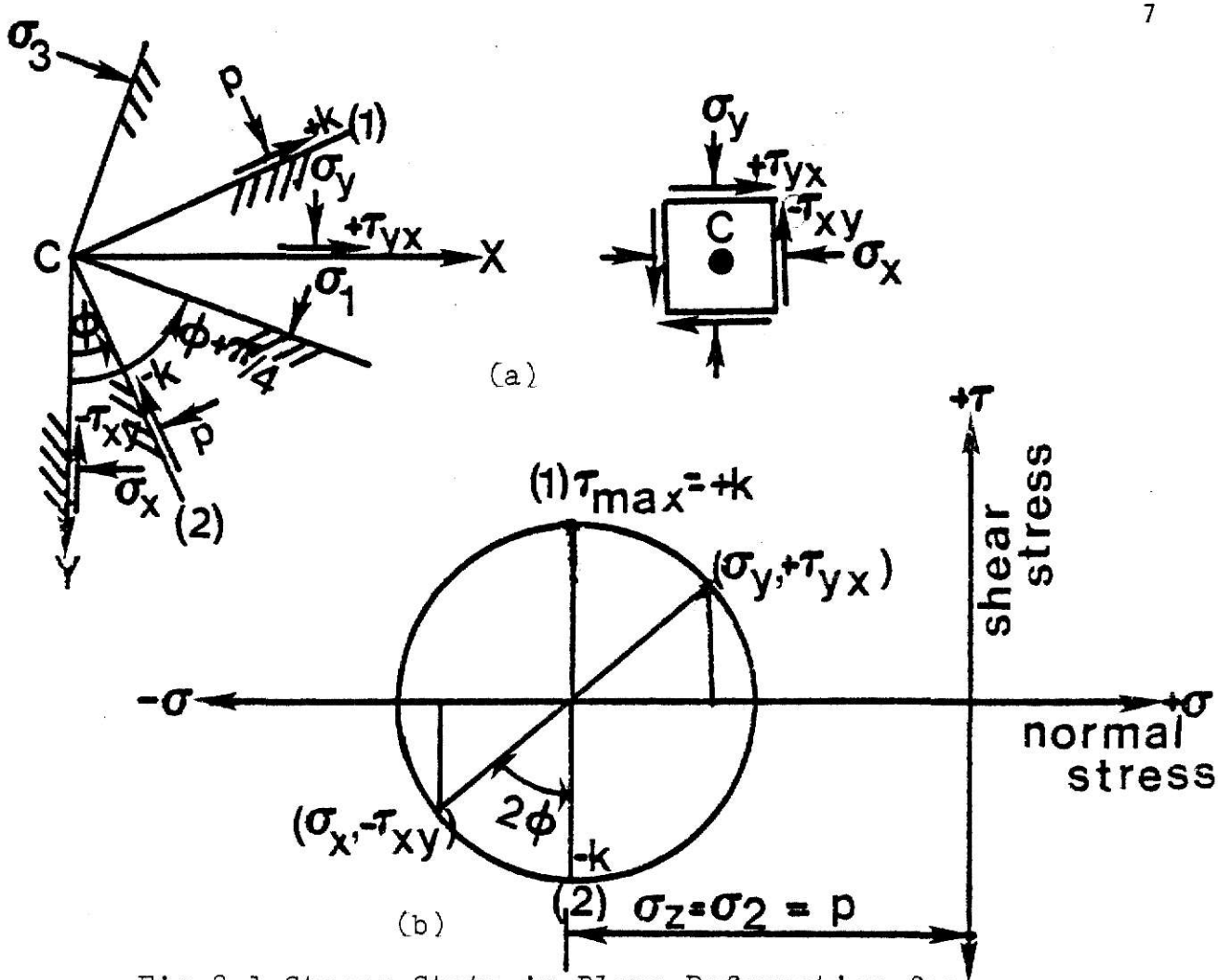

Fig.2.1.Stress State in Plane Deformation for a Rigid Perfectly Plastic Material Showing (a)the Physical Plane,and,(b)the Mohr Stress Circle Diagram.

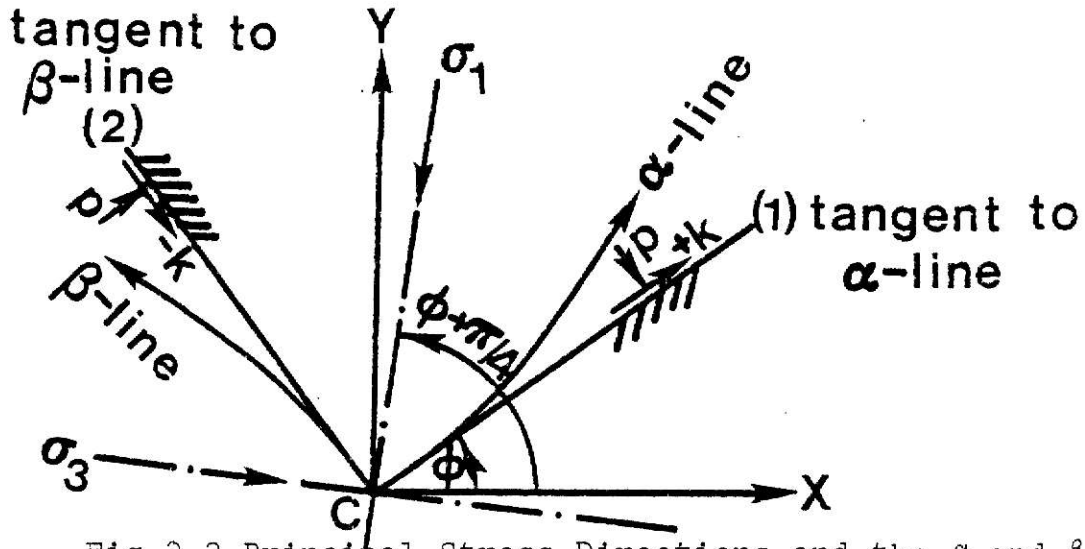

Fig.2.2.Principal Stress Directions and the α and β Directions at a Point in a Plastically Deforming Region.

angles of ±45° with the principal directions. If curves are drawn in the X - Y plane such that at every point on each curve the tangent coincides with the direction of maximum shear stress, then two orthogonal families of curves are obtained which are termed shear lines or slip lines. These two families of curves are usually designated as α-lines and β-lines. To distinguish between these two lines, the usual convention is that where the α and β-lines form a right-handed coordinate system of axes, then the line of action of the algebraic maximum principal stress, σ_1, as shown in Fig. 2.2 falls in the first and third quadrants. The anti-clockwise rotation, $\emptyset$, of the α-line from the chosen X-direction is then considered positive.

2.3.2 Hencky Stress Equations

The state of stress at a point can be expressed in terms of the independent quantities p, K and $\emptyset$ as in equations (2.10). Thus, the equilibrium equations (2.6) and (2.7) can be expressed in terms of these quantities as follows:

$$\begin{aligned} 2K \sin \emptyset \frac{\partial \emptyset}{\partial y} + \frac{\partial p}{\partial x} + 2K \cos 2\emptyset . \frac{\partial \emptyset}{\partial x} = 0 \\ 2K \sin \emptyset \frac{\partial \emptyset}{\partial x} + \frac{\partial p}{\partial y} - 2K \cos 2\emptyset . \frac{\partial \emptyset}{\partial y} = 0 \end{aligned} \qquad (2.11)$$

Equations (2.11) are the partial differential equations of equilibrium for the plane strain deformation of a rigid perfectly plastic material and are hyperbolic. The characteristics of the hyperbolic equations in this case, coincide with the slip lines.

The choice of X and Y axes is arbitrary. If we rotate the axes through $\emptyset$ such that the α and β lines coincide with the X, Y axes, $\emptyset$ becomes zero in equations (2.11) and as a result:

$$\frac{\partial p}{\partial x} + 2K\frac{\partial \phi}{\partial x} = 0$$

$$\frac{\partial p}{\partial y} - 2K\frac{\partial \phi}{\partial y} = 0 \qquad (2.12)$$

integrating (2.12), we have the Hencky equations

$$p + 2K\phi = C_1 \quad , \text{ along an } \alpha\text{-line}$$

$$p - 2K\phi = C_2 \quad , \text{ along a } \beta\text{-line} \qquad (2.13)$$

C_1 and C_2 are constants and their values generally vary from one slip-line to another.

2.3.3 Geiringer Velocity Equations

From Fig. 2.3 the velocity components in the X and Y directions are respectively

$$u_x = u \cos \phi - v \sin \phi$$
$$v_y = v \cos \phi + u \sin \phi \qquad (2.14)$$

Differentiating with respect to x and y respectively, and rotating the X - Y axes through ϕ so that the X-axis coincides with the α-line, that is, ϕ=0. We have

$$\frac{\partial u_x}{\partial x} = \frac{\partial u}{\partial x} - v\frac{\partial \phi}{\partial x}$$
$$\frac{\partial v_y}{\partial y} = \frac{\partial v}{\partial y} + u\frac{\partial \phi}{\partial y} \qquad (2.15)$$

Since the rate of extension along a slip-line is zero

$$\left(\frac{\partial u_x}{\partial x}\right)_{\phi=0} = \left(\frac{\partial v_y}{\partial y}\right)_{\phi=0} = 0 \qquad (2.16)$$

Thus equations (2.15) become:

$$du - v\,d\phi = 0 \quad \text{along an } \alpha\text{-line}$$
$$dv + u\,d\phi = 0 \quad \text{along a } \beta\text{-line} \qquad (2.17)$$

Equations (2.17) are the velocity compatiblity equations and are known as Geiringer's equations.

In many cases, it is possible to construct a graphical representation

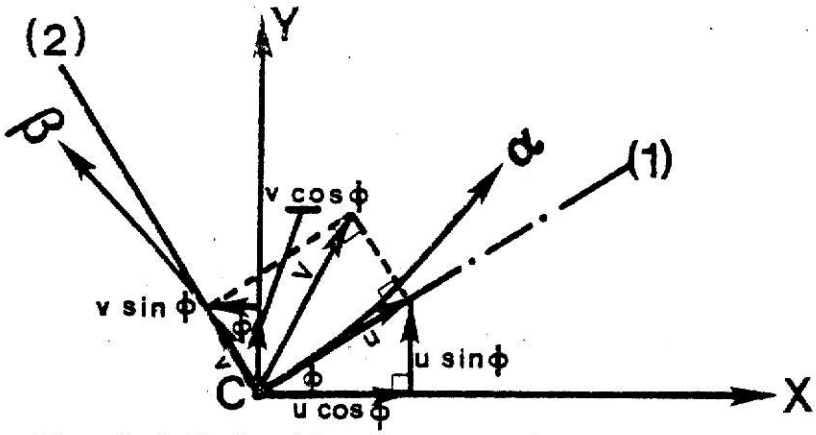

Fig.2.3.Velocity Components.

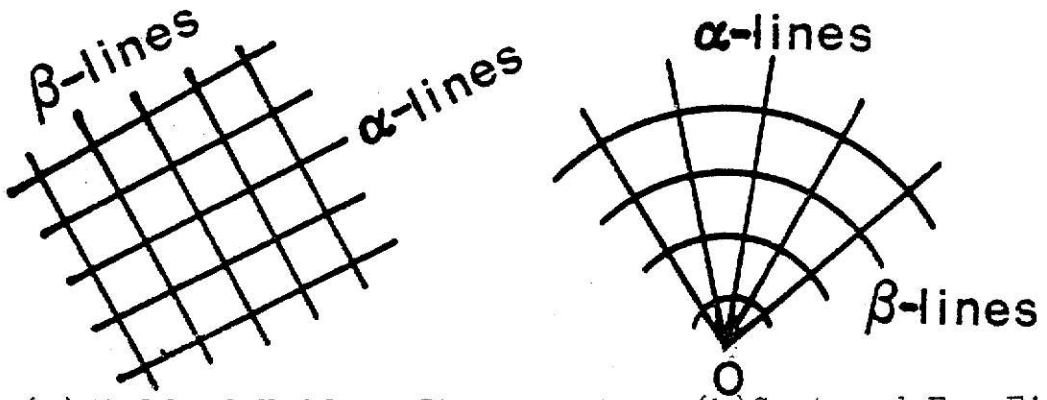

(a)Field of Uniform Stress. (b)Centered Fan Field.

Fig.2.4.Slip-Lines of Simple Stress States.

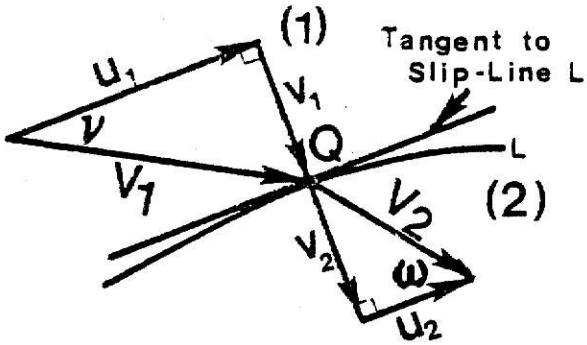

(a)Physical Plane.

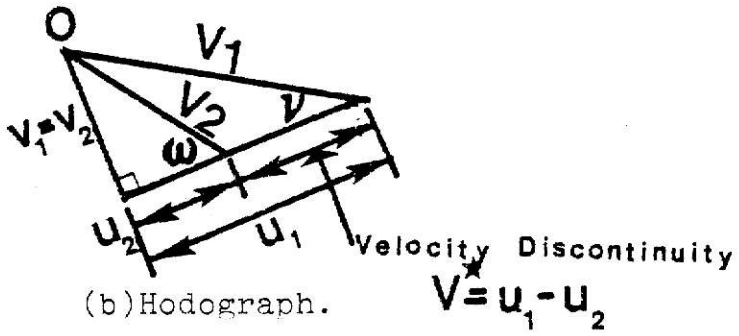

(b)Hodograph.

Fig.2.5.Velocity Discontinuity.

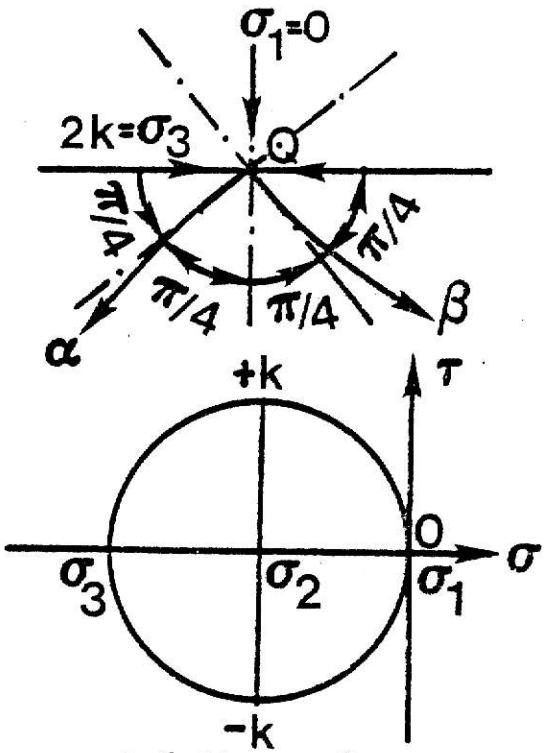

Fig.2.6.Stress Free Surface.

of the velocity at each point in a plastically deforming region. This is known as a hodograph The hodograph permits the evaluation of the magnitude and direction of the velocity at a point which is indicated as a vector.

2.3.4 Simple Stress-States

Fig. 2.4(a) shows a slip-line field generated by two orthogonal families of parallel straight lines. Using Hencky's stress equations (2.13) it can be shown that if the slip lines are straight then the angle, $\emptyset$, is constant along the slip lines and the hydrostatic pressure, p, remains constant. Also the stress components σ_x, σ_y, and σ_z must be constant. Thus the slip-line field of Fig. 2.4(a) represents a uniform stress state.

The slip-line field shown in Fig. 2.4(b) consists of a set of radial lines, say α-lines, intersected orthogonally by a set of concentric circular arcs, say β-lines. From the first of Hencky's stress equations (2.13), since $\emptyset$ is constant along an α-line, the hydrostatic pressure, p, must also be constant along an α-line. From the second of Hencky's stress equations, since $\emptyset$ varies linearly with distance along a β-line, the hydrostatic pressure, p, varies linearly with distance along a β-line. This type of slip-line field is known as the centered fan. The center of the fan, 0, is a point of stress singularity, and it can have any one of an infinite number of values.

In general a slip-line field can be constructed by combining both the uniform stress state and the centered fan fields.

2.3.5 Velocity Discontinuities

For a rigid-perfectly plastic material the displacements throughout the deforming material need not be continous. It is possible for there to be relative slipping between neighbouring zones in the deforming material.

The line of velocity discontinuity is a slip-line. As shown in Fig. 2.5(a) consider the material at Q crossing a slip-line. Let the material to the left of Q have a velocity V_1 with components v_1 and u_1 which are normal and tangential to the slip-line respectively. After crossing the slip-line its velocity changes to V_2 with corresponding components v_2 and u_2. Continuity at Q demands $v_1=v_2$; hence normal components of velocity when crossing a slip-line are always the same magnitude on either side of the slip line. However, it is possible for there to exist a velocity discontinuity of magnitude, $V^*=u_1-u_2$, tangential to the slip-line at the point Q, as shown in the hodograph in Fig. 2.5(b).

The magnitude of the tangential stress along a line of velocity discontinuity is equal to $\tau=\pm K$. In passing through such a line, an element experiences a finite shear in the direction in which the tangential stresses act and thus changes its direction of motion. The jump velocity, $V^*=u_1-u_2$ and the sense of the tangential stress, τ, are related by the condition that the plastic energy dissipation be positive: $\tau(u_1-u_2)>0$. Therefore, if the jump $V^*=u_1-u_2>0$, $\tau=+K$ and if $V^*=u_1-u_2<0$ then $\tau=-K$.

In general, once a velocity discontinuity is established across a slip-line there always exists a velocity discontinuity across any extension to the slip-line. Another general rule on slip-lines across which there is a discontinuity in the tangential component of velocity, is that, these slip-lines either form the boundary of the deforming region, or originate and/or terminate at a point of stress singularity within the field. These restrictions are necessary, otherwise compatibility of the velocity solution is violated.

2.3.6 Boundary Conditions for Stresses

2.3.6.1 Stress Free Surface

At a stress free surface there are no normal or shear components of

stress. The stress free surface is, therefore, a principal plane on which the principal stress is zero. It follows that the direction tangential to the free surface is a principal stress direction. The slip-lines indicate directions of maximum shear stress at anypoint in the material and intersect the free surface at angles of $\pm 45°$ as shown in Fig. 2.6(a).

The normal stress at the point Q can be considered as a zero compressive stress. Since the other principal stresses are also compressive and have greater magnitudes, the zero normal stress is the algebraic maximum principal stress, that is, $\sigma_1=0$. The algebraic minimum principal stress is $\sigma_3=-2K$. The Mohr's circle diagram is shown in Fig 2.6(b). The algebraic maximum principal stress, σ_1, has its direction contained in the first and third quadrants of the right-handed $\alpha-\beta$ co-ordinate system. Hence the α and β-lines are designated as shown in Fig. 2.6(a).

2.3.6.2 Friction Present at the Interface

At the tool-workpiece interface there can exist both shear and normal stresses. The shear stress tangential to the interface arises from friction conditions. If the magnitude of the shear and normal stresses are known the angle at which the family of slip-lines intersects the boundary can be found from the Mohr's circle as shown in Fig. 2.7(c). One slip-line will intersect the interface at some angle $\eta < 45°$. The determination of the magnitude of the shear and normal stress from a given friction condition will be discussed in Section 5.1.2.

In the case of no friction at the interface, the slip-lines intersect the interface at angles of $\eta = \pm 45°$. If the frictional stress becomes so high that the workpiece material will yield in shear at the interface, one slip-line meets the interface tangentially and the other normally. Under these conditions the interface is usually referred to as being perfectly rough.

2.3.7 Requirements for a Complete Solution

2.3.7.1 General Requirements

A complete solution to the plane strain deformation of a rigid-perfectly plastic material requires:

1. A statically admissible stress field which satisfies the equilibrium equations and the stress boundary conditions and nowhere is the yield criterion to be violated.

2. A kinematically admissible velocity field that is compatible with the stress field.

3. The rate of plastic work is everywhere positive.

4. The yield criterion is not violated in the material adjacent to the plastic region. That is, the material must be capable of supporting the stresses transmitted across the boundary without yielding.

2.3.7.2 Check of Positive Rate of Work

Plastic work is always positive, that is, work has to be done on materials to cause permanent deformation. It is necessary to check that any slip-line solution does not violate this fact at any point throughout the field.

The following method of verifying that the plastic energy dissipation be positive was suggested by Ford [33]. In Fig. 2.8(a), a curvilinear element ABCD is bounded by a pair of α and β-lines. The corresponding hodograph is shown in Fig. 2.8(b). The plastic energy dissipation in the element will be positive provided the velocity of C relative to A represented by the vector, $\overrightarrow{ac}$, in the hodograph is positive, that is, having a sense from A to C, and the velocity of D relative to B represented by the vector $\overrightarrow{bd}$ is positive, that is, having a sense from D to B corresponding with the sign of the shear stresses in the physical plane of Fig. 2.8(a).

Velocity discontinuities need to be considered separately. The jump

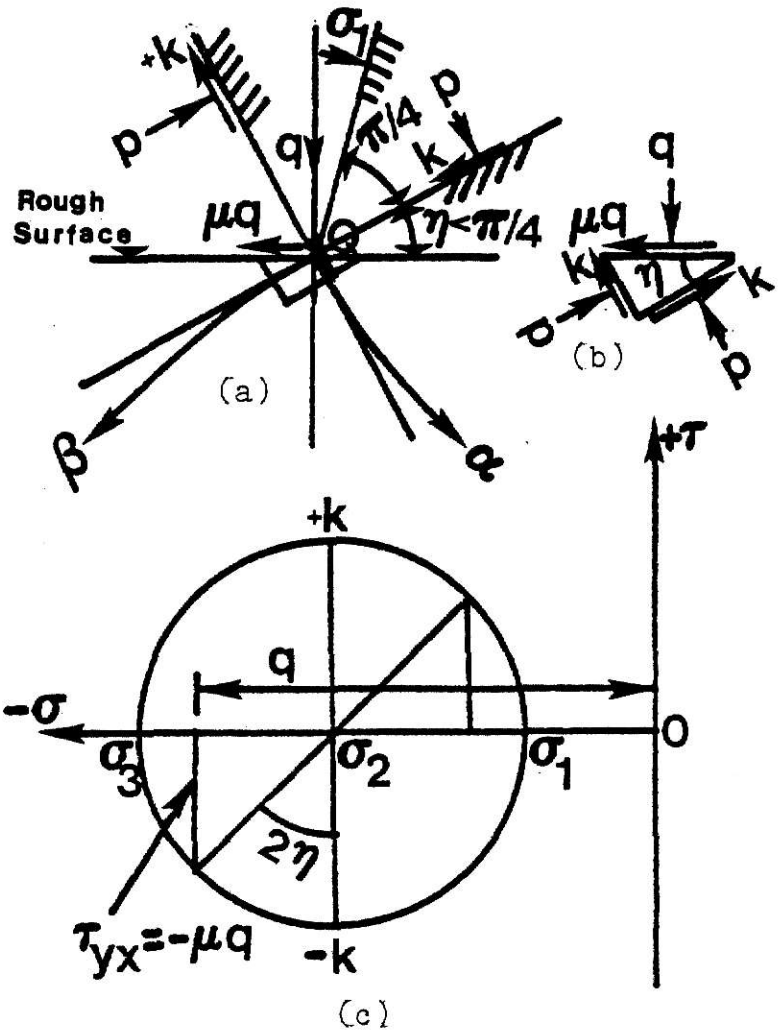

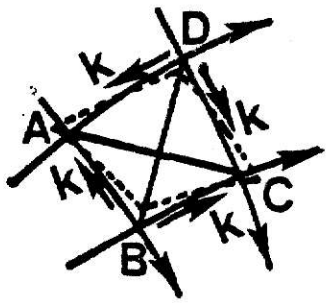

(a) Physical Plane

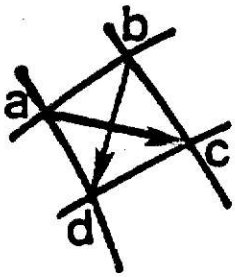

(b) Hodograph.

Fig.2.8.Verification of Positive Plastic Energy Dissipation.

Fig.2.7.Rough Surface,(a)Intersection of the Slip-Lines at Point Q in an Interface where Friction is Present (b)Stresses Acting on an Element, (c)Mohr Stress Circle Diagram.

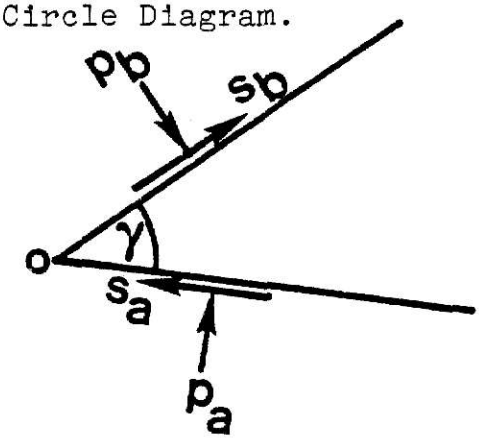

Fig,2.9. State of Stress at a Vertex.

in velocity, $V^*=u_2-u_1$, as discussed in Section 2.3.5, must be in the same direction of the shear stress on the same side of the discontinuity line.

2.3.7.3 Yield Criterion Not Violated at Points of Stress Singularity.

Hill [30] showed that in order that yielding of the vertex, Fig 2.9, shall not occur, the following inequalities must apply:

$$\gamma \geq |\Omega_a - \Omega_b| \tag{2.18}$$

$$\left(\frac{p_b-p_a}{2K}\right)_{\max} \leq \begin{cases} \frac{1}{2}[\text{Cos } 2\Omega_a+\text{Cos } 2\Omega_b]-\text{Cos}(\gamma+\Omega_a+\Omega_b) & \text{, for } \gamma+\Omega_a+\Omega_b \frac{\pi}{2} \\ \frac{1}{2}[\text{Cos } 2\Omega_a+\text{Cos } 2\Omega_b]+(\gamma+\Omega_a+\Omega_b-\pi/2) & \text{, for } \gamma+\Omega_a+\Omega_b \frac{\pi}{2} \end{cases}$$

$$\left(\frac{p_b-p_a}{2K}\right)_{\min} \geq \begin{cases} -\frac{1}{2}[\text{Cos } 2\Omega_a+\text{Cos } 2\Omega_b]+\text{Cos}(\gamma-\Omega_a-\Omega_b) & \text{, for } \gamma-\Omega_a-\Omega_b \leq \frac{\pi}{2} \\ -\frac{1}{2}[\text{Cos } 2\Omega_a+\text{Cos } 2\Omega_b]-(\gamma-\Omega_a-\Omega_b-\pi/2) & \text{, for } \gamma-\Omega_a-\Omega_b \geq \frac{\pi}{2} \end{cases} \tag{2.19}$$

where,
$$\Omega_a = \frac{1}{2}\,\text{Sin}^{-1}\frac{S_a}{K}$$
$$\Omega_b = \frac{1}{2}\,\text{Sin}^{-1}\frac{S_b}{K} \tag{2.20}$$

and both Ω_a and Ω_b lie between $\frac{-\pi}{4}$ and $\frac{+\pi}{4}$.

Some particular singularities which frequently occur in plasticity solutions are given as follows:

case(i): Only normal pressures p_a and p_b are applied.

$$S_a = S_b = 0, \quad \Omega_a = \Omega_b = 0, \text{ requires } \gamma \geq 0$$

$$\left|\frac{p_b-p_a}{2K}\right| \leq \begin{cases} 1-\text{Cos } \gamma & , \gamma \leq \frac{\pi}{2} \\ 1+\gamma-\frac{1}{2}\pi & , \gamma \geq \frac{\pi}{2} \end{cases}$$

case(ii): The shearing stresses are the largest possible and are both directed either towards or away from the vertex.

$$S_a = -S_b = \pm K \quad , \Omega_a = -\Omega_b = \pm\frac{\pi}{4} \quad , \text{ requires } \gamma \geq \frac{\pi}{2}$$

$$\left|\frac{p_b - p_a}{2K}\right| \leq \gamma - \frac{\pi}{2}$$

case(iii): One shear stress (S_a) is directed towards and the other (S_b) away from the vertex.

$$S_a = S_b = K\ ,\quad \Omega_a = \Omega_b = \frac{\pi}{4}\ ,\ \text{requires}\ \gamma \geq 0$$

$$\gamma \geq \frac{p_b - p_a}{2K} \geq \begin{cases} \text{Sin}\gamma & ,\ \gamma \leq \pi \\ -(\gamma - \pi) & ,\ \gamma \geq \pi \end{cases}$$

case(iv): On one side there is no shearing stress, but on the other the maximum possible.

$$S_a = 0,\quad S_b = K,\ \Omega_a = 0,\quad \Omega_b = \frac{\pi}{4}\ \text{requires}\ \gamma \geq \frac{\pi}{4}$$

$$1 + 2(\gamma - \tfrac{\pi}{4}) \geq \frac{p_b - p_a}{K} \geq \begin{cases} 2\ \text{Cos}(\gamma - \pi/4) - 1 & ,\ \frac{\pi}{4} \leq \gamma \leq \frac{3}{4}\pi \\ -2\ (\gamma - \frac{3}{4}\pi) - 1 & ,\ \gamma \geq \frac{3}{4}\pi \end{cases}$$

2.3.8 Methods of Solution

If the problem is statically determinate, the slip-line field and the stresses can be defined from equations (2.13) and the stress boundary conditions. The velocities can be determined from equations (2.17) using the boundary conditions. However, if the problem is statically indeterminate, when the stress boundary conditions are insufficient to obtain a unique slip-line field, then Hencky's stress equations must be solved simultaneously with the Geiringer velocity equations using both the stress boundary conditions and the velocity boundary conditions. Except for the cases where the slip-line fields are of the simplest kind, the numerical solution to statically indeterminate problems is extremely difficult.

Sometimes such problems can be treated by a semi-inverse method. First, the stress field is determined with guesses made for the unattended boundary conditions. If a valid hodograph, that satisifies the velocity boundary conditions, can be constructed for a field so obtained; and the rate of energy dissipation is non-negative throughout the field, the slip-

line is kinematically admissible. Furthermore, in the stress field at stress singularities if the vertices are not overstressed, and if the stress field can be extended in a statically admissible manner into the non-deforming regions of the velocity field, the stress field is unique in the deforming regions and the solution is complete.

A solution that does not include an extension of the stress field into all the non-deforming regions of the velocity field, but is otherwise complete, yields an upper bound for the surface tractions [24].

3.0 FORMULATION OF THE PROBLEM

3.1 Introduction

In the metal cutting process, a surface layer of metal is removed by a tool that travels parallel to the surface at a chosen depth of cut. Most metal cutting operations are three dimensional, however, only orthogonal cutting, where the tool is moved in a direction at right angles to the cutting edge is considered. This simplifies the analysis of the mechanics of metal cutting.

The chip formed is assumed to be continuous and thus the process is considered to be steady motion. The rake angle, α, of the tool, which is the angle between the upper face of the tool and the normal to the workpiece surface is considered to be negative and is shown in Fig. 3.2. It is assumed that the state of friction over the area of contact between the tool and the plastic flow of the work material can be represented by an adhesion coefficient, m. The given conditions are then, the values of the rake angle (α), the adhesion coefficient (m), the depth of cut (D), the width of cut (W), and the workpiece physical properties (Y' or K). The problem is to determine the shape of the plastic region around the cutting edge and to calculate the forces on the face of the tool, and the thickness of the chip, d. Since the width of the tool, W, is generally very large compared with the depth of cut, D, the deformation is essentially plane strain.

For plane strain plastic deformation, the governing equilibrium differential equations (2.11) which are hyperbolic are known, but

for statically indeterminate problems like negative rake angle cutting, direct solutions are extremely difficult. However, considering the characteristics of the differential equations which are the slip-lines, the problem is reduced to determining the field of slip-lines. The construction of a slip-line field is usually based on experimental observation and the intuition of the investigator. Once the slip-line field is determined, a valid velocity field (hodograph) is constructed. If a valid hodograph cannot be found the procedure of finding a new slip-line is continued until a slip-line field with a kinematically admissible field is found. If the slip-line field found satisfies all the requirements of a complete solution as discussed in Section 2.3.7, it is a complete solution to the problem. However, if the stress field used is not extended to the non-deforming regions of the velocity field, it is an upper bound solution.

The trial and error procedure of determining the slip-line field for large negative rake is more complex than many types of forming processes such as extrusion and sheet drawing. One of the main reasons is that, in the cutting process the material of the workpiece first lifts up and then divides into two parts under the tool. One of them flows up the tool face to become a stress free chip, while the second one flows down the tool face to rejoin the workpiece material.

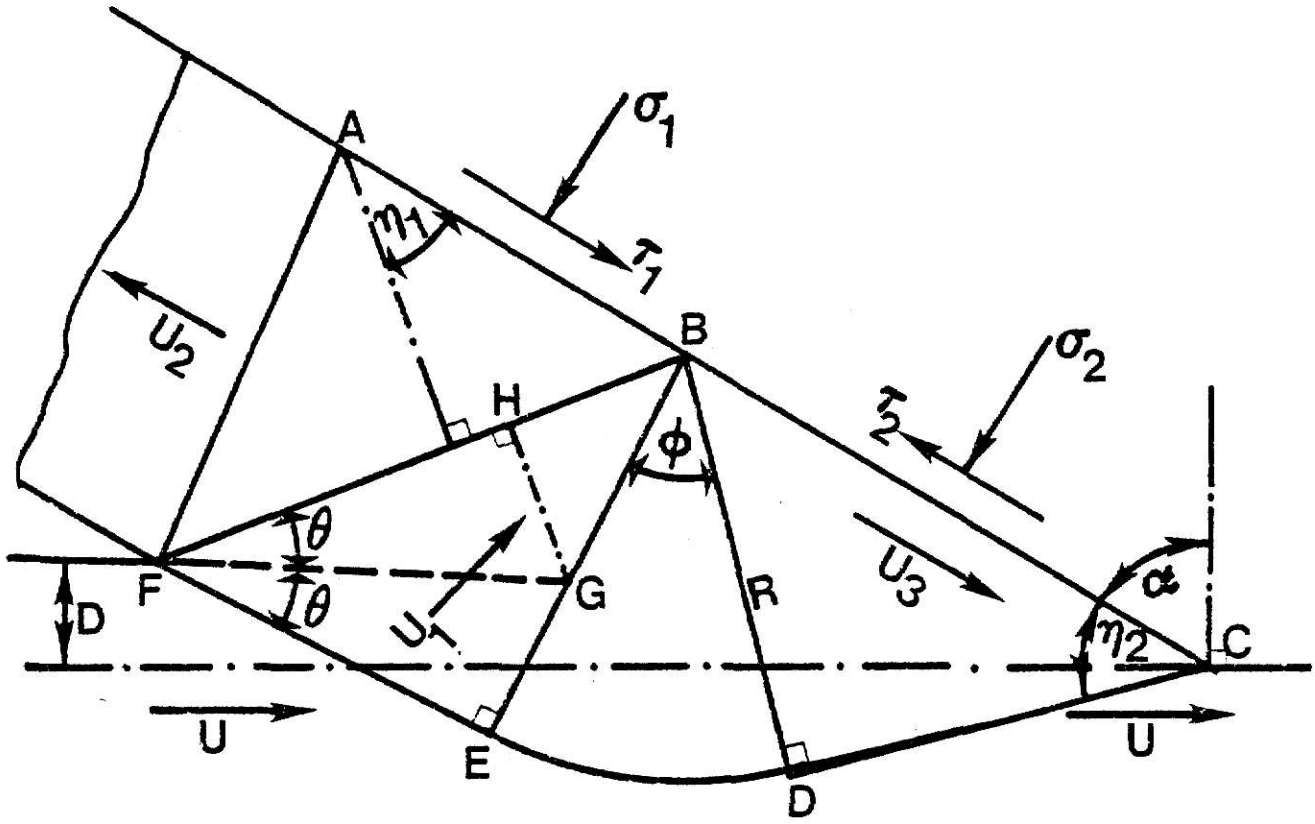

(a)Slip-Line Field.

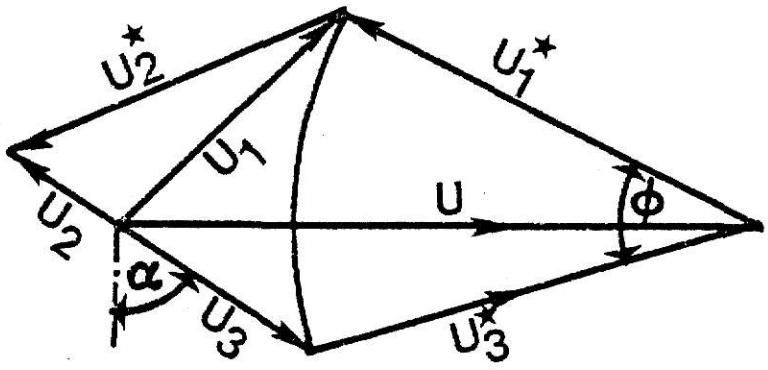

(b)Hodograph.

Fig.3.1.Slip-Line Field with its Hodograph [35].

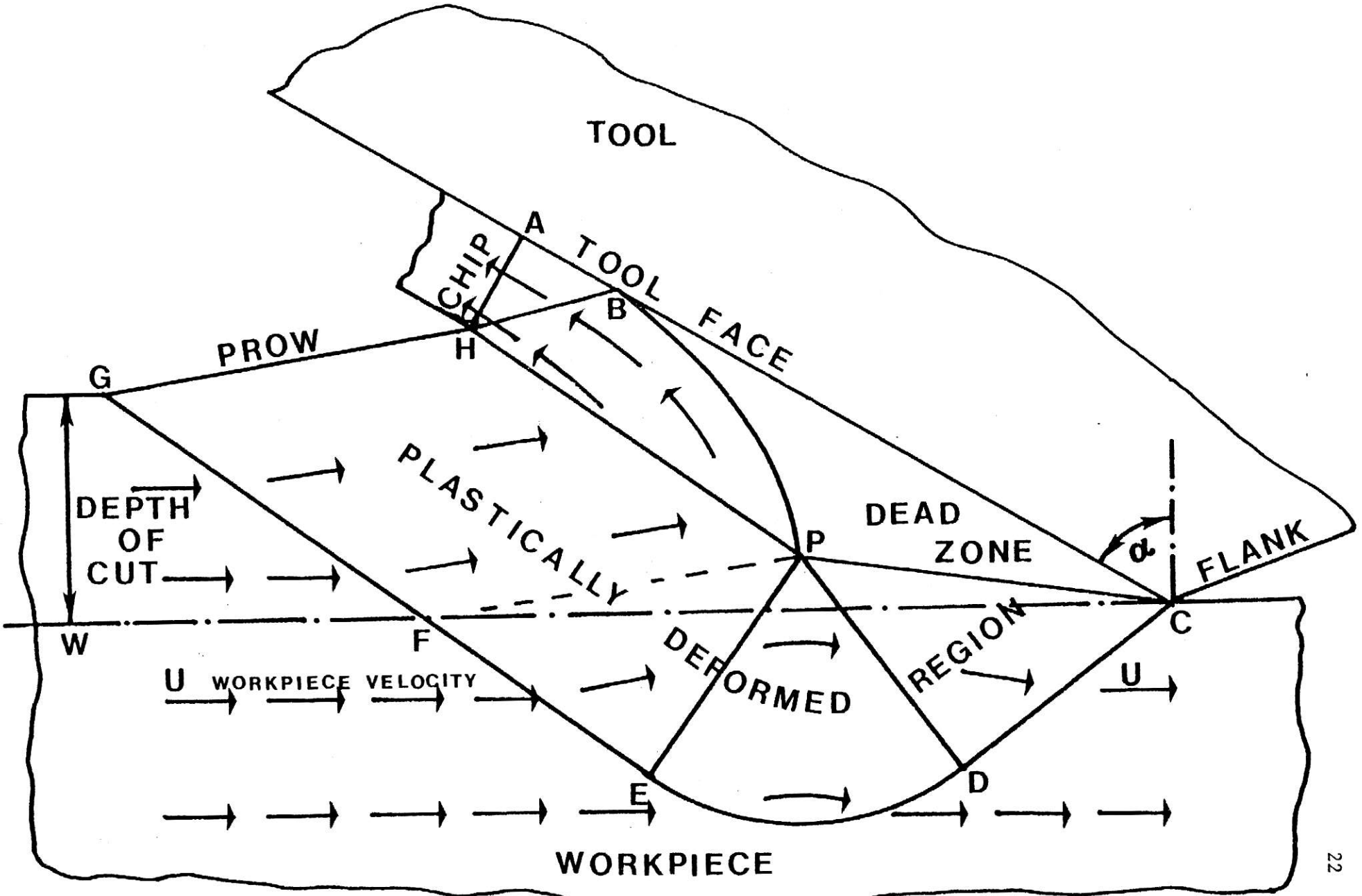

Fig.3.2.Schematic of Cutting with a Large Negative Rake Tool.

3.2 Previously Proposed Slip-Line Field

Slip-line fields for negative rake angle cutting are proposed by Hein [35] and Challen [31]. The one proposed by Challen does not consider the division of the plastic flow into two parts. Since the divided flow has been proved experimentally [11,33], Challen's slip-line field will not be discussed further. Hein's proposal which is an upper bound solution type will now be discussed.

Hein's proposed slip-line field is shown in Fig. 3.1(a). It has a valid hodograph as shown in Fig. 3.1(b). Point B is the stagnation point where the workpiece material is divided into two parts. One flows towards A to become a chip, and the other flows towards C. The region BGH is overstressed and violates the yield criterion necessary for a complete slip-line solution, however, the solution leads to an upper-bound approximate solution. The results obtained predict that there is a maximum allowable negative rake angle, beyond which it is impossible to form a chip. The fact that there is a critical angle is supported experimentally [11,14,28], even though the numerical value is not in agreement. Also, using the slip-line field it is found that the normal component of the cutting force is greater than the tangential component, and both force components increase as the rake angle increases. These facts are also in good agreement with experimental results [11,28,36].

The results obtained by this trial slip-line, which is the first of its kind, shows that the slip-line method of solution is

suited to the type of problem under consideration. Thus, one is tempted to search for an improved slip-line field which will be a better solution by taking into account additional cutting features not previously considered.

3.3 Newly Proposed Slip-Line Field

In setting up the slip-line field it is assumed that the tool is stationary and rigid, and the depth of cut is comparatively bigger than the radius of curvature at the tip of the cutting edge of the tool.

Only a few experiments have been done on negative rake angle cutting; and all that appear in the literature [12,14,36] observed that a stagnation region appears in front of the tool. This region divides the plastic flow into upward and downward directions over the tool face. Thus, the slip-line to be constructed should take this fact into consideration. Also it is observed experimentally [13] that there exists a buildup of material ahead of the tool which is called a prow, and this too should be included in the slip-line field. Other experiments relating to wear indicate that the tool wears on the bottom side of the tool, which is called the flank. This suggests that the slip-line field proposed should extend beyond the cutting tip. However, this feature is not included as it makes the problem of finding the slip-line field more difficult.

Hein's slip-line field, Fig. 3.1(a), assumes that at a single point B on the tool face the plastic flow is divided into upward and downward directions. This assumption makes the construction of a

slip-line field difficult and thus the over-stressed region BGH is created. In order to avoid this over-stress it will be considered that there is a dead zone of some shape in front of the tool. In addition, it seems that the trial slip-line field should include a prow. Thus, considering the region ABF, BDE and BCD of the trial slip-line field with a dead zone and a prow, a new slip-line field consisting of simple stress regions is sought. After many trial attempts a successful upper bound solution was found as shown in Fig. 3.2.

The proposed slip-line field consists of the dead zone BCP and prow GH. The chip leaves from the work material, with zero stress, along the stress-free line AH. The work material, with a horizontal uniform velocity U, enters and leaves the plastic zone along the velocity discontinuity slip-line GC. That entering along the line GF, first flows parallel to the prow GH, then the velocity discontinuity slip-line PH makes the flow parallel to the tangent to the curved surface BP at P. Then the centered fan field BHP causes the flow to follow a path similar to the curve BP. Next the velocity discontinuity slip-line BH straightens the flow out parallel to the tool face and finally it emerges as a chip along the stress-free surface line AH. Material entering along FE first flows parallel to GH, is then directed by the centered fan field to flow parallel to the surface PC, and finally the velocity discontinuity slip-line DC makes the flow horizontal with velocity U. Material entering below

E is directed by the fan to change directions and leave from the plastic region crossing ED again which makes the flow horizontal with a magnitude of U. Here it can be seen that the dead zone BPC acts as a divider of the plastic flow.

For this slip-line field GW is the depth of cut, D. The friction conditions on the surfaces AB, BP and PD are given by the angle η_1, η_2 and η_3, respectively. The determination of the magnitude of these angles is discussed in Section 5.1.2.

4.0 SLIP-LINE FIELD SOLUTION

4.1 Geometrical Properties

Figure 4.1 is the slip-line field proposed. It consists of the uniform stress state regions ABH, GHPE and PCD, the centered fan regions HBP and PED, and the dead zone BPC. The center of the circular arc BP is at O. Angles α, η_1, η_2 and η_3 and the depth of cut D are known for a given problem. Since the depth of cut D can be expressed in terms of the fan PED radius, R is also assumed known. The geometrical relationships of the slip-lines are given in Appendix I.

The depth of cut D is

$$D = R \frac{1}{\sin\eta_3} \frac{\sin(180-\eta_1-\theta-\Delta+\eta_2)}{\sin(\eta_1-\eta_2+\frac{\theta}{2})} \frac{\sin(90-\frac{\theta}{2}+\eta_2)}{\sin\theta} \sin(\eta_1+\theta-\alpha) \tag{4.1}$$

The chip thickness d is

$$d = R \frac{1}{\sin\eta_3} \frac{\sin(180-\eta_1-\theta-\Delta+\eta_2)}{\sin(\eta_1-\eta_2+\frac{\theta}{2})} \frac{\sin(90-\frac{\theta}{2}-\eta_2)}{\sin\theta} x$$

$$\frac{\sin(90-\eta_1)}{\sin(45+\eta_1)} \cos(45-\eta_1) \tag{4.2}$$

At point P all the angles should sum to 360°. Thus the geometric condition at P requires that

$$\phi + \Delta - \eta_3 + \eta_2 = 90 \tag{4.3}$$

In order that a chip be formed, it is necessary to have

$$\eta_1 + \theta - \alpha > 0. \tag{4.4}$$

Also in order to form the dead zone

$$180-(\eta_1 + \theta + \Delta - \eta_2) > 0. \tag{4.5}$$

For frictional stresses to be in proper directions

$$0 \leq \eta_1 \leq 45, \quad 0 \leq \eta_2 \leq 45, \quad 0 \leq \eta_3 \leq 45. \tag{4.6}$$

4.2 Velocity Field

4.2.1 Hodograph

The hodograph of the slip-line field is shown in Fig. 4.2. It is assumed that velocity discontinuities shall occur along the slip-line GC and the radial lines of the centered fan field of HPB and PED. The numerical relationships of the velocities in each region of the slip-line field in terms of the velocity U of the work-piece are given in Appendix I.

4.2.2 Continuity Requirements

The material entering across the slip-line GF should come out as a chip along the free surface line HA. This requires that the volume cut should be equal to the volume of chip.

Referring to Fig. 4.1 and Fig. 4.2

$$\text{Volume cut} = U\ W = U\ HQ$$
$$= \frac{U\ R}{\sin\eta_3} \frac{\sin(180-\eta_1-\theta-\Delta+\eta_2)}{\sin(\eta_1-\eta_2+\theta/2)} \frac{\sin(90-\theta/2+\eta_2)}{\sin\theta} \sin(\eta_1+\theta-\alpha) \tag{4.7}$$

and it can be shown also that

$$\text{Volume of chip} = U_{BA}\ HA\ \cos(45-\eta_1)$$

$$= \frac{U\ R}{\sin\eta_3}\ \frac{\sin(180-\eta_1-\theta-\Delta+\eta_2)}{\sin(\eta_1-\eta_2+\theta/2)}\ \frac{\sin(90-\theta/2+\eta_2)}{\sin\theta}\ \sin(\eta_1+\theta-\alpha). \tag{4.8}$$

Equations (4.7) and (4.8) are equal in magnitude. Hence the volume cut equals the volume of chip. Thus, physically there is no restriction on the angles θ and Δ which are unknown.

4.2.3 Velocity Discontinuity Requirements

The velocity discontinuity along the whole length of the slip-line GC should be equal. Thus, referring to the hodograph of Fig. 4.2, it means that the velocity discontinuities U^*_{EG} and U^*_{DC} should be identical. Hence, the following condition follows

$$U^*_{EG} = U\ \frac{\sin(45-\eta_1-\theta+\alpha)}{\sin\ 135}$$

$$U^*_{DC} = U\ \frac{\sin(\eta_1+\theta+\Delta-\eta_2-\alpha-90)}{\sin(180-\eta_3)}$$

Therefore,

$$U\ \frac{\sin(45-\eta_1-\theta+\alpha)}{\sin\ 135} = U\ \frac{\sin(\eta_1+\theta+\Delta-\eta_2-\alpha-90)}{\sin(180-\eta_3)} \tag{4.9}$$

Solving for θ,

$$\theta = \text{Arctan}\left[\frac{\sin(180-\eta_3)\ \sin(45-\eta_1+\alpha)-\sin135\ \sin(\eta_1+\Delta-\eta_2-\alpha-90)}{\sin(180-\eta_3)\ \cos(45-\eta_1+\alpha)+\sin135\ \cos(\eta_1+\Delta-\eta_2-\alpha-90)}\right] \tag{4.10}$$

and solving for Δ in Eq. (4.9) and using the relationship of Eq. (4.3)

$$\phi = \eta_3+\eta_1-\alpha+\theta-\sin^{-1}\left[\frac{\sin(180-\eta_3)\ \sin(45-\eta_1-\theta+\alpha)}{\sin135}\right] \tag{4.11}$$

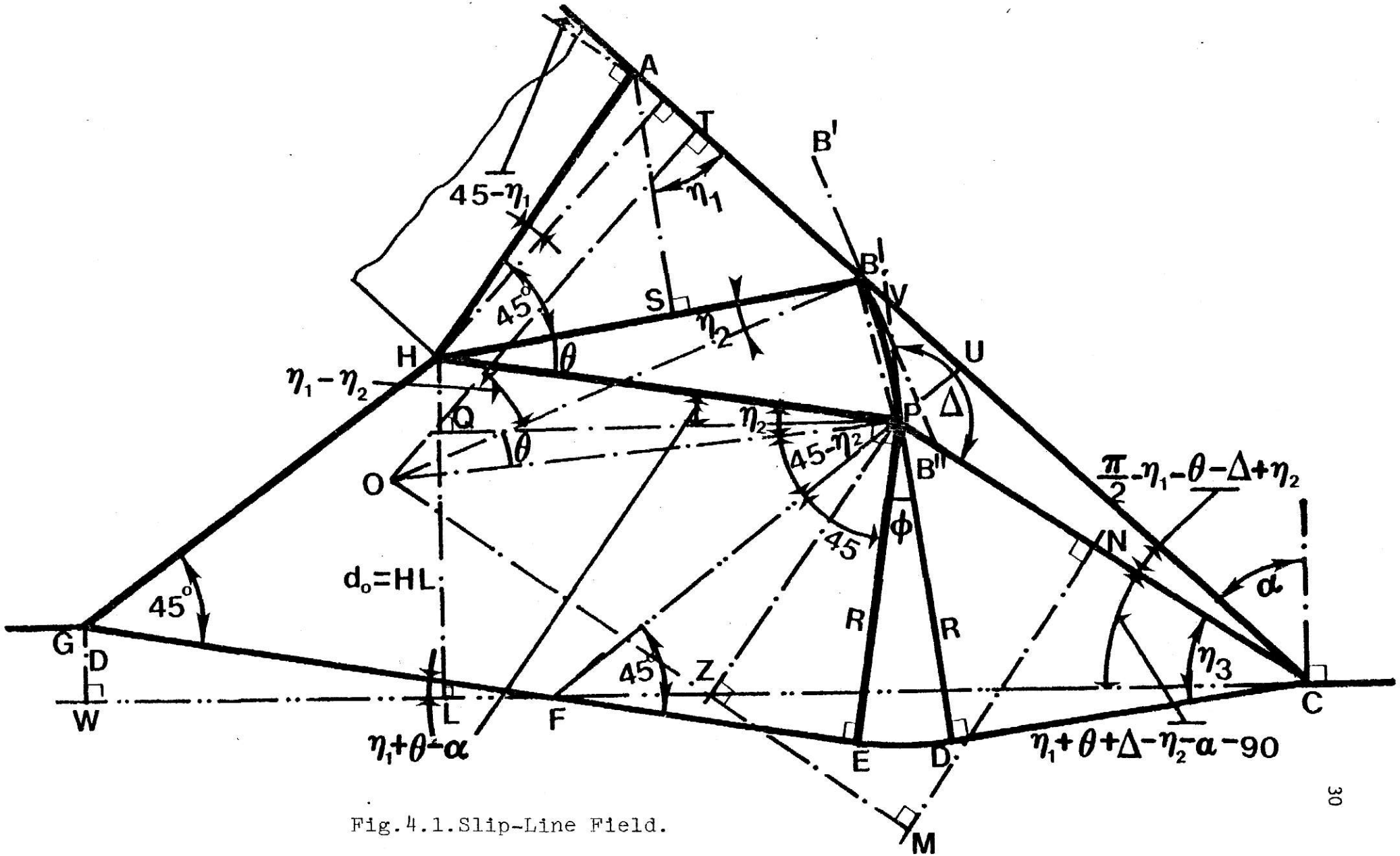

Fig.4.1.Slip-Line Field.

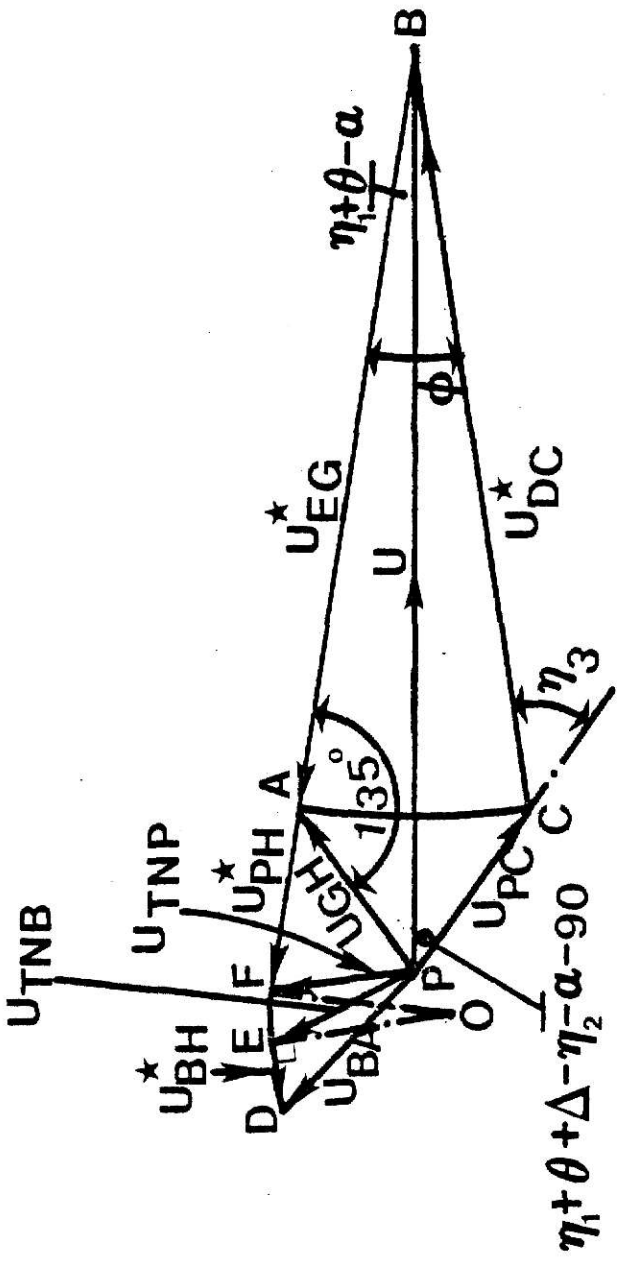

Fig.4.2, Hodograph

Angles

EPF = θ
EOF = θ
DPE = $\eta_1-\eta_2$
PDE = $90-\eta_1$
OFP = η_2
PFA = $90-\eta_2$
PAF = 45
OEF = $90-\frac{\theta}{2}$

Physically this means that the only ϕ angle that keeps the line FC in Fig. 4.1 horizontal is the relationship given by the equation (4.11).

4.3 Stress Distribution

The chip flows from the work-material along the stress free line HA, as shown in Fig. 4.3(a). It is assumed that the chip has no stress, thus $p_1=0$ and $p_2= -2k$ as shown in the Mohr's circle diagram of Fig. 4.3(b). Thus, the maximum principle stress is p_1. The α and β lines as described in Sec. 2.3.1 are shown in Fig. 4.3(a). The hydrostatic pressure in region ABH is k and the states of stress along AB and HB are shown on the Mohr's circle.

In the centered fan HBP, the radial lines are the β-lines and the circular arcs are the α-lines. According to Hencky's, Eq. (2.13) the pressure varies linearly with θ along the circular arc (α-line), and thus

$$p_6 + 2k(-\theta_6) = p_8 + 2k(-\theta_8).$$

Thus,

$$p_8 = p_6 + 2k(\theta_8-\theta_6), \quad \theta_8-\theta_6 = \theta$$

or

$$p_8 = p_6 + 2k\theta \ . \tag{4.12}$$

The state of stress in the regions HBP and HPEG can be found using the Mohr's circle of Fig. 4.3(b).

The centered-fan PED has α radial lines and β circular arcs. Thus using Hencky's equation on the β-lines

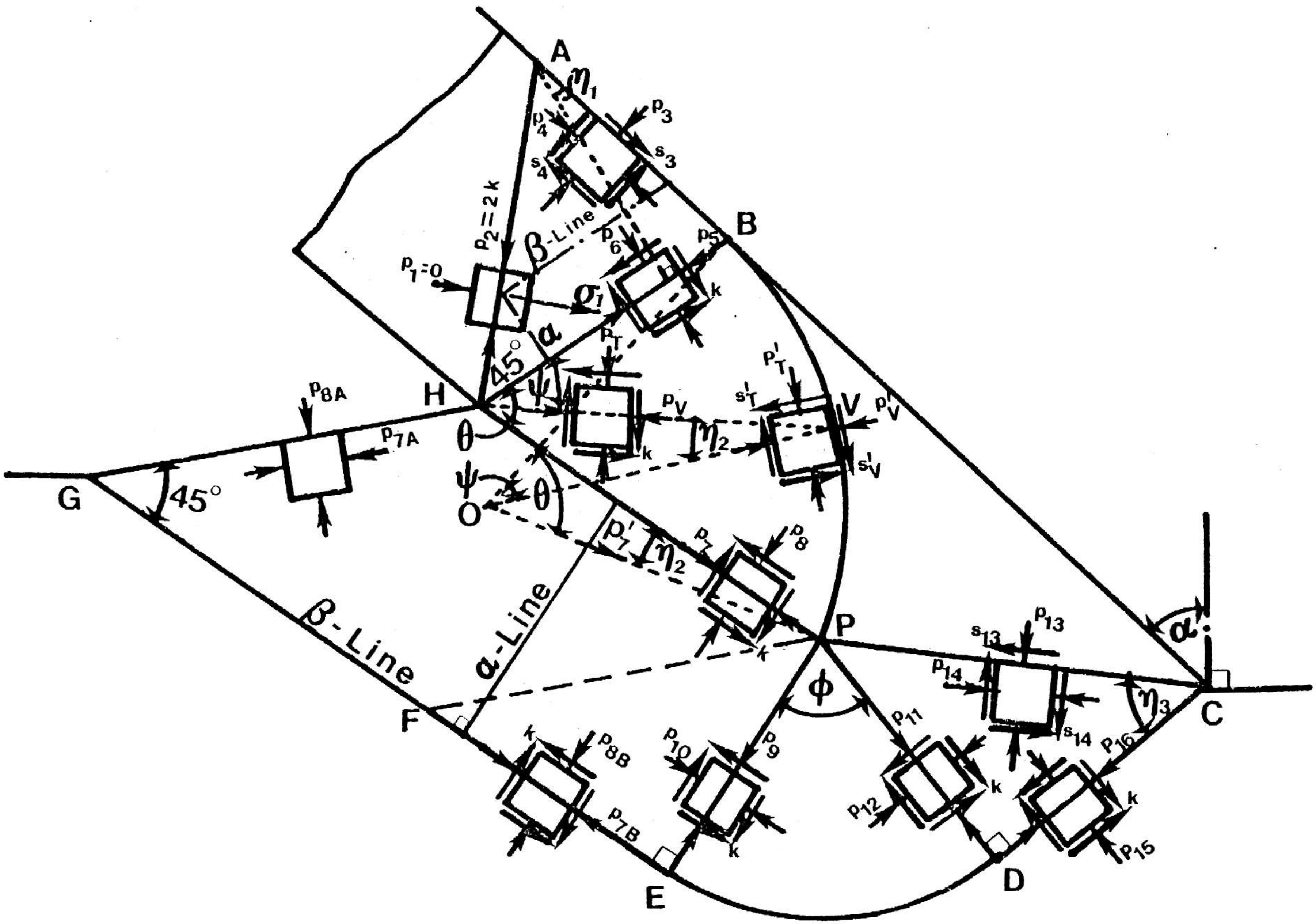

Fig.4.3.(a).Stress Distribution in the Slip-Line Field.

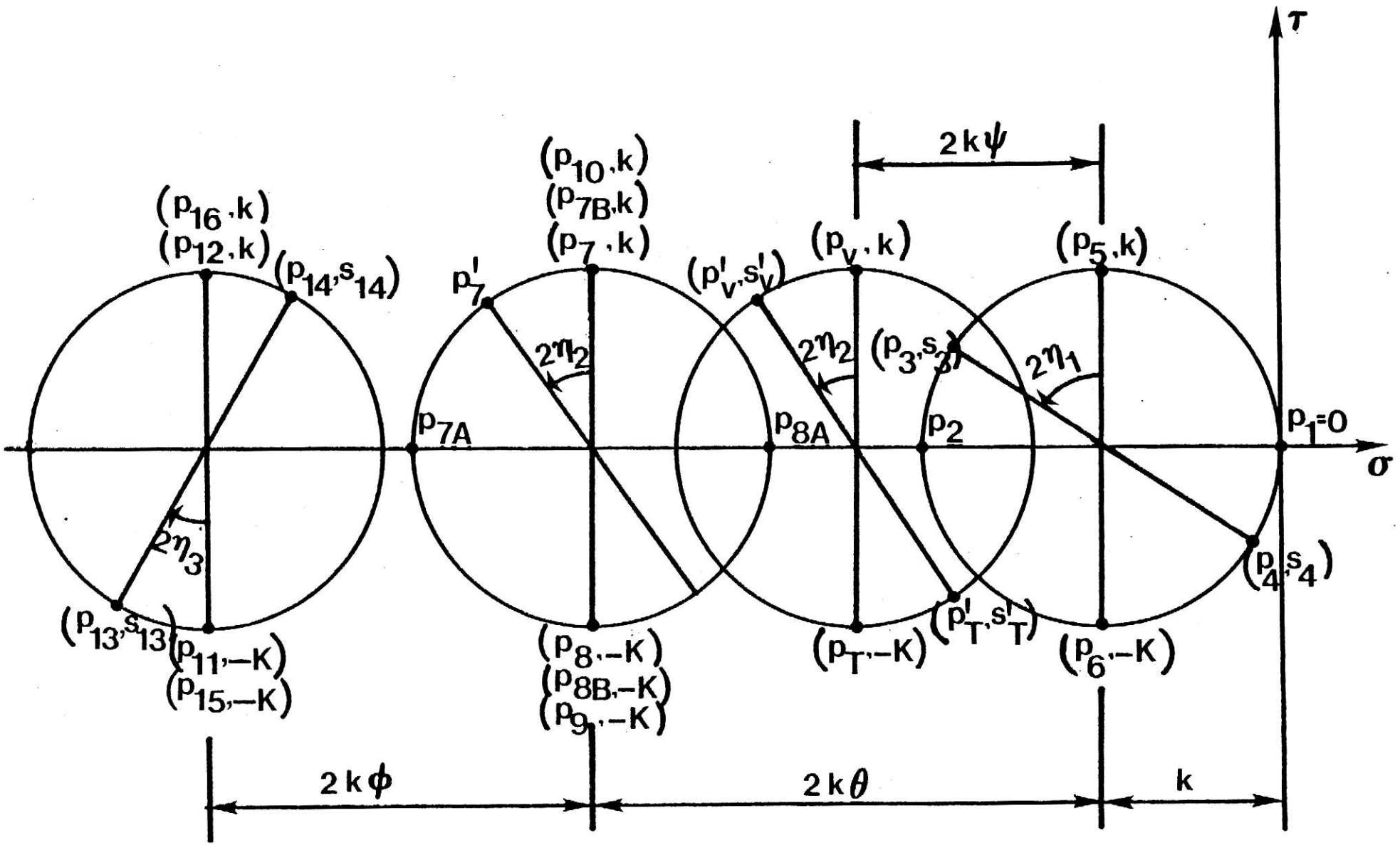

Fig.4.3.(b).Mohr Stress Circle Diagram indicating the Stress State on Slip-Lines and Interfaces.

$$p_{12} - 2k\phi_{12} = p_{10} - 2k\phi_{10}.$$

That is,

$$p_{12} = p_{10} + 2k(\phi_{12}-\phi_{10}), \quad \phi_{12}-\phi_{10} = \phi$$

or

$$p_{12} = p_{10} + 2k\phi. \tag{4.13}$$

The state of stress in the regions PED and PCD are shown in the Mohr's circle diagram of Fig. 4.3(b).

As shown in Fig. 4.3(a) the α-lines make angle η_1 with the tool interface AB, the β-lines make angle η_2 with the radius of the dead zone circular interface BP, and the β-lines make η_3 with the dead-zone interface PC. The frictional stresses on the interface AB and BP oppose the plastic flow that enters across the slip-line GF; and the frictional stress on side PC opposes the flow that enters through slip-line FE. The angles η_1, η_2 and η_3 represent friction conditions on AB, BP and PC, respectively, and the determination of their numerical values is discussed in Section 5.1.2.

The values of the stresses on the interfaces as determined from the Mohr's circle diagram of Fig. 4.3(b) is discussed in Appendix I. Some of the results are as follows:

$$p_3 = -k(1+\sin 2\eta_1)$$
$$s_3 = k \cos 2\eta_1 . \tag{4.14}$$

On side BP, at any point $\bar{V}$

$$p'_v = -k(1+2\psi + \sin 2\eta_2)$$
$$s'_v = k\cos 2\eta_2. \tag{4.15}$$

On side PC

$$p_{13} = -k\ (1+2\theta+2\phi+\sin 2\eta_3)$$

$$s_{13} = -k\ \cos\ 2\eta_3. \qquad (4.16)$$

Referring to Fig. 4.2 and Fig. 4.3(a) it is observed that the plastic flow velocity discontinuities are in the directions of $\overrightarrow{EG}$, $\overrightarrow{PH}$, $\overrightarrow{BH}$, $\overrightarrow{PE}$, $\overrightarrow{PD}$ and $\overrightarrow{DC}$, and are in the same directions as shear stresses across these slip-lines. Thus, the plastic work done in deforming the work-piece is positive as required by slip-line theory. In the slip-line field proposed all deformation occurs along the velocity discontinuity lines and thus the check for positive plastic work is complete.

4.4 Check of Yield Criterion

In the slip-line field of Fig. 4.3(a), the vertices of the simple stress regions HAB, HBP, HPEG, PED and PCD are not over-stressed as shown in Appendix II. The analysis to find whether a stress field satisfying equilibrium exists in the non-plastic regions is not attempted as we are interested in an upper-bound solution. However, the stability of the vertex BPC of the dead zone, which is thought to be very critical in the sense that it acts as a cutting tip, is checked.

From the Mohr's circle of Fig. 4.3(b)

$$p_d = \frac{p_7' - p_{13}}{2k} = \frac{1}{2}\ (2\phi + \sin 2\eta_3 - \sin 2\eta_2). \qquad (4.17)$$

The conditions for the vertex BPC to not be overstressed, as shown in Appendix II, are as follows. The maximum and minimum values of p_d allowed are:

For $\Delta + \eta_2 - \eta_3 \geq \pi/2$

$$P_{dmax} = \frac{1}{2} (\sin 2\eta_3 + \sin 2\eta_2) + (\Delta + \eta_2 - \eta_3 - \pi/2)$$

For $\Delta + \eta_2 - \eta_3 \leq \pi/2$

$$P_{dmax} = \frac{1}{2} (\sin 2\eta_3 + \sin 2\eta_2) - \cos (\Delta + \eta_2 - \eta_3) \qquad (4.18)$$

For $\Delta + \eta_3 - \eta_2 \geq \pi/2$

$$P_{dmin} = -\frac{1}{2} (\sin 2\eta_3 + \sin 2\eta_2) - (\Delta + \eta_3 - \eta_2 - \pi/2)$$

For $\Delta + \eta_3 - \eta_2 \leq \pi/2$

$$P_{dmin} = -\frac{1}{2} (\sin 2\eta_3 + \sin 2\eta_2) + \cos(\Delta + \eta_3 - \eta_2).$$

So in determining the unknown angles ϕ or Δ, the value of p_d given by Eq. (4.17) should satisfy the inequality

$$P_{dmin} \leq P_d \leq P_{dmax}. \qquad (4.19)$$

4.5 Forces Exerted by the Cutting Tool

4.5.1 Equilibrium Requirements on the Dead Zone

In Fig. 4.4, BPC is the dead zone. Due to plastic deformation the normal and tangential forces that act on the surfaces BP and PC are PVT, SVT and P13T, S13T, respectively, as shown in Fig. 4.4. The magnitudes of these forces are as follows:

Assume the width of the tool to be unity. As shown in Appendix I.

$$S13T = s_{13} \, PC$$

$$= K R \cos 2\eta_3 / \sin\eta_3$$

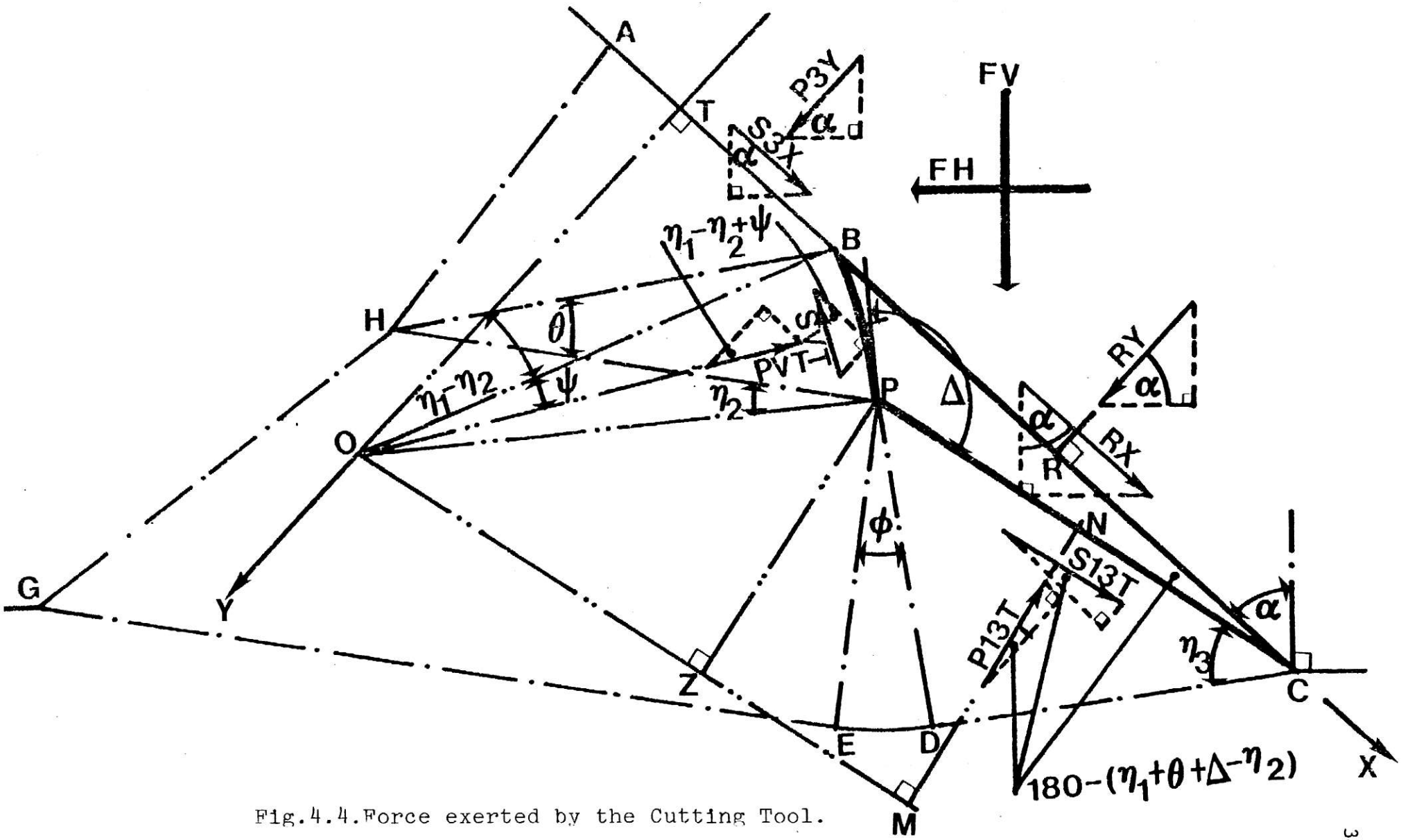

Fig.4.4.Force exerted by the Cutting Tool.

$$P13T = p_{13}\ PC$$

$$= K\ R\ (1 + 2\theta + 2\phi + \sin 2\eta_3)/\sin\eta_3$$

$$PVT = \int_0^{\theta} p_v'\ OB\ d\psi = K\ OB \int_0^{\theta} (1 + 2\psi + \sin 2\eta_2)\ d\psi$$

$$= K\ R\ \frac{\sin(90-\theta/2)}{\sin\theta}\ \frac{\sin(180-\eta_1-\theta-\Delta+\eta_2)}{\sin(\eta_1-\eta_2+\theta/2)}\ \frac{1}{\sin\eta_3} \int_0^{\theta} (1+2\psi+\sin 2\eta_2)\ d\psi$$

$$SVT = \int_0^{\theta} s_v'\ OB\ d\psi$$

$$= K\ R\ \cos 2\eta_2\ \frac{\sin(90-\theta/2)}{\sin\theta}\ \frac{\sin(180-\eta_1-\theta-\Delta+\eta_2)}{\sin(\eta_1-\eta_2+\theta/2)}\ \frac{1}{\sin\eta_3} \int_0^{\theta} d\psi$$

For the dead zone to be in static equilibrium the tool has to exert the forces RY and RX which act normal and tangential to its face, respectively. These forces can be determined as follows:

Referring to Fig. 4.4,

$$\Sigma F_x = 0$$

$$RX = SVTX + P13TX - S13TX - PVTX \qquad (4.20)$$

where, $S13TX = S13T \cos(180-\eta_1-\theta-\Delta+\eta_2) = \dfrac{K\ R \cos 2\eta_3 \cos(180-\eta_1-\theta-\Delta+\eta_2)}{\sin\eta_3}$

$$P13TX = P13T \sin(180-\eta_1-\theta-\Delta+\eta_2) = K\ R\ (1+2\theta+2\phi+\sin 2\eta_3)\ x$$

$$\sin(180-\eta_1-\theta-\Delta+\eta_2)/\sin\eta_3$$

$$PVTX = \int_0^{\theta} PVT \sin(\eta_1-\eta_2+\psi)\ d\psi$$

$$= K\ R\ \frac{\sin(90-\theta/2)}{\sin\theta}\ \frac{\sin(180-\eta_1-\theta-\Delta+\eta_2)}{\sin(\eta_1-\eta_2+\theta/2)}\ \frac{1}{\sin\eta_3}\ x$$

$$\Big[-\cos(\eta_1-\eta_2+\theta) + \cos(\eta_1-\eta_2) + 2\,\{\sin(\eta_1-\eta_2+\theta) -$$

$$\theta\,\cos(\eta_1-\eta_2+\theta) - \sin(\eta_1-\eta_2)\} - \sin 2\eta_2\,\{\cos(\eta_1-\eta_2+\theta)$$

$$-\cos(\eta_1-\eta_2)\}\Big]$$

$$SVTX = \int_0^{\theta} SVT\,\sin(90-\eta_1+\eta_2-\psi)\,d\psi$$

$$= K\,R\,\cos 2\eta_2\,\frac{\sin(90-\theta/2)}{\sin\theta}\,\frac{\sin(180-\eta_1-\theta-\Delta+\eta_2)}{\sin(\eta_1-\eta_2+\theta/2)}\,\frac{1}{\sin\eta_3}\,x$$

$$(\cos(90-\eta_1+\eta_2-\theta) - \cos(90-\eta_1+\eta_2))$$

Assuming uniform shear stress on BC, the shearing stress is given by SBC=RX/BC. Thus, the following inequality should not be violated

$$0 \le \frac{RX}{BC} \le K\ . \tag{4.21}$$

$$\Sigma F_y = 0$$

$$RY = S13TY + P13TY + PVTY + SVTY \tag{4.22}$$

where

$$P13TY = P13T\,\cos(180-\eta_1-\theta-\Delta+\eta_2)$$

$$= K\,R\,(1 + 2\theta+2\phi+\sin 2\eta_3)\,\cos(180-\eta_1-\theta-\Delta+\eta_2)/\sin\eta_3$$

$$S13TY = S13T\,\sin(180-\eta_1-\theta-\Delta+\eta_2)$$

$$= K\,R\,\cos 2\eta_3\,\sin(180-\eta_1-\theta-\Delta+\eta_2)/\sin\eta_3$$

$$PVTY = \int_0^{\theta} PVT\,\cos(\eta_1-\eta_2+\psi)\,d\psi$$

$$= K\,R\,\frac{\sin(90-\theta/2)}{\sin\theta}\,\frac{\sin(180-\eta_1-\theta-\Delta+\eta_2)}{\sin(\eta_1-\eta_2+\theta/2)}\,\frac{1}{\sin\eta_3}\,(\sin(\eta_1-\eta_2+\theta) -$$

$$\sin(\eta_1-\eta_2) + 2\,\{\cos(\eta_1-\eta_2+\theta) + \theta\,\sin(\eta_1-\eta_2+\theta) - \cos(\eta_1-\eta_2)\}$$

$$-\sin 2\eta_2\,\{\sin(\eta_1-\eta_2+\theta) - \sin(\eta_1-\eta_2)\})$$

$$SVTY = \int_0^{\theta} SVT \cos(90-\eta_1+\eta_2-\psi)\, d\psi$$

$$= K\, R \cos 2\eta_2 \frac{\sin(90-\theta/2)}{\sin\theta} \frac{\sin(180-\eta_1-\theta-\Delta+\eta_2)}{\sin(\eta_1-\eta_2+\theta/2)} \frac{1}{\sin\eta_3} \times$$

$$(\sin(90-\eta_1+\eta_2) - \sin(90-\eta_1+\eta_2-\theta))$$

The location of these forces can be determined by taking moments about 0. That is,

$$\Sigma M_0 = 0; \quad RX\ OT + RY\ TR - P13T\ OM + S13T\ PZ - SVTO = 0.$$

Hence,

$$TR = \frac{P13T\ OM - S13T\ PZ + SVTO - RX\ OT}{R\,Y} \tag{4.23}$$

where

$$SVTO = \int_0^{\theta} S_v\ OB\ OB\, d\psi$$

$$= K\, R^2 \left[\frac{\sin(90-\theta/2)}{\sin\theta} \frac{\sin(180-\eta_1-\theta-\Delta+\eta_2)}{\sin(\eta_1-\eta_2+\theta/2)} \frac{1}{\sin\eta_3}\right]^2 \cos 2\eta_2\ \theta$$

$$OM = OZ + ZM$$

$$= R \left[\frac{\sin(180-\eta_1-\theta-\Delta+\eta_2)}{\sin(\eta_1-\eta_2+\theta/2)} \frac{\sin(90-\theta/2)}{\sin\theta} \frac{\cos(\eta_2+\eta_3-\phi)}{\sin\eta_3} + \frac{1}{2\sin\eta_3}\right]$$

$$PZ = R \left[\frac{\sin(180-\eta_1-\theta-\Delta+\eta_2)}{\sin(\eta_1-\eta_2+\theta/2)} \frac{\sin(90-\theta/2)}{\sin\theta} \frac{\sin(\eta_2+\eta_3-\phi)}{\sin\eta_3}\right]$$

$$OT = R \frac{\sin(180-\eta_1-\theta-\Delta+\eta_2)}{\sin(\eta_1-\eta_2+\theta/2)} \frac{\sin(90-\theta/2)}{\sin\theta} \frac{\cos(\eta_1-\eta_2)}{\sin\eta_3}\ .$$

To have the dead zone in equilibrium it is required that

$$TB < TR < TC \tag{4.24}$$

4.5.2 Force Reactions on the Tool Face

The forces that act on the tool face in response to plastic deformation stresses, as shown in Fig. 4.4, are the tangential forces S3X and RX, and the normal forces P3Y and RY.

The magnitudes of these forces using Appendix I are:

$$S3X = s_3\ AB$$

$$= K\ R\ \frac{\cos 2\eta_1}{\sin\eta_3}\ \frac{\sin(180-\eta_1-\theta-\Delta+\eta_2)}{\sin(\eta_1-\eta_2+\theta/2)}\ \frac{\sin(90-\theta/2-\eta_2)}{\sin\theta}\ \frac{\sin 45}{\sin(45+\eta_1)}$$

$$P3Y = p_3\ AB$$

$$= K\ R\ \frac{(1+\sin 2\eta_1)}{\sin\eta_3}\ \frac{\sin(180-\eta_1-\theta-\Delta+\eta_2)}{\sin(\eta_1-\eta_2+\theta/2)}\ \frac{\sin(90-\theta/2-\eta_2)}{\sin\theta}\ \frac{\sin 45}{\sin(45+\eta_1)}$$

RX and RY are given in Eqs. (4.20) and (4.22), respectively. On the face of the tool, denoting the tangential force, FT, and the normal force, FN, we have the following relationship,

$$FT = S3 + RX \tag{4.25}$$

$$FN = P3Y + RY\ .$$

4.5.3 Force Exerted by Tool

The horizontal and vertical force components exerted by the tool on the work material are denoted by FH and FV, respectively, and are shown in Fig. 4.4.

The magnitudes are

$$FH = FN\cos\alpha - FT\sin\alpha$$

$$FV = FN\sin\alpha + FT\cos\alpha. \tag{4.26}$$

The ratio of the vertical force to horizontal force is,

$$VOH = FV/FH. \tag{4.27}$$

4.5.4 Dimensionless Forces

All the force equations are expressed in terms of the maximum shear stress, K, and the radius, R, of the fan PED. To make these forces dimensionless, the force equations are divided by K and R. Thus, the dimensionless tangential force on the face of the tool, the horizontal and the vertical force component exerted by the tool on the workpiece are denoted by FTD, FHD, and FVD, respectively. Their magnitudes are expressed as,

$$\begin{aligned} FTD &= FT/K\,R \\ FHD &= FH/K\,R \\ FVD &= FV/K\,R \end{aligned} \tag{4.28}$$

5.0 THEORETICAL RESULTS

5.1 Friction at High Normal Pressures

5.1.1 Theory

In negative rake angle metal cutting the normal pressures on friction surfaces are very high, and the relationship of shear stress and normal stress given by Amonton's friction law are not valid. This is proved experimentally by Wanheim [25,29]. The relation between frictional shear stress and normal stress appear as in Fig. 5.1. From the graphical relationships of shear and normal stress given by Wanheim, Hein [35] developed equations that relate frictional shear stress with normal stress using the newly defined term called the adhesive friction coefficient, m. Here it is discussed briefly.

The dimensionless frictional shear stress is related to the real area of contact AR by the equation

$$\frac{\tau}{k} = m\ AR\ . \tag{5.1}$$

The dimensionless normal stress limit of proportionality is given by the expression

$$\left(\frac{\sigma_n}{2k}\right)_{lim} = \frac{\sqrt{2}(1+\pi/2+2\xi+\sin 2\xi)}{2\sqrt{2} + 4\sin\xi} \tag{5.2}$$

where $\xi = \frac{1}{2}\cos^{-1} m$, $m \neq 0$.

The limit of the real area of contact, AR, is approximated by

$$AR_{lim} \doteq 1-0.52\ (1-m)^{0.325}. \tag{5.3}$$

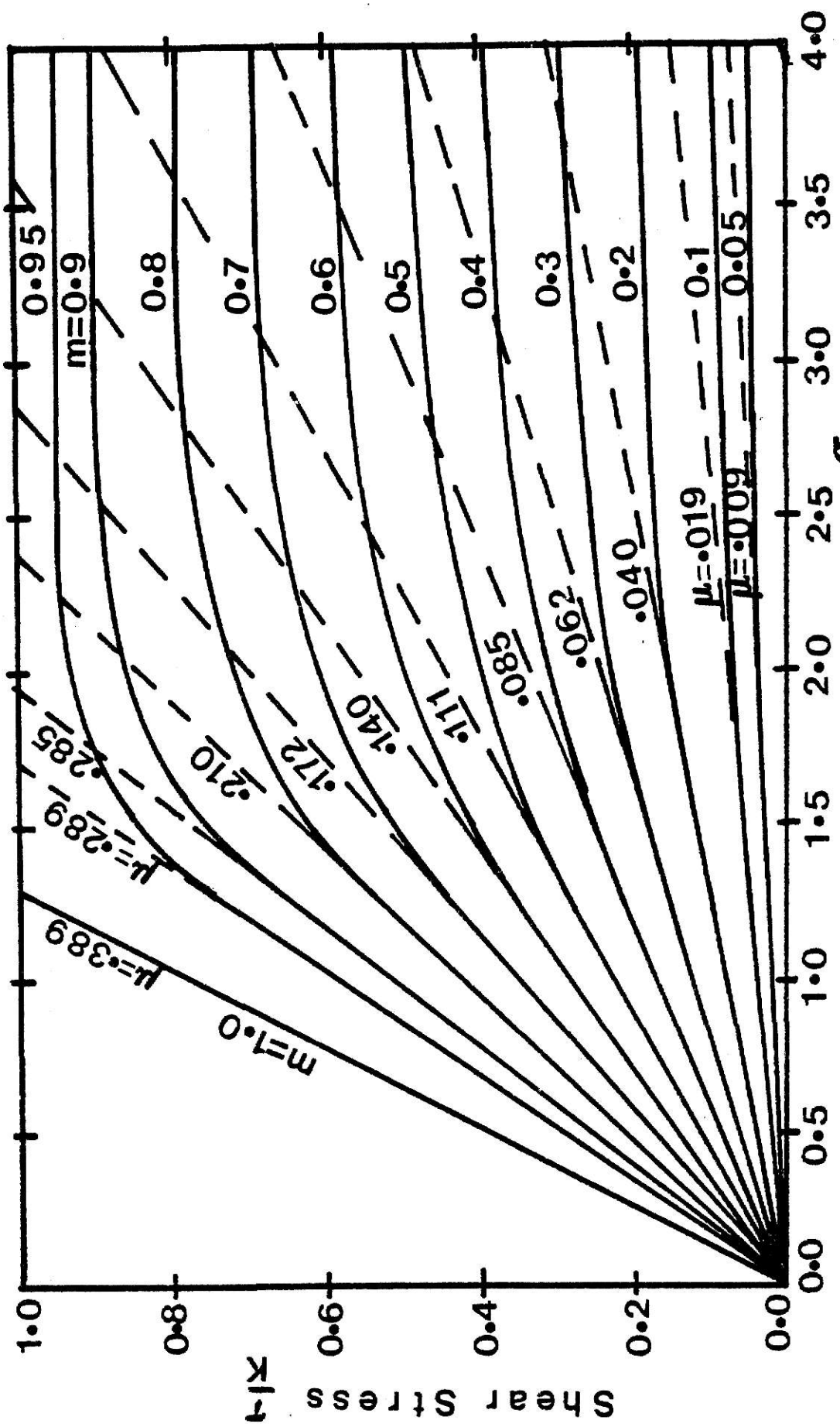

Fig.5.1.Relation between Dimensionless Frictional Shear Stress and Dimensionless Normal Stress [25].

For normal stresses below the proportional limit, that is, $0 \leq \frac{\sigma n}{2k} \leq \left(\frac{\sigma n}{2k}\right)_{lim}$, the dimensionless frictional shear stress is given by

$$\frac{\tau}{k} = \frac{m\ AR_{lim}}{\left(\frac{\sigma n}{2k}\right)_{lim}} \frac{\sigma n}{2k} . \tag{5.4}$$

For normal stresses greater than the proportional limit, that is, $\left(\frac{\sigma n}{2k}\right)_{lim} \leq \frac{\sigma n}{2k}$, the real area of contact is given by

$$AR = 1-\beta_1\ e^{-\beta_2 \left(\frac{\sigma n}{2k}\right)} \tag{5.5}$$

where, $\beta_2 = \frac{AR_{lim}}{(1-AR_{lim})\ \left(\frac{\sigma n}{2k}\right)_{lim}}$, (5.6)

and $\beta_1 = (1-AR_{lim})\ e^{\beta_2 \left(\frac{\sigma n}{2k}\right)_{lim}}$, (5.7)

and the dimensionless shear stress is

$$\frac{\tau}{k} = m\ (1-\beta_1\ e^{-\beta_2 \left(\frac{\sigma n}{2k}\right)}). \tag{5.8}$$

The friction coefficient, μ, is defined as usual as

$$\mu = \frac{\tau}{\sigma_n} . \tag{5.9}$$

The relationship between the dimensionless shear stress and the normal stress in terms of the adhesion friction coefficient m, and in terms of the friction coefficient, μ, is shown in Fig. 5.1

5.1.2 Determination of the Angles η_1, η_2, and η_3

As shown in Fig. 4.3(a), η_1 is the angle between the α-slip lines and the tool face AB, η_2 is the angle between the β-slip lines and the curved side of the dead zone BPC, and η_3 is the angle between the β-slip lines and the side of the dead zone PC.

From the Mohr's circle of Fig. 4.3(b), on interface AB,

$$s_3 = k\cos 2\eta_1; \quad p_3 = -k(1+\sin 2\eta_1)$$

and thus from Eq. (5.1)

$$\frac{s_3}{k} = \cos 2\eta_1 = m\ AR.$$

Hence, for $0 \leq \left|\frac{p_3}{2k}\right| \leq \left(\frac{\sigma n}{2k}\right)_{lim}$, from Eq. (5.4)

$$\cos 2\eta_1 = \frac{m\ AR_{lim}}{\left(\frac{\sigma n}{2k}\right)_{lim}} \frac{p_3}{2k}.$$

That is,

$$\cos 2\eta_1 = \frac{m\ AR_{lim}}{\left(\frac{\sigma n}{2k}\right)_{lim}} \left(\frac{1+\sin 2\eta_1}{2}\right) \tag{5.10}$$

and for $\left|\frac{p_3}{2k}\right| \geq \left(\frac{\sigma n}{2k}\right)_{lim}$, from Eq. (5.8)

$$\cos 2\eta_1 = m\left(1-\beta_1 e^{-\beta_2\left(\frac{1+\sin 2\eta_1}{2}\right)}\right). \tag{5.11}$$

On interface BP, the normal pressure varies linearly with angle θ. To simplify the calculation, the average normal stress is used in determining the angle η_2. It is assumed that the error

introduced in determining η_2 does not significantly affect the general result.

The average pressure p_{va}, on BP, from Appendix I and Fig. 4.3(b) is

$$p_{va} = \frac{\int_0^{\theta} p_v' \, OB d\psi}{\int_0^{\theta} OB d\psi} = -k\,(1+\theta+\sin 2\eta_2).$$

Thus, for $0 \leq \left|\frac{pv_a}{2k}\right| \leq \left(\frac{\sigma n}{2k}\right)_{lim}$

$$\cos 2\eta_2 = \frac{m\ AR_{lim}}{\left(\frac{\sigma n}{2k}\right)_{lim}} \frac{(1+\theta+\sin 2\eta_2)}{2} \tag{5.12}$$

for $\left|\frac{pv_a}{2k}\right| \geq \left(\frac{\sigma n}{2k}\right)_{lim}$

$$\cos 2\eta_2 = m\,(1-\beta_1\, e^{-\beta_2 \left(\frac{1+\theta+\sin 2\eta_2}{2}\right)}) \tag{5.13}$$

On interface PC, for $0 \leq \left|\frac{P_{13}}{2k}\right| \leq \left(\frac{\sigma n}{2k}\right)_{lim}$

$$\cos 2\eta_3 = \frac{m\ AR_{lim}}{\left(\frac{\sigma n}{2k}\right)_{lim}} \left(\frac{1+2\theta+2\phi+\sin 2\eta_3}{2}\right) \tag{5.14}$$

and for $\left|\frac{P_{13}}{2k}\right| \geq \left(\frac{\sigma n}{2k}\right)_{lim}$

$$\cos 2\eta_3 = m\,(1-\beta_1\, e^{-\beta_2 \left(\frac{1+2\theta+2\phi+\sin 2\eta_3}{2}\right)}) \tag{5.15}$$

Equations (5.10) to (5.15) are non-linear and the direct solution of η_1, η_2, and η_3 is extremely difficult. Thus, iteration is used in solving for them.

5.2 Method of Solving

The angle the tool inclines with the workpiece, that is, the rake angle, the amount of material to be removed, that is, the depth of cut D and the width of cut W, are known. If the nature of friction, in this case, the value of the adhesion coefficient, m, is known for the cutting condition under consideration, the cutting forces FH and FV can be determined from Eqs. (4.26). However, the determination of FH and FV is complex.

After selecting the appropriate value of m, the value of η_1 can be determined using some kind of iteration on Eqs. (5.10) or (5.11). The same procedure can be applied for determining η_2 from Eqs. (5.12) or (5.13). But, since the determination of η_2 involves the value of θ which is unknown, the iterations are not direct. The angle θ as can be seen in Eq. (4.10) depends on η_2, η_3, and on Δ which are unknown. Thus, to determine η_2, the value of θ has to be guessed first.

To determine η_3 from Eqs. (5.14) or (5.15) the same problem as in determining η_2 arises since the value of ϕ is unknown. So, in this case too, the value of ϕ is guessed in addition to the value of θ guessed above; and the calculation is carried out. Then the value θ given by the expression (4.10) is calculated and checked against the initial guessed value. If the two values are not within the

desired error limits, the procedure is repeated until the desired result is obtained. During these computations the value of ϕ is kept constant.

Once the unknown angles are determined, the dimensionless forces can be computed taking care of all the requirements imposed by the slip-line solution method and its consequences. Since for different values of ϕ an infinite number of results can be obtained, the one that requires minimum cutting energy is chosen as the best solution. This assumption is made by the logical intuition that metal cutting operations can be performed by minimum horizontal cutting force.

The computer program developed for the computations described above is given in Appendix III.

5.3 Numerical Results

The numerical results obtained from the computer program are given in Appendix IV. However, for better understanding some of the results are shown graphically.

The variation of the dimensionless cutting forces, FHD and FVD, with increasing rake angle, α, for certain values of adhesion coefficient, m, are shown in Fig. 5.2 and Fig. 5.3, respectively. The dimensionless tangential force, FTD, plotted against the rake angle for certain values of m is shown in Fig. 5.4. The ratio of the vertical cutting force component to the horizontal cutting force component as m changes for constant rake angle is shown in Fig. 5.6. The variation

of FHD and FVD with m for a given rake angle can be seen in Fig. 5.7 and 5.8, respectively. The critical angle which is defined as the maximum rake angle beyond which the tool does not cut is plotted against m and shown in Fig. 5.5. Figure 5.9 shows the ratio of chip thickness to depth of cut plotted against m for different values of α. The variation, with m, of shear stresses and normal stresses on the tool face and dead zone are shown in Fig. 5.10, and Fig. 5.11, respectively.

Using the numerical results calculated, some slip-line fields are drawn to scale for different rake angles and adhesion coefficients, and are shown in Fig. 5.12 and Fig. 5.13.

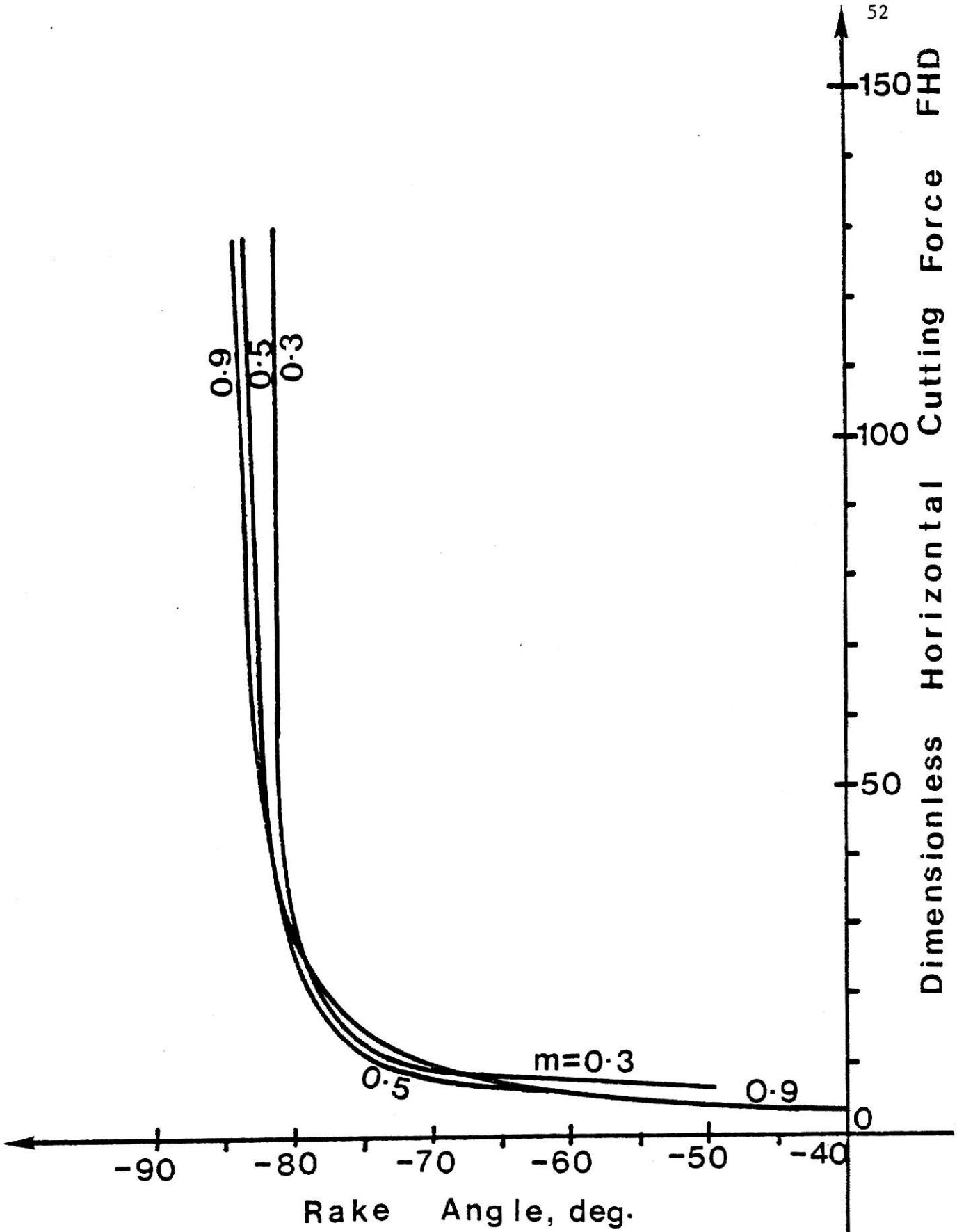

Fig.5.2. Relation between Dimensionless Horizontal Cutting Force,FHD,and Rake Angle with respect to Adhesion Coefficient,m.

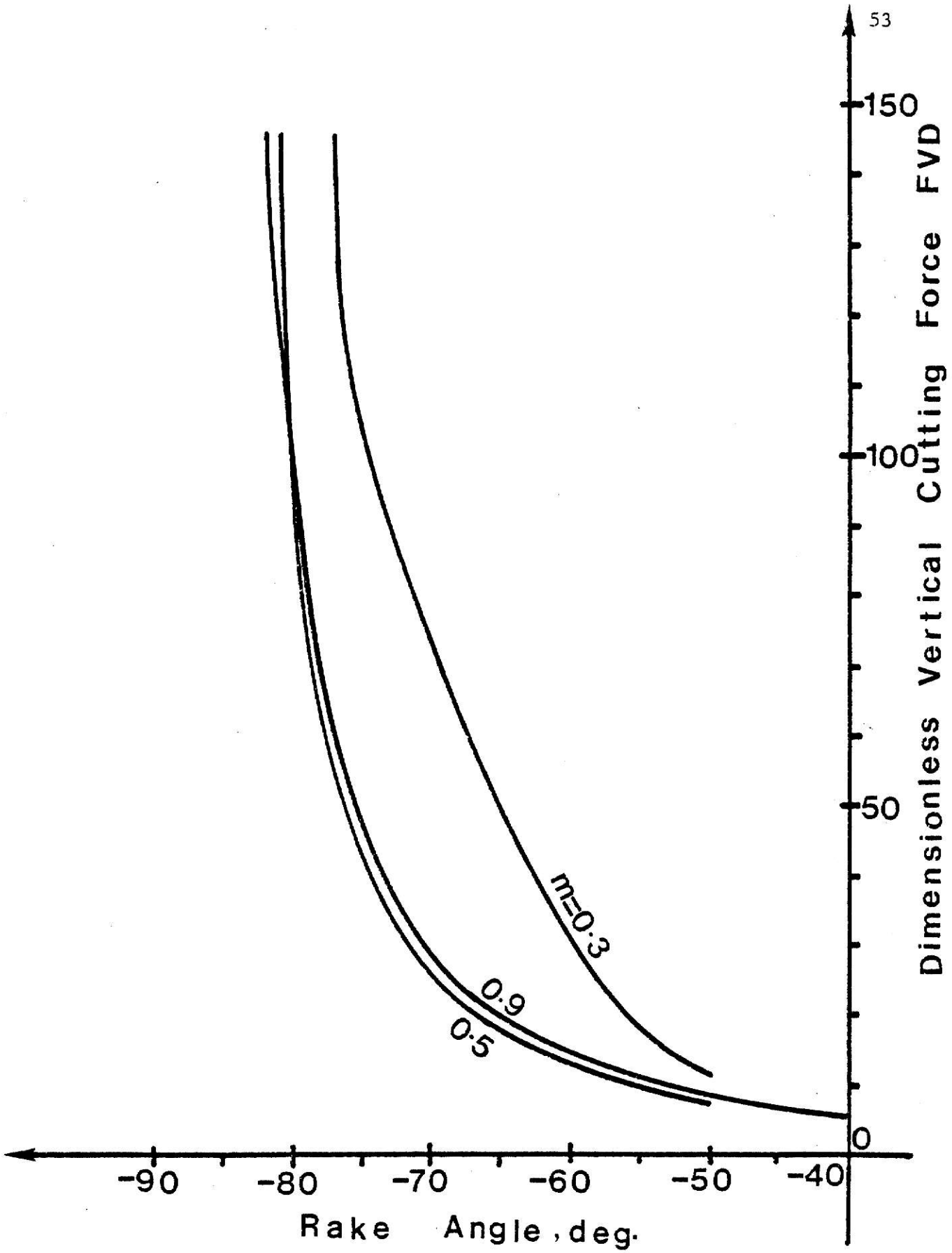

Fig.5.3. Relation between Dimensionless Vertical Cutting Force FVD, and Rake Angle with respect to Adhesion Coefficient, m.

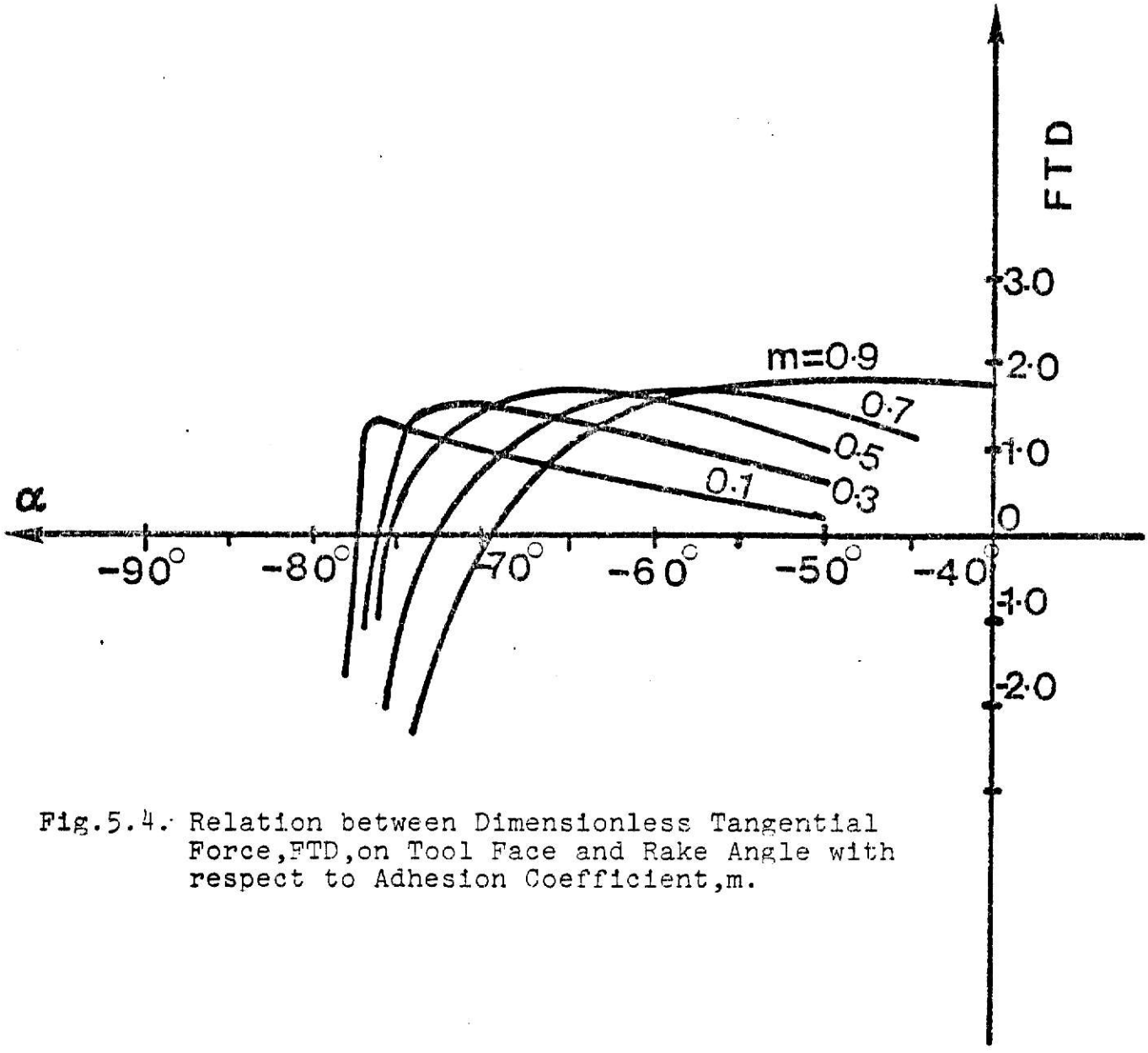

Fig.5.4. Relation between Dimensionless Tangential Force,FTD,on Tool Face and Rake Angle with respect to Adhesion Coefficient,m.

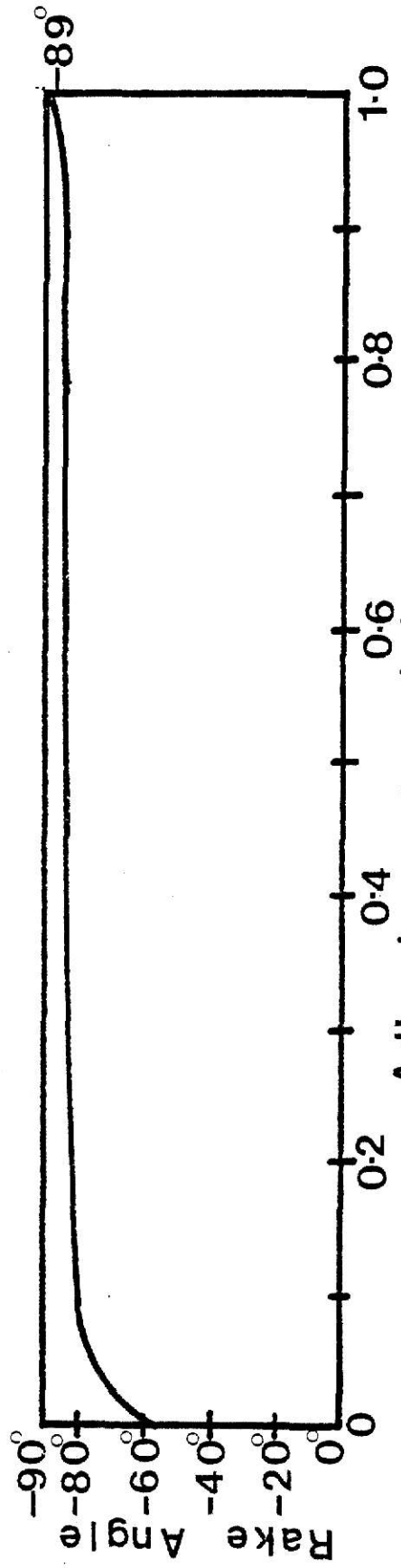

Fig.5.5. The Maximum Rake Angle at which the Tool can cut in relation to Adhesion Coefficient,m.

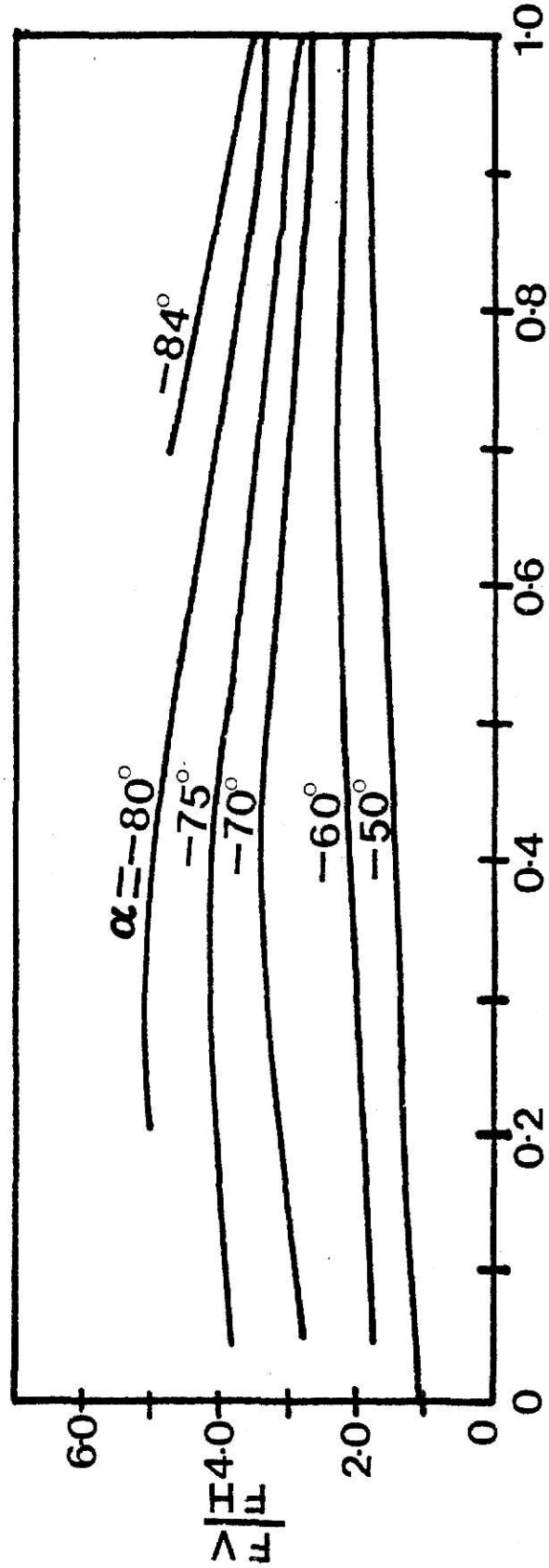

Fig.5.6. Relation between the Ratio of the Vertical Cutting Force,FV,to Horizontal Cutting Force,FH,and Adhesion Coefficient,m,with respect to Rake Angle.

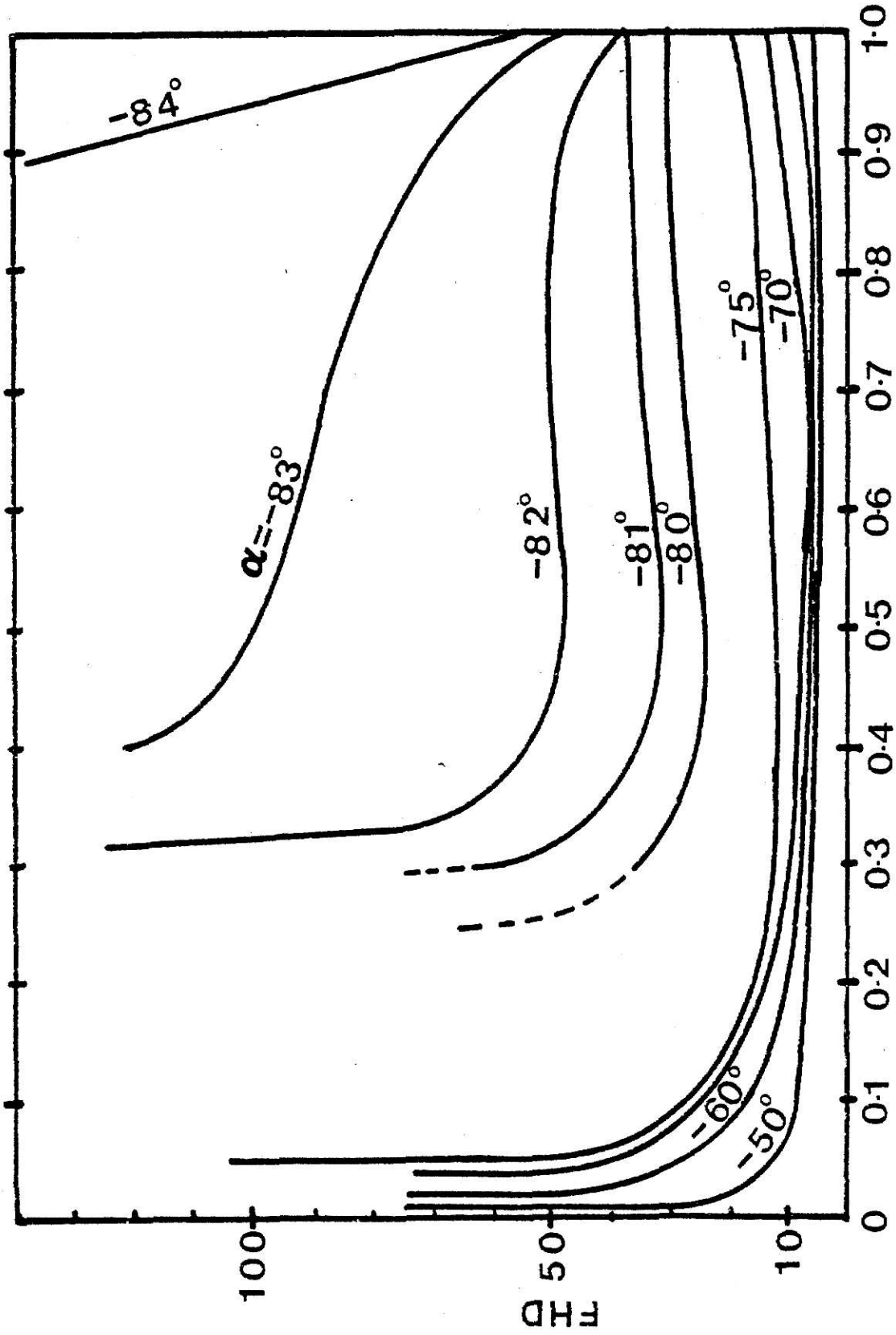

Fig.5.7 Relation between Dimensionless Horizontal Cutting Force, FHD, and Adhesion Coefficient, m, with respect to Rake Angle.

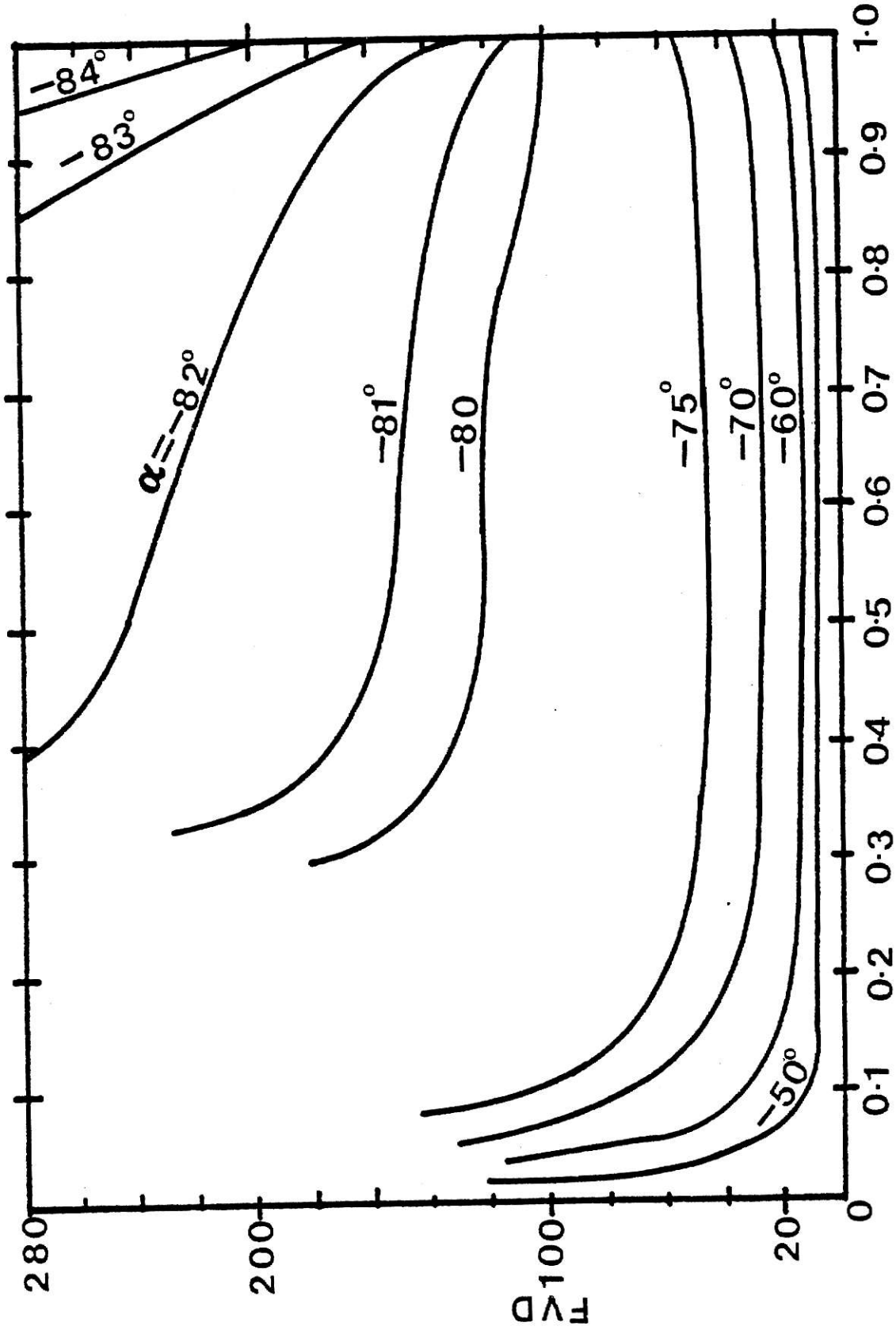

Fig.5.8. Relation between Dimensionless Vertical Cutting Force, FVD, and Adhesion Coefficient, m, with respect to Rake Angle.

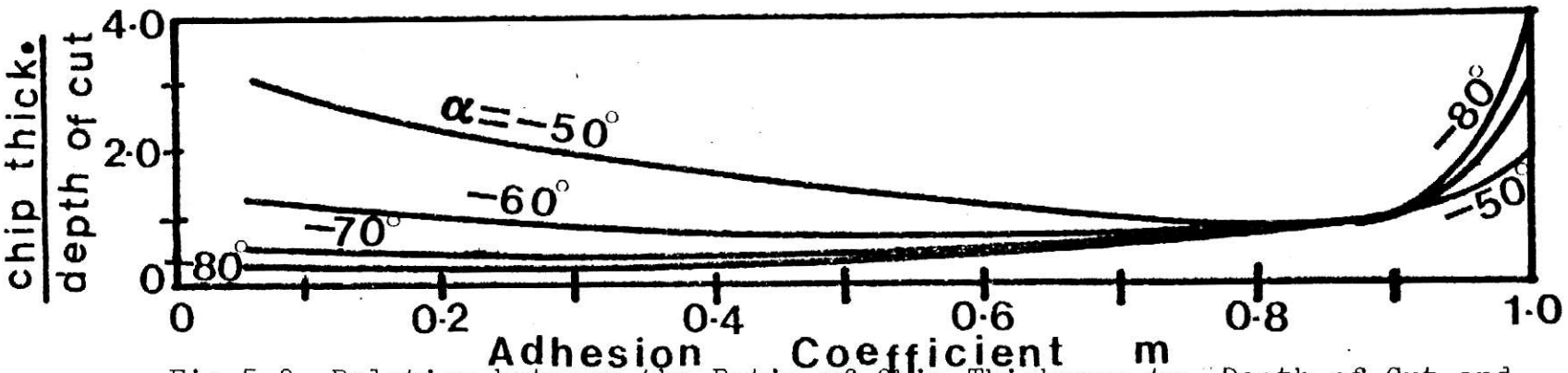

Fig.5.9. Relation between the Ratio of Chip Thickness to Depth of Cut and Adhesion Coefficient,m.

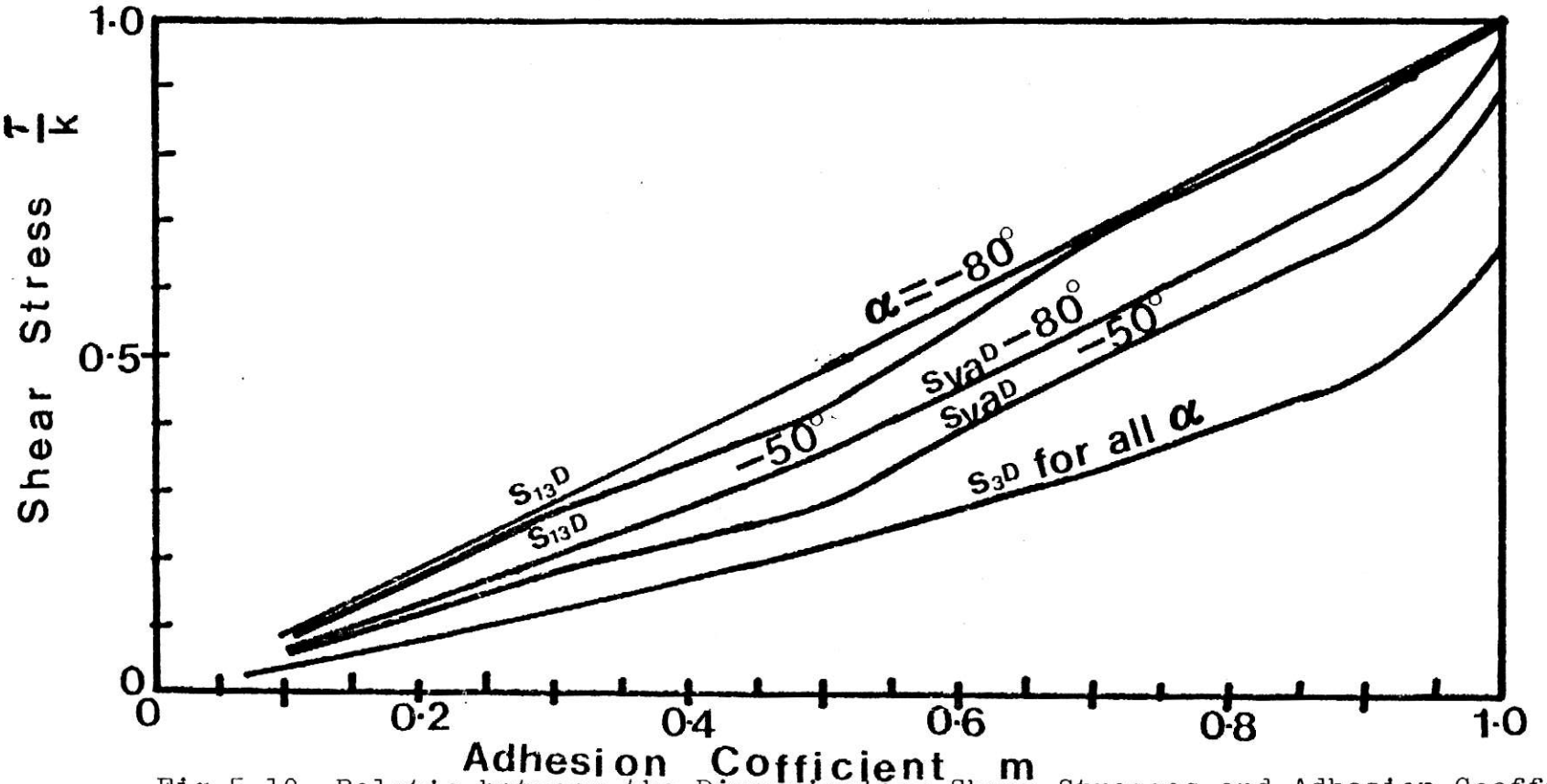

Fig.5.10. Relatio between the Dimensionless Shear Stresses and Adhesion Coefficient,m

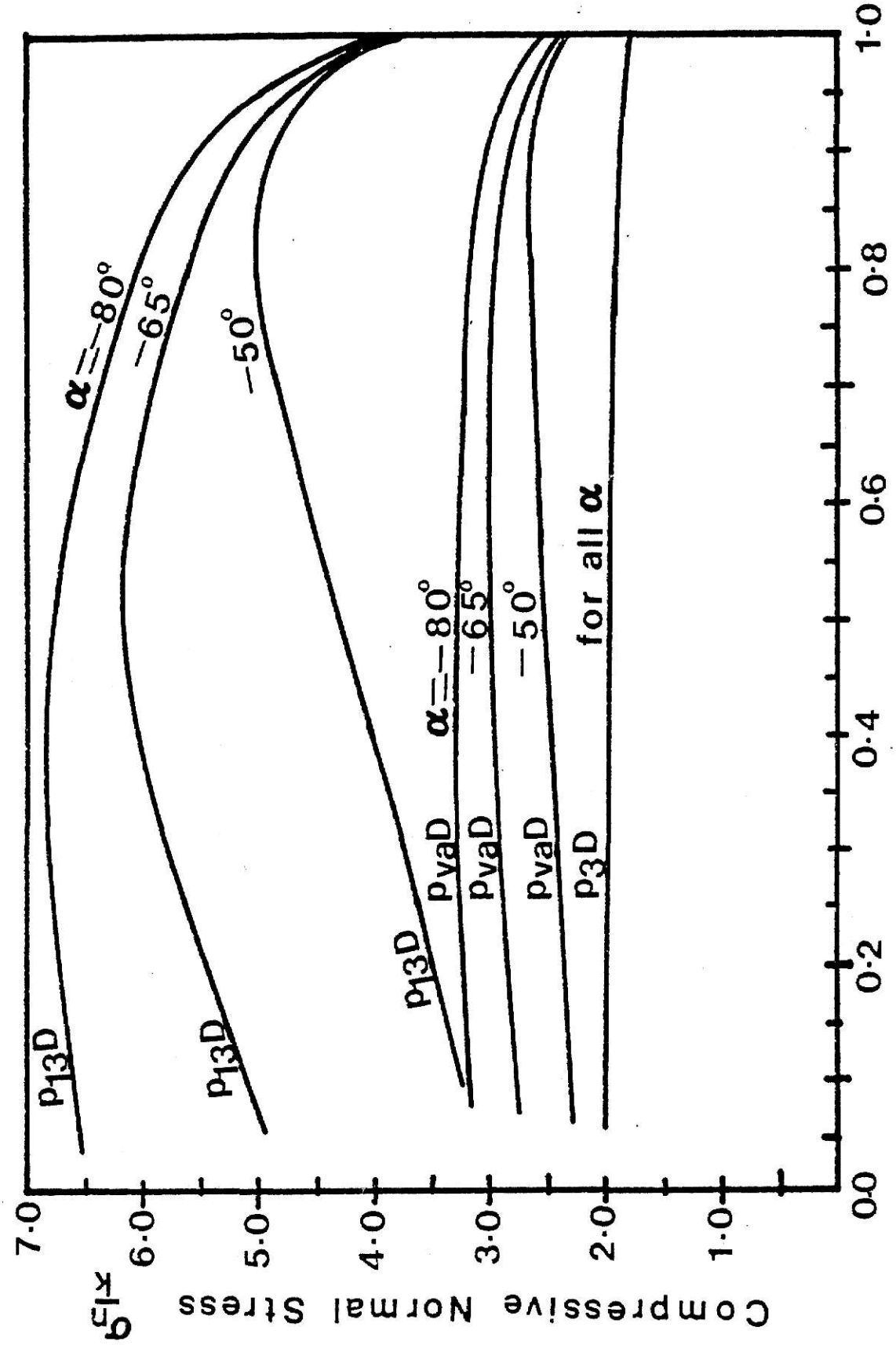

Fig.5.11. Relation between the Dimensionless Normal Stresses and Adhesion Coefficient,m,with respect to Rake Angle.

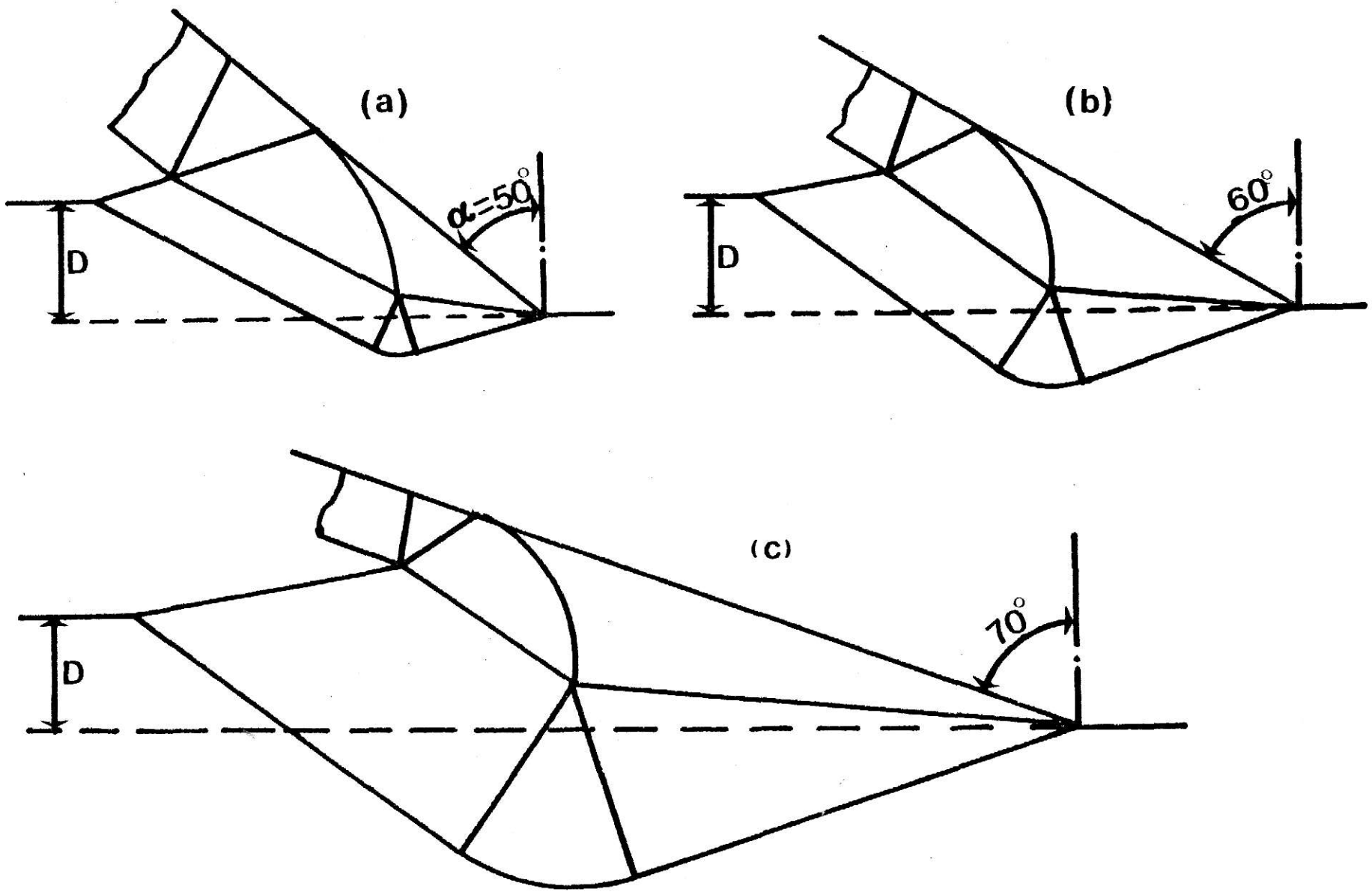

Fig.5.12. Slip-Line Fields for Adhesion Coefficient,m=0.7,same Depth of Cut,D, and for Rake angles (a) -50deg. (b)-60deg. (c)-70deg.

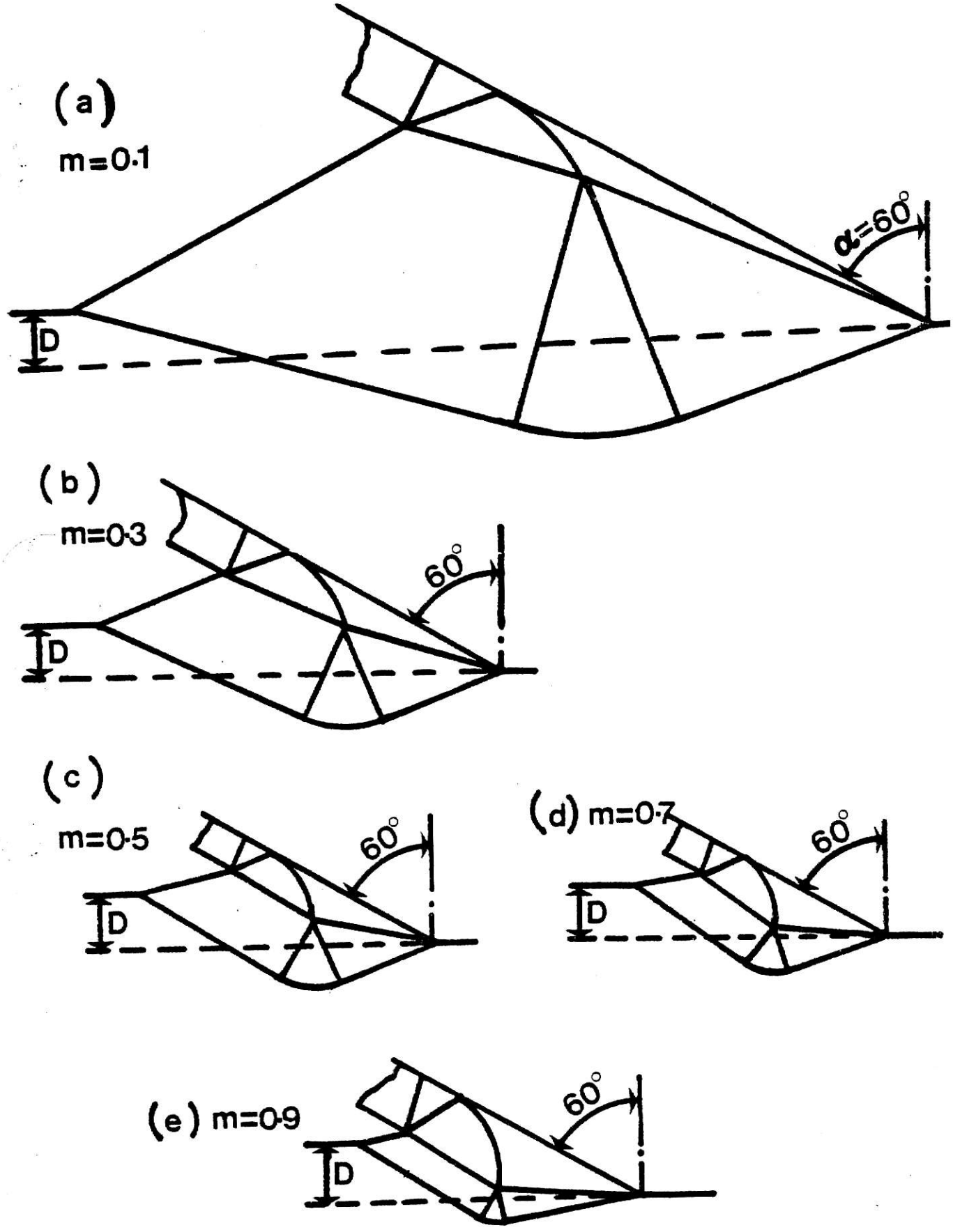

Fig.5.3.Slip-Line Fields for Rake Angle -60deg.,same depth of Cut,D,and Adhesion Coefficient,m,for (a) 0.1, (b) 0.3,(c) 0.5,(d) 0.7,(e) 0.9.

6.0 COMPARISON WITH EXPERIMENTAL RESULTS

6.1 Introduction

Very few experiments have been done on negative rake angle metal cutting. The works of Komanduri[14], Abdelmoneim [28], and Y. Kita [36] are discussed here. In all the experiments performed the cutting forces are measured. Thus, it is required to convert the theoretical dimensionless forces FVD, FHD and FTD to actual forces. If the adhesion coefficient, m, is known for a certain rake angle cutting, the theoretical dimensional forces can be computed by multiplying the dimensionless forces by the yield shear stress, K, the depth of cut and width of cut. It is assumed that in metal cutting the adhesion coefficient, m, is between 0.5 and 1.0. However, the values of 0.1, 0.5, and 0.9 are selected to compare with experimental results. The value of K which is the mechanical property of the work material is taken from reference books.

6.2 Comparison with Komanduri's Experiments [14]

In these experiments it is observed that chips formed for all rake angles down to -75 deg. and no chip is obtained at -85 deg. rake. The value of the cutting forces for the depth of cut 0.0004 in. and width of cut 0.15 in. for different values of negative rake angles are compared graphically in Figs. 6.1, 6.2 and 6.3. It is assumed that the yield stress in tension of the work material is about $Y' = 50{,}000$ psi, and thus the yield stress is $K = Y'/\sqrt{3} = 28{,}900$ psi.

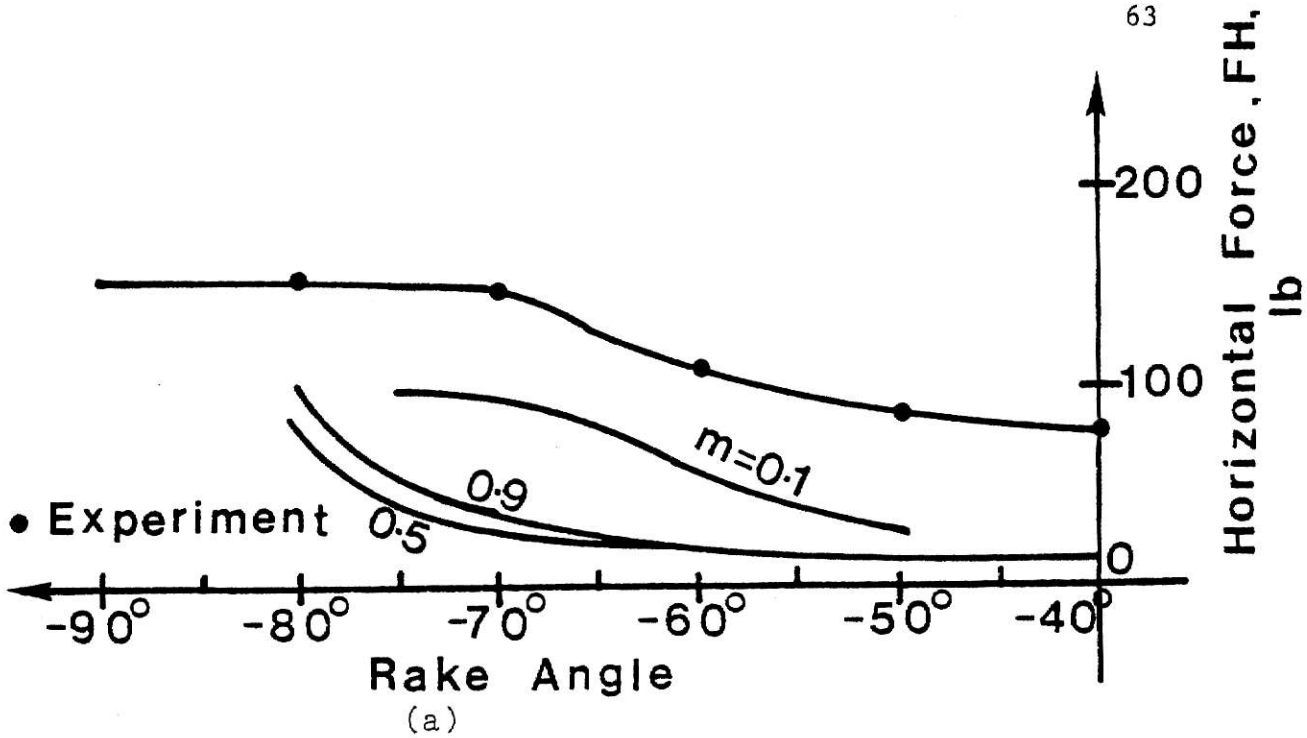

(a)

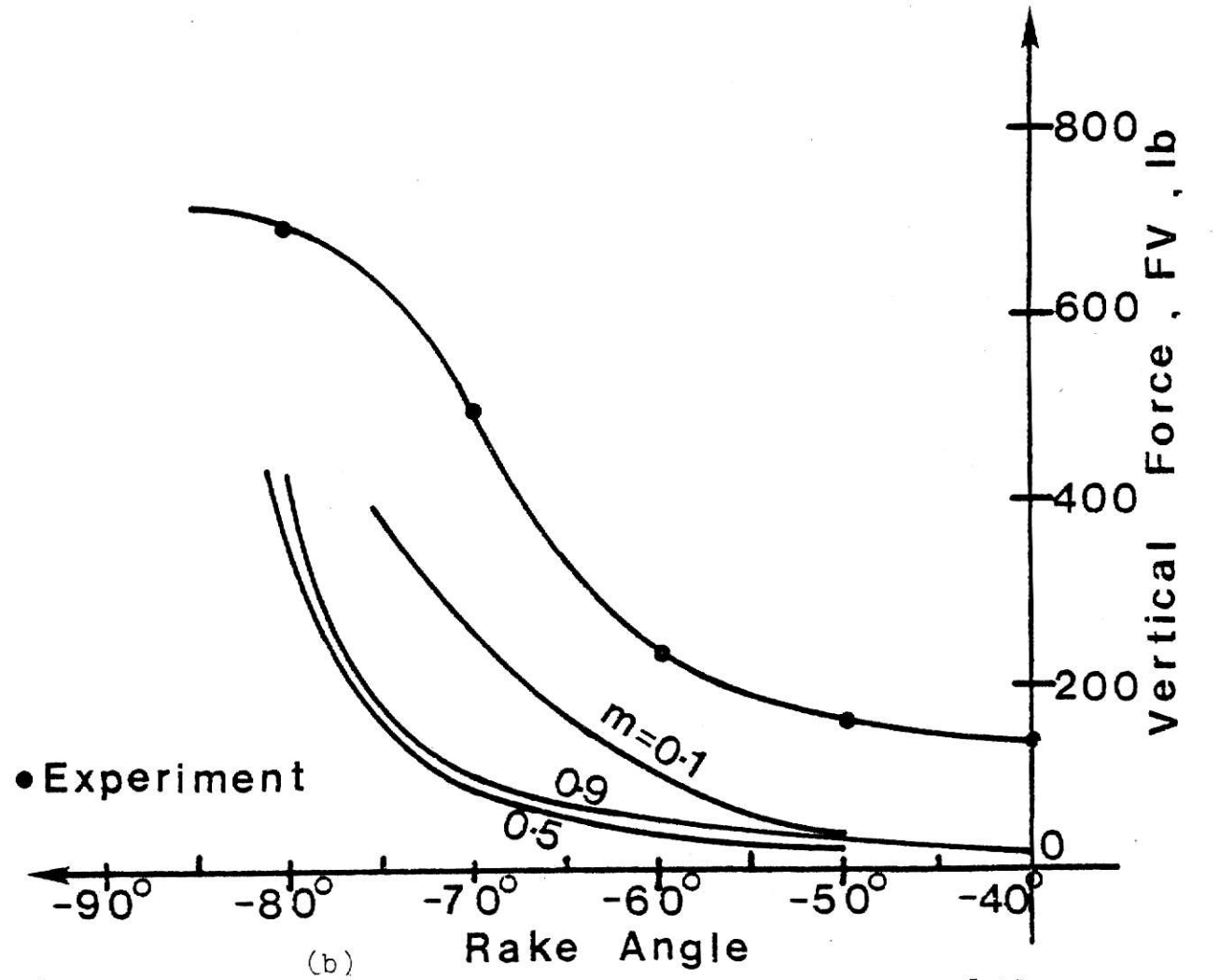

(b)

Fig.6.1.Theortical Cutting Forces compared to Komanduri[14] Experimental Results.

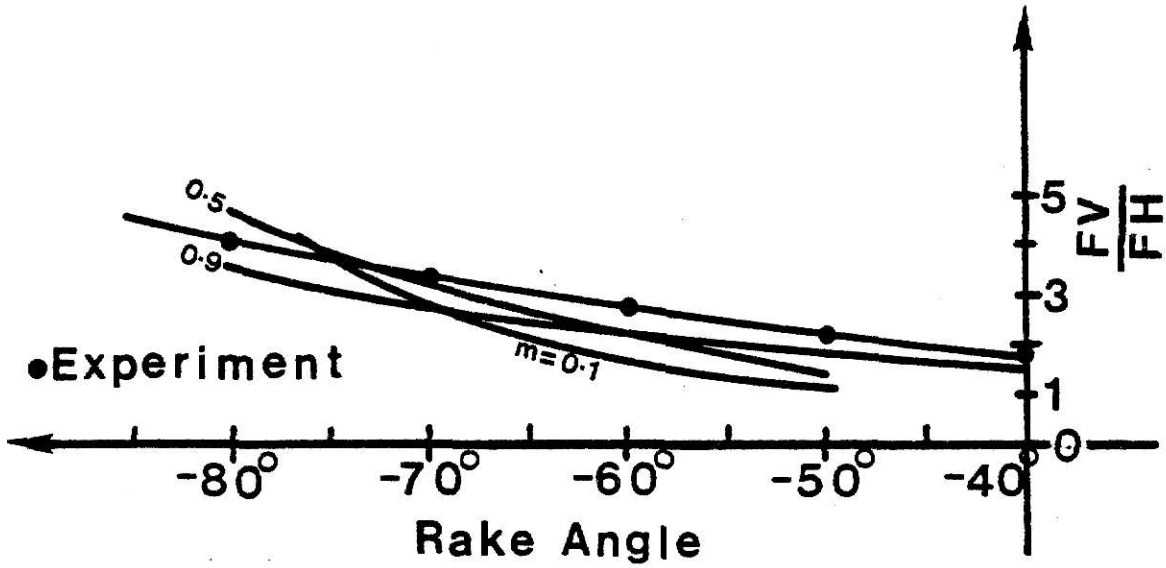

Fig.6.2.Theoretical Ratio of Vertical Cutting Force to Horizontal Cutting Force compared to Komanduri [14] Experimental Results.

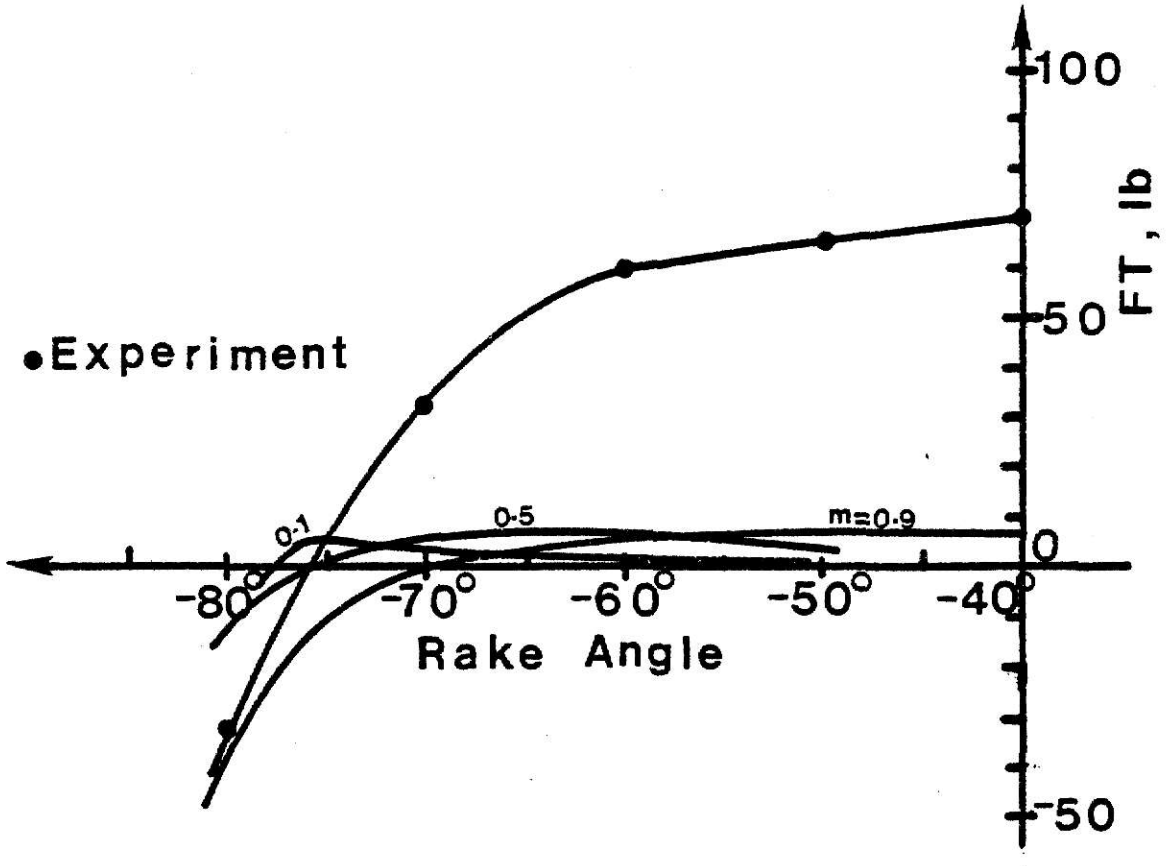

Fig.6.3.Theoretical Tangential Force on the Tool Face compared to Komanduri [14] Experimental Results.

In Fig. 6.1(a) and Fig. 6.1(b) the theoretical cutting forces are compared with the experimental values. It is seen that the experimental values are about 10 times greater than the theoretical values. The experimental values obtained for zero rake angle are compared with theories [21] which are good for positive and small negative rake angles and it is found the experimental horizontal and vertical forces are 6 and 12, respectively, times greater than the theoretical values of these forces. Thus, it is assumed that due to the very small depth of cut of 0.0004 in., the experimental values obtained have to account for some factors which are unknown to this author. Therefore, in this comparison the magnitude of forces are not given much attention. From Fig. 6.1(a) and 6.1(b) it can be observed that the shape of the theoretical curves in particular for m = 0.5 and m = 0.9 have the same shape as the experimentally obtained curve. The ratio of the theoretical vertical force to horizontal force shown in Fig. 6.2 is in general agreement both in shape and magnitude to the experimental results.

In Fig. 6.3 the tangential force on the tool face for different rake angles is shown. It is seen that the shape of the theoretical curves is similar to the experimental one. The surprising result is that the zero force obtained experimentally, which is for rake angle -76 deg., is between the theoretically obtained values of -68 to -77 deg. for m = 0.9 and 0.1, respectively. For m = 0.5 the force is zero for rake angle -75 deg.

6.3 Comparison with Abdelmoneim's Experiments [28]

This experiment has experimental results for machining brass with the depth of cut 0.004 in. The yield stress in tension for brass is 37,000 psi and thus, K = 21,360 psi. The experimental results are compared with the theoretical results in Fig. 6.4(a) and Fig. 6.4(b). The experimental values are higher than the theoretical values as expected. However, unlike the comparison with Komanduri's result, the theoretical values are in reasonable agreement with the experimental results; considering, the difficulties in measuring the cutting forces and the slip-line theory assumptions used in calculating the theoretical forces. In Fig. 6.5 the tangential forces are compared; and it can be seen that the shapes of the curves and the magnitudes of the forces are in reasonable agreement. Also in Fig. 6.4 it can be observed that there is a certain value of m which gives very close result to the experimentally obtained forces.

6.4 Comparison with Y. Kita [36]

This experiment is done using lead as a work material. It is observed in this experiment that at -60 deg. rake the horizontal cutting force is 100 kg, and the vertical cutting force is 200 kg, for cutting at a depth of 3 mm and width 2.20 mm. Also at -60 deg. rake it is observed that the ratio of the depth of cut to the height of chip formation, is $D/d_o = 0.5$. The value of $K = 2\ kg/mm^2$ is given by the author.

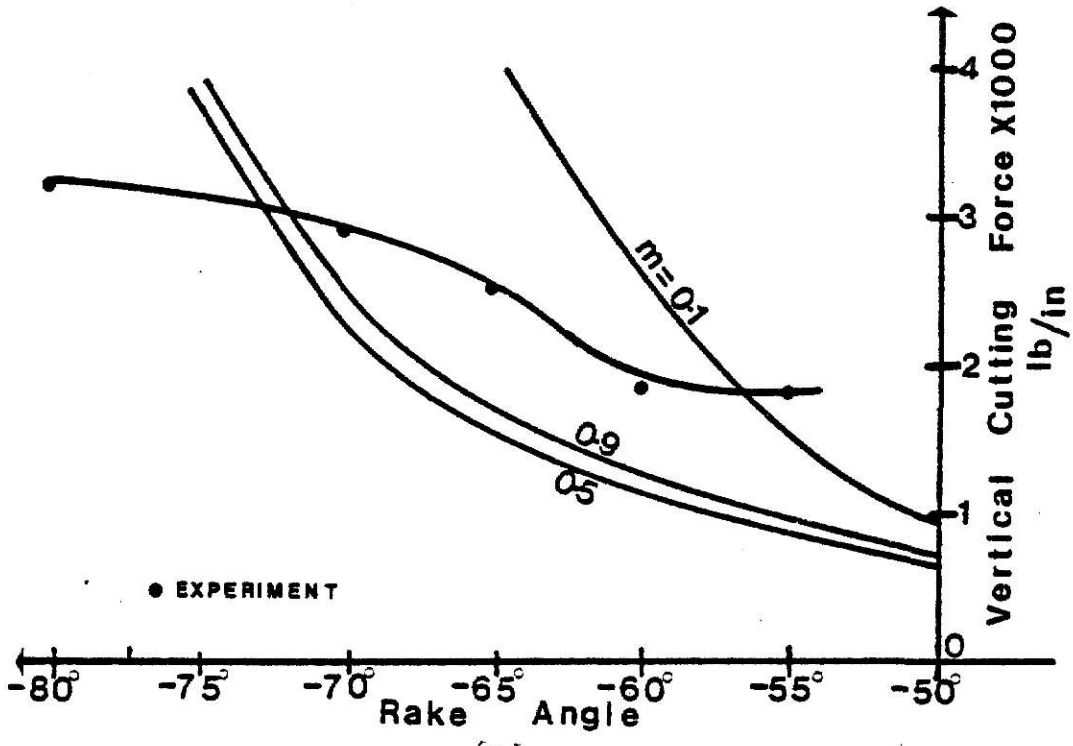

(a)

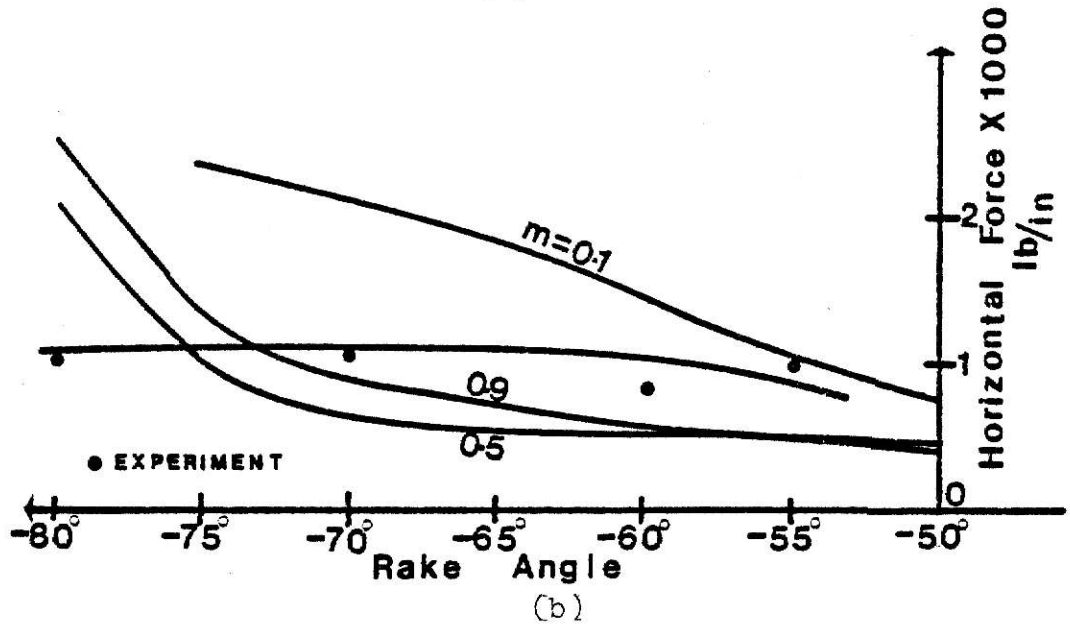

(b)

Fig.6.4.Theoretical Cutting Forces Compared to Abdelmoneim[28] Experimental Results.

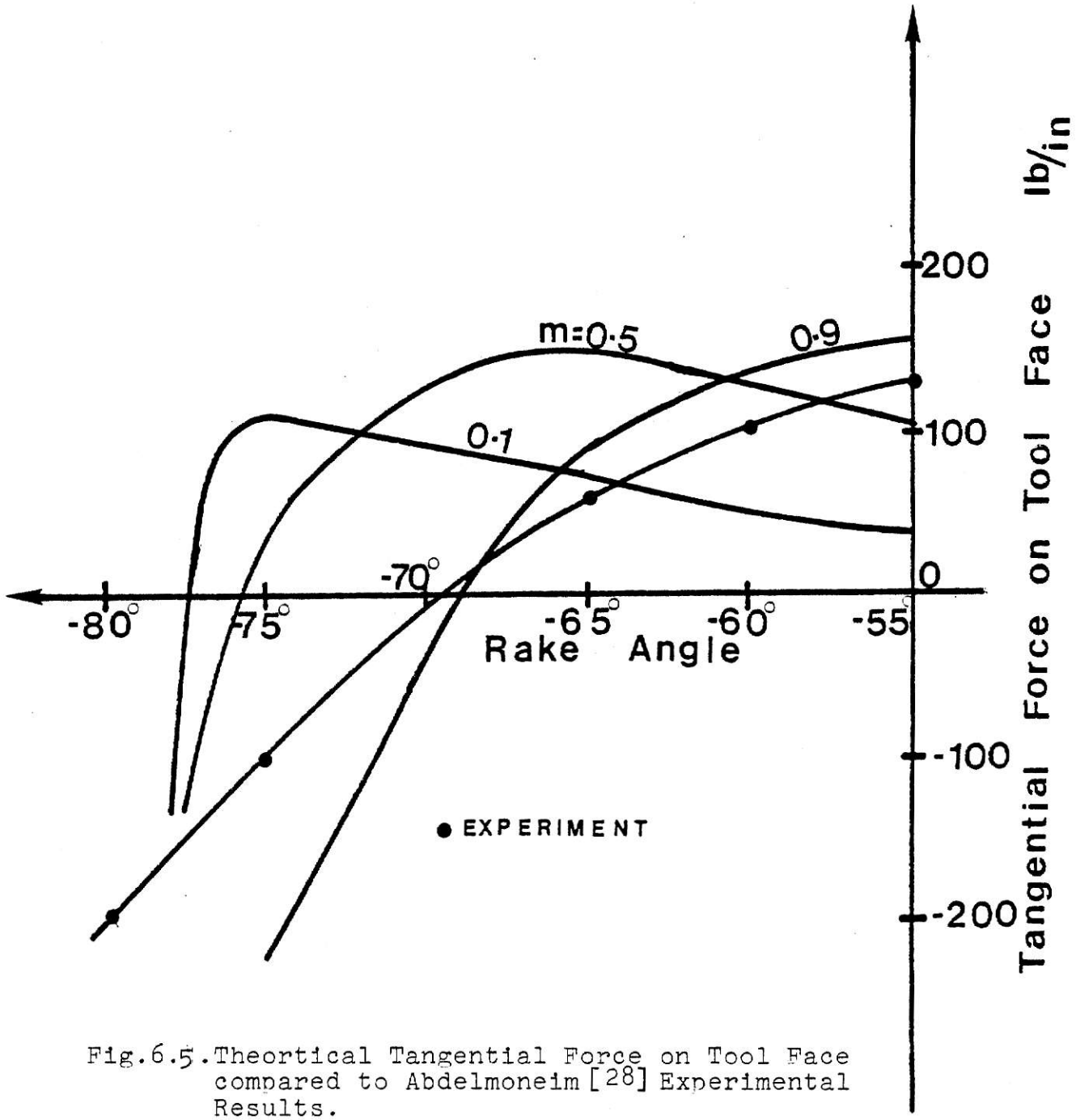

Fig.6.5. Theortical Tangential Force on Tool Face compared to Abdelmoneim [28] Experimental Results.

The theoretical values for m = 0.1, 0.5 and 0.9 are given in Table 6.1. From this table it can be seen that for m = 0.5 and 0.9 the theoretical cutting forces, and the theoretical ratio D/d_o are very close to the experimental values. In this experiment special care was taken to achieve plain-strain and to reduce the heat effect on the material properties.

Table 6.1. Theoretical Results for α = -60 deg.

Adhesion Coefficient m	Horizontal Force FH (kg)	Vertical Force FV (kg)	Ratio FV/FH	$\frac{D}{d_o}$
0.1	228	409	1.80	.18
0.5	80	177	2.23	.58
0.9	88	192	2.21	.57

7.0 CONCLUSIONS

The slip-line solution which was developed to solve the problem of metal cutting with large negative rake angles is considered to be a good approximation to the real solution. The solution presented is an upper-bound type. This slip-line solution considers the experimental facts that a bulge or prow forms ahead of the tool before the chip is formed, and that the workpiece material flows in opposite directions on the tool face. It accounts for the experimental facts that: there is a critical rake angle beyond which metal cutting ceases; that the vertical component of the cutting force is larger than the horizontal component; and that there is a certain rake angle at which the tangential force on the tool face is zero. The numerical results of the cutting forces agree reasonably well with experimental results of Abdelmoneim [28] and Y. Kita [36]. Thus, the slip-line field suggested is believed to be close to the real one, even though in reality the slip-line field may not consist of simple stress state regions.

Analyzing the numerical results of this slip-line solution other interesting facts can be concluded. In Fig. 5.5 it can be seen that the critical rake angle, which is defined as the maximum rake angle beyond which the tool does not cut, has different values for different values of adhesion coefficient, m. The critical rake angle varies from about -55 deg. for m near 0 to about -89 deg. for m near 1. The adhesion coefficient is related to friction conditions. Thus, one can conclude that the friction conditions during cutting

determine whether a certain negative rake angle can cut or not. With the presence of high friction coefficients the critical angle is more negative than with low friction coefficients.

The variation of the vertical and horizontal components of the cutting force with adhesion coefficient, m, for a fixed rake angle are shown in Fig. 5.7 and Fig. 5.8, respectively. From these figures it can be speculated that there is a certain value of adhesion coefficient, for a given negative rake angle, for which the cutting force is minimum. As expected it is not the lowest friction coefficient or adhesion coefficient, m, that gives this value. It is a value of m greater than 0.3 that gives this minimum value. Besides, from these figures one can conclude that m values greater than 0.2 help in cutting more than values less than 0.1. The above conclusion is presented pictorially in Fig. 5.13. In this figure the rake angle is kept constant at -60 deg. and the slip-line fields for various adhesion coefficients, m, which have the same depth of cut are drawn to scale from the numerical values obtained. It can be seen in the figures that for large m the size of the slip-line field is smaller than for lower values of m. This means to cut the same depth an m value less than 0.1 needs a larger plastically deformed region than higher values of m.

The vertical and horizontal components of the cutting force for a given value of m increase as the rake angle becomes more negative. This is shown in Fig. 5.3 and Fig. 5.2, respectively. The value of these forces increases very fast as the rake angle

approaches the value of the critical angle. The behavior of the plastically deformed region as the rake angle becomes more negative is shown in Fig. 5.12. From this figure it can be concluded that to cut the same depth at a given value of m, higher negative rake angles need larger size of deformed region than lower negative rake angles. The value of the vertical force is greater than the horizontal force, and is shown in Fig. 5.6.

The value of the tangential force on the tool face becomes zero for a certain value of m at a certain value of rake angle. This fact is shown in Fig. 5.4. The values of these rake angles range from -77 deg. for m=0.1 to about -68 deg. for m=0.9. This range includes the experimental result obtained by Komanduri shown in Fig. 6.3 and by Abdelmoneim shown in Fig. 6.5. The reason that the tangential force becomes zero at a certain rake angle is that, the division of the metal flow in front of the tool creates shear stresses that cause friction forces on the tool face that have opposite sense; and at some rake angle these forces become equal and cancel out. Since the theoretical value of the rake angle at which the tangential force on the tool face is zero is supported by experiments, the shape of the dead zone used in the development of the slip-line field, is believed to be close to the real one.

The results obtained in using the slip-line solution in solving metal cutting problems with high negative rake are encouraging. However, it would be valuable to conduct experiments to test the accuracy of the proposed slip-line field.

To further improve the theory the curved surface BP should be changed so that the friction conditions are satisfied at each point along the curve. This will be more complex than the present theory in which average conditions are used. It is also believed that the region outside the plastic region may be overstressed and that this can be overcome by extending the plastic region (slip-line field) around and under the tip of the tool for a short distance. This would provide important information about the stresses on the flank of the tool which would help explain and predict flank wear of the tool.

REFERENCES

1. Ernst, H., and Merchant, M. E., "Chip Formation, Friction, and High Quality Machined Surfaces," from "Surface Treatment of Metals," Trans. Am. Soc. Metals, 29: 299-328 (1941).

2. Merchant, M. E., "Basic Mechanics of the Metal Cutting Process," Jour. Appl. Mech., 15, 1944 A-168.

3. Merchant, M. E., "Mechanics of the Metal Cutting Process-I: Orthogonal Cutting and the Type 2 Chip," Jour. Appl. Phys., 16, 1945, 267.

4. Merchant, M. E., "Mechanics of the Metal Cutting Process-II: Plasticity Conditions in Orthogonal Cutting," Jour. Appl. Phys., 16, 1945, 318.

5. Lee, E. H., and Shaffer, "The Theory of Plasticity Applied to a Problem of Machining," Trans. ASME, J. Appl. Mech. 18: 405-413 (1951).

6. Hill, R., "The Mechanics of Machining: A New Approach," J. Mech. Phys. Solids, 3: 47-53 (1954).

7. Albrecht, P., "New Developments in the Theory of the Metal-Cutting Process, Part I: The Ploughing Process in Metal Cutting," Jour. Eng. Ind., Nov., 1960, 348.

8. Shaw, M. C., "A New Theory of Grinding," Mech. and Chem. Eng. Trans. of Inst. of Engrs., Australia, V. MC8, May 1972, 73.

9. Appl, F. C. and Rowley, D. S., "Analysis of the Cutting Action of a Single Diamond," Jour. Soc. Pet. Eng., September, 1968.

10. Rowley, D. S. and Appl, F. C., "Analysis of Surface Set Diamond Bit Performance," Jour. Soc. Pet. Eng., September, 1969.

11. Rubenstein, C., Groszman, F. K., and Koenigsberger, F., "Force Measurements During Cutting Tests and Single Point Tools Simulating the Action of a Single Abrasive Grit," Science and Technology of Industrial Diamonds, 1967, Proc. Int. Indust. Dia. Conf., Oxford, 1966.

12. Connolly, R. and Rubenstein, C., "The Mechanics of Continuous Chip Formation in Orthogonal Cutting," Int. Jour. Mach. Tool Des. Res., V. 8, 1968, 159.

References - continued

13. Rowe, G. W. and Wetton, A. G., "Theoretical Considerations in the Grinding of Metals," Jour. Inst. Metals, V. 97, 1969, 193.

14. Komanduri, R., "Some Aspects of Machining with Negative Rake Tools Simulating Grinding," Int. Jour. Mach. Tool Des. Res., Vol. 11, 1971.

15. Lal, G. K. and Shaw, M. C., "Experiments with Spherical Tools," Wear, V. 29, 1974, 153.

16. Abdelmoneim, M. ES. and Scrutton, R. F., "Tool Edge Roundness and Stable Build-up Formation in Finish Machining," Jour. Eng. Ind., Nov., 1974, 1259.

17. Sakamoto, T. and Tsukizoe, T., "Friction and Prow Formation in a Scratch Process of Copper by a Diamond Cone," Wear, V. 44, 1977, 393.

18. Basuray, P. K., Misra, B. K., and Lal, G. K., "Transition From Ploughing to Cutting During Machining with Blunt Tools," Wear, Vol. 43, 1977, 341.

19. Bitans, K. and Brown, R. H., "An Investigation in Orthogonal Cutting," Int. Jour. Mach. Tool Des. Res., Vol. 5, 1965, 155.

20. Hill, R., The Mathematical Theory of Plasticity, Oxford: The Clarendon Press, 1950.

21. Thomsen, E. G. and Yang, C. T. and Kobayashi, S., Mechanics of Plastic Deformation in Metal Processing, New York: The MacMillan Company, 1965.

22. Black, P. H., Theory of Metal Cutting, New York: McGraw Hill Book Co., 1961.

23. Crandall, S. H., Engineering Analysis, New York: McGraw Hill Book Co., 1956.

24. Johnson, W. and Sowerby, R., Plane-Strain Slip-Line Fields: Theory and Bibliography, New York: American Elsevier Pub. Co., 1970.

25. Wanheim, T., Bay, N. and Peterson, A. S., "A Theoretically Determined Model for Friction in Metal Work Processes," Wear, V. 28, 1974, 251.

References - continued

26. Bowden, F. P. and Tabor, D., The Friction and Lubrication of Solids, London: The Oxford University Press, 1950.

27. Yoshihiro Kita, Mamoru Ido and Shigeki Hata, "The Mechanism of Metal Removal by an Abrasive Tool," Wear, 47 (1978) 185-193.

28. Abdelmoneim, M. Es. and Scrutton, R. F., "Post-Machining Plastic Recovery and the Law of Abrasive Wear," Wear, 24 (1973) 1-13.

29. Bay, N., Wanheim, T., "Real Area of Contact and Friction Stress at High Pressure Sliding Contact," Wear, 38 (1976) 201-209.

30. Hill, R., "On the Limits Set by Plastic Yielding to the Intensity of Singularities of Stress," Journal of the Mechanics and Physics of Solids, 1954, Vol. 2, pp. 278-285.

31. Challen, J. M., and Oxley, P. L. B., "An Explanation of the Different Regimes of Friction and Wear Using Asperity Deformation Models," Wear, 53 (1979) 229-243.

32. Slater, R. A. C., Engineering Plasticity: Theory and Application to Metal Forming Processes, London: A Halsted Press Book, The MacMillan Press Ltd., 1977.

33. Hugh Ford, Advanced Mechanics of Materials, London: Longmans, Green & Co., 1963.

34. Kachanov, L. M., Foundations of the Theory of Plasticity, Amsterdam: North-Holland Publishing Company, 1971.

35. Hein, J. W., "Theoretical Analysis of Metal Cutting with Large Negative Rake Cutting Tools," Master's Thesis, Kansas State University, 1979.

36. Yoshihiro Kita, Mamoru Ido, Naomichi Kawasaki, "A Study on the Cutting Mechanism with Large Negative Rake Angle." (In Japanese, Abstract appears in TECHNOCRAT Vol. 11-No. 10, Oct. 1978; p. 98).

APPENDIX I

SLIP-LINE ANALYSIS

Angles and Lengths

In the slip-line field of Fig. 4.1, the following angles are denoted by:

angle SAB = η_1

angle BHP = angle BOP = θ

angle HBO = angle HPO = η_2

angle PCD = η_3

angle EPD = ϕ

From the geometry of the slip-line fields it is required to have

angle AHB = angle HAS = 45°

angle FEP = angle CDP = 90°

angle OPV = angle OB'' = 90°

angle HPF = angle FPE = 45°.

The rake angle is α.

In triangle PDC

angle CDP = 90°, angle DPC = $90^\circ - \eta_3$

In triangle BOP

angle BOP = θ, angle OBP = angle OPB = $\frac{180-\theta}{2}$

In triangle BHP

angle BHP = θ, angle HPO = η_2

angle HPB = $90^\circ - \theta/2 - \eta_2$, angle HBP = $90 - \theta/2 + \eta_2$

In triangle BPV

angle OPV = 90°, angle BPV = angle OPV - angle OPB = $\theta/2$

In triangle HAB

angle HBA = $90^{\circ} - \eta_1$

At point B

angle HBA + angle HBO + angle OBP + angle PBC = 180°

angle PBC = $\eta_1 - \eta_2 + \theta/2$

In triangle BPC

angle BPC = $\Delta + \theta/2$

angle BCP = $180^{\circ} - (\Delta + \theta + \eta_1 - \eta_2)$

At point P

angle EPD + angle DPC + angle CPB + angle OPB

+ angle OPF + angle FPE = 360°

Hence, $\phi - \eta_3 + \Delta - \eta_2 = 90^{\circ}$

Angle VPU

FPU is a straight line, so angle OPF + angle OPB

+ angle BPV + angle VPU = 180°

Hence, angle VPU = $45^{\circ} + \eta_2$

Angle ABB'

angle ABB' = 90° - angle HBA - angle OBH = $\eta_1 - \eta_2$

In triangle OTB

angle OTB = 90°, angle OBT = $90 - \eta_1 + \eta_2$

angle TOB = $\eta_1 - \eta_2$

In Quadrilateral OPNM

angle OMN = angle PNM = 90°

angle POM = 360° - angle OMN - angle PNM - angle OPC

= $\eta_2 + \eta_3 - \phi$

Angle PCF

angle BCF = $90 - \alpha$

angle PCF = angle BCF - angle BCP

= $\eta_1 + \theta + \Delta - \eta_2 - \alpha - 90$

In triangle FPC

angle PFC = 180° - angle PCF - angle FPC

= $135^{\circ} - (\eta_1 + \theta + \Delta + \phi - \eta_2 - \eta_3 - \alpha)$

but $\phi + \Delta - \eta_2 - \eta_3 = 90^{\circ}$

hence, angle PFC = $45^{\circ} + \alpha - \eta_1 - \theta$

In triangle HPQ

angle HPQ = angle CFE

angle CFE = 45 - angle PFC

angle CFE = angle HPQ = $\eta_1 + \theta - \alpha$

In determining the lengths, the sine law is used, that is,

$$\frac{a}{\sin A} = \frac{b}{\sin B} = \frac{c}{\sin C} .$$

Let PD = PE = R

In triangle PDC

PC = $PD/\sin\eta_3$

DC = $PC \cos\eta_3$

In triangle BPC

$$PB = PC \frac{\sin(180-\eta_1-\theta-\Delta+\eta_2)}{\sin(\eta_1-\eta_2+\theta/2)}$$

$$BC = PC \frac{\sin(\Delta+\theta/2)}{\sin(\eta_1-\eta_2+\theta/2)}$$

In triangle HPB

$$HB = PB \frac{\sin(90-\theta/2-\eta_2)}{\sin\theta}$$

$$HP = PB \frac{\sin(90-\theta/2+\eta_2)}{\sin\theta}$$

In triangle BOP

$$OB = OP = PB \frac{\sin(90-\theta/2)}{\sin\theta}$$

In triangle HPQ

angle HQP = 90°

$$HQ = HP \sin(\eta_1+\theta-\alpha)$$

but, HQ = Depth of cut, D

Hence,

$$D = R \frac{1}{\sin\theta_3} \frac{\sin(180-\eta_1-\theta-\Delta+\eta_2)}{\sin(\eta_1-\eta_2+\theta/2)} \frac{\sin(90-\theta/2+\eta_2)}{\sin\theta} \sin(\eta_1+\theta-\alpha)$$

In triangle HAB

$$AB = HB \frac{\sin 45}{\sin(45+\eta_1)}$$

$$HA = HB \frac{\sin(90-\eta_1)}{\sin(45+\eta_1)}$$

The chip thickness, $d = HA \cos(45-\eta_1)$

Hence, $$d + R \frac{1}{\sin\eta_3} \frac{\sin(180-\eta_1-\theta-\Delta+\eta_2)}{\sin(\eta_1-\eta_2+\theta/2)} \frac{\sin(90-\theta/2-\eta_2)}{\sin\theta} \cos(45-\eta_1)$$

In triangle OTB

$$TB = OB \sin(\eta_1-\eta_2)$$

$$OT = BO \cos(\eta_1-\eta_2)$$

In triangle OZP

$$OZ = OP \cos(\eta_2+\eta_3-\phi)$$

$$PZ = OP \sin(\eta_2+\eta_3-\phi)$$

In triangle FPE

$$PF = PE/\sin 45$$

$$FE = FP \cos 45$$

Other lengths required in the analysis are

$$QL = FP \sin(45-\eta_1-\theta+\alpha)$$

$$ZM = PC/2$$

$$OM = OZ + ZM$$

$$HL = HQ + QL = d_o$$

Velocity Relationship

The hodograph is shown in Fig. 4.2. From the slip-line field of Fig. 4.1 the following angles in the hodograph can be determined.

In triangle PBA

angle PAB = 135, angle PBA = $\eta_1+\theta-\alpha$

angle APB = $45-(\eta_1+\theta-\alpha)$

In triangle PCB

angle CPB = $\eta_1+\theta+\Delta-\eta_2-\alpha-90$ angle PCB = $180-\eta_3$

angle PBC = $\eta_3-\eta_1-\theta-\Delta+\eta_2+\alpha+90$

In triangle FPA

angle PAF = 45^{o}, angle FPA = $45+\eta_2$

angle PFA = $90-\eta_2$

In triangle PEF

angle EPF=θ, angle PFE = $90-\theta/2$

angle PEF = $90-\theta/2-\eta_2$

In triangle PDE

angle PED=90, angle DPE = $\eta_1-\eta_2$

angle PDE = $90-\eta_1$

Let the unit velocity be PB=U

Using the law's of sine, the velocity discontinuities can be determined as

In triangle PAB

$$U^{*}_{EG} = U \frac{\sin(45-\eta_1-\theta+\alpha)}{\sin 135}$$

$$U_{GH} = U \frac{\sin(\eta_1+\theta-\alpha)}{\sin 135}$$

In triangle PCB

$$U^{*}_{DC} = U \frac{\sin(\eta_1+\theta+\Delta-\eta_2-\alpha-90)}{\sin(180-\eta_3)}$$

$$U_{PC} = U \frac{\sin(\eta_3-\eta_1-\theta-\Delta+\eta_2+\alpha+90)}{\sin(180-\eta_3)}$$

In triangle PFB

$$U_{TNP} = U \frac{\sin(\eta_1+\theta-\alpha)}{\sin(90-\eta_2)}$$

In triangle PEF

$$U_{TNB} = U \frac{\sin(\eta_1+\theta-\alpha)}{\sin(90-\eta_2)} \frac{\sin(90-\theta/2+\eta_2)}{\sin(90-\theta/2-\eta_2)}$$

In triangle DPE

$$U_{BA} = U \frac{\sin(\eta_1+\theta-\alpha)}{\sin(90-\eta_2)} \frac{\sin(90-\theta/2+\eta_2)}{\sin(90-\theta/2-\eta_2)} \frac{\sin(90+\eta_2)}{\sin(90-\eta_1)}$$

$$U^*_{BH} = U \frac{\sin(\eta_1+\theta-\alpha)}{\sin(90-\eta_2)} \frac{\sin(90-\theta/2+\eta_2)}{\sin(90-\theta/2-\eta_2)} \frac{\sin(\eta_1-\eta_2)}{\sin(90-\eta_1)}$$

Stress Distributions

The normal stresses p_1 to p_{16} in Fig. 4.3(a) are compressive. The stresses on an element on a slip-line can be determined from the Mohr's circles of Fig. 4.3(b). The values are given as follows:

On HA

$p_1=0$, free surface

$p_2= -2k$

No shear stresses, $s_1=s_2=0$

On AB

$p_3= -k(1+\sin 2\eta_1)$

$p_4= -k(1-\sin 2\eta_1)$

$s_3=k\cos 2\eta_1$

$s_4= -k\cos 2\eta_1$

On HB

$p_5=p_6= -k$

$s_5=k$

$s_6= -k$

On HP

$p_7 = -k(1+2\theta)$

$p_8 = -k(1+2\theta)$

$s_7 = k$

$s_8 = -k$

On HV

$p_v = -k(1+2\psi)$

$p_T = -k(1+2\psi)$

$s_v = k, \; s_T = -k$

On OV at V

$p_v' = -k(1+2\psi+\sin 2\eta_2)$

$p_T' = -k(1+2\psi-\sin 2\eta_2)$

$s_v' = k\cos 2\eta_2, \; s_T' = -k\cos 2\eta_2$

On GH

$p_{7A} = -2k(1+\theta)$

$p_{8A} = -2k\theta$

$s_{7A} = s_{8A} = 0$

On GE

$p_{7B} = -k(1+2\theta)$

$p_{8B} = -k(1+2\theta)$

$s_{7B} = k, \; s_{8B} = -k$

On PE

$p_9 = -k(1+2\theta)$

$p_{10} = -k(1+2\theta)$

$s_9 = -k, \; s_{10} = k$

On PD

$$p_{11} = -k(1+2\theta+2\phi)$$

$$p_{12} = -k(1+2\theta+2\phi)$$

$$s_{11} = -k,\ s_{12} = k$$

On PC

$$p_{13} = -k(1+2\theta+2\phi+\sin 2\eta_3)$$

$$p_{14} = -k(1+2\theta+2\phi-\sin 2\eta_3)$$

$$s_{13} = -k\cos 2\eta_3,\ s_{14} = k\cos 2\eta_3$$

On DC

$$p_{15} = -k(1+2\theta+2\phi)$$

$$p_{16} = -k(1+2\theta+2\phi)$$

$$s_{15} = -k,\ s_{16} = k$$

On OP

$$p_7' = -k(1+2\theta+\sin 2\eta_2)$$

APPENDIX II

Check of Yield Criterion at Points of Stress Singularity

In order that yielding of the vertices in Fig. 2.9 shall not occur the inequalities mentioned in Section 2.3.7.3 must apply.

Vertex PHB; angle PHB=θ

This is case (iii) as described in Section 2.3.7.3. That is,

$$0 \leq \frac{P_6 - P_8}{2k} \geq \begin{cases} \sin\theta\ , & \theta \leq \pi \\ -(\theta-\pi), & \theta \geq \pi \end{cases}$$

but here, from Appendix I

$$\frac{P_6 - P_8}{2k} = \theta$$

Therefore, the above inequality becomes

$$\theta \geq \theta \geq \sin\theta, \quad \text{for } 0 < \theta \leq \pi$$

and thus there is no restrictions on θ.

Vertex EPD; angle EPD=ϕ

This is the same case as vertex PHB. Here,

$$\frac{P_{10} - P_{12}}{2k} = \phi$$

and the condition of stability becomes

$$\phi \geq \phi \geq \sin\phi, \quad \text{for } 0 < \phi \leq \pi$$

which is true for any ϕ.

Vertex HGF, angle HGF=45^{o}

This is case (iv). Hence,

$$1+2\ (\alpha - \tfrac{\pi}{4}) \geq \frac{P_{8A} - P_{8B}}{k} \geq 2\cos(\alpha - \tfrac{\pi}{4}) - 1, \quad \tfrac{\pi}{4} \leq \alpha \leq \tfrac{3}{4}\pi$$

or

$$1 \geq \frac{P_{8A}-P_{8B}}{k} \geq 1$$

Here,

$$\frac{P_{8A}-P_{8B}}{k} = 1$$

Therefore, the vertex HGF is not overstressed.

Vertex AHB

angle AHB=45°

This is case (iv) with p_1=0. That is

$$1 \geq \frac{P_1-P_6}{k} \geq 1$$

Here,

$$\frac{P_1-P_6}{k} = 1$$

Therefore, the vertex is not overstressed.

Vertex DPC, angle DPC=$90-\eta_3$

The shearing stresses are directed towards the vertex according to Eq. (2.18), since

$$\phi_{13} = \frac{1}{2} \sin^{-1} \frac{s_{13}}{k} = -(45-\eta_3)$$

and,

$$\phi_{12} = \frac{1}{2} \sin^{-1} \frac{s_{12}}{k} = 45$$

It is necessary that,

$$\text{angle DPC} \geq |\phi_{13}-\phi_{12}| = 90-\eta_3.$$

This is true in this case. From Eqs. (2.20)

$$\left(\frac{P_{12}-P_{13}}{2k}\right)_{max} = \frac{1}{2}\left[\cos(90)+\cos(-90+2\eta_3)\right]+\left[90-\eta_3+45-45+\eta_3 - \frac{\pi}{2}\right]$$

$$= \frac{1}{2} \sin 2\eta_3$$

Similarly,

$$\left(\frac{P_{12}-P_{13}}{2k}\right)_{min} = \frac{1}{2}\sin 2\eta_3$$

Here,

$$\frac{P_{12}-P_{13}}{2k} = \frac{1}{2}\sin 2\eta_3.$$

Thus, the yielding inequalities are satisfied for any η_3.

Vertex PCD, angle PCD=η_3

One shear stress (s_{15}) is directed towards, and the other (s_{13}) away from the vertex. According to Eq. (2.18). Since,

$$\phi_{13} = \frac{1}{2}\sin^{-1}\frac{s_{13}}{k} = 45-\eta_3$$

$$\phi_{15} = \frac{1}{2}\sin^{-1}\frac{s_{15}}{k} = 45.$$

It is necessary that, angle PCD $\geq |\phi_{13}-\phi_{15}| = \eta_3$, which is true in this case.

From the yield inequality Eqs. (2.20), it can be shown that

$$\left(\frac{P_{15}-P_{13}}{2k}\right)_{max} = \frac{1}{2}\sin 2\eta_3$$

$$\left(\frac{P_{15}-P_{13}}{2k}\right)_{min} = \frac{1}{2}\sin 2\eta_3.$$

Here, $\frac{P_{15}-P_{13}}{2k} = \frac{1}{2}\sin 2\eta_3$.

Therefore, the yield criterion is satisfied for any η_3.

Vertex ABH, angle ABH=90-η_1

Both shear stresses are directed toward the vertex. Since,

$$\phi_3 = \frac{1}{2} \sin^{-1} \frac{s_3}{k} = -(45-\eta_1)$$

$$\phi_6 = 45.$$

It is necessary that, angle ABH $\geq |\phi_3 - \phi_6| = 90-\eta_1$, which is true in this case.

From the yield inequality equations

$$\left(\frac{P_6-P_3}{2k}\right)_{max} = \frac{1}{2} \sin 2\eta_1, \quad \left(\frac{P_6-P_3}{2k}\right)_{min} = \frac{1}{2} \sin 2\eta_1.$$

But, at the vertex from Mohr's circle of Fig. 4.3(b)

$$\frac{P_6-P_3}{2k} = \frac{1}{2} \sin 2\eta_1.$$

Thus, the yield criterion is satisfied for any η_1.

Vertex HAB, angle HAB=$45+\eta_1$.

On one side there is no shearing stress, but on the other s_3. We have

$$\phi_1=0, \text{ and } \phi_3 = \frac{1}{2} \sin^{-1} \frac{s_3}{k} = 45-\eta_1.$$

It is required that, angle HAB $\geq |\phi_3-\phi_1| = 45-\eta_1$, which is true at the vertex.

From Equations 2.20

$$\left(\frac{P_1-P_3}{2k}\right)_{max} = \frac{1}{2} (1+\sin 2\eta_1); \quad \left(\frac{P_1-P_3}{2k}\right)_{min} = -\frac{1}{2} (1+\sin 2\eta_1)+\cos 2\eta_1.$$

At the vertex, $\frac{P_1-P_3}{2k} = \frac{1}{2} (1+\sin 2\eta_1)$.

Therefore, $\frac{1}{2}(1+\sin 2\eta_1) \geq \frac{1}{2} (1+\sin 2\eta_1) \geq -\frac{1}{2} (1+\sin 2\eta_1) + \cos 2\eta_1$

which is true for any η_1. So the vertex does not yield.

Vertex HBP, angle HBB'' = $90+\eta_2$.

Both shear stresses are directed away from the vertex. Hence, with $\phi_6 = \frac{1}{2}\sin^{-1}\frac{s_6}{k} = -45$, $\phi_v = \frac{1}{2}\sin^{-1}\frac{s'_v}{k} = 45-\eta_2$. It is necessary that, angle HBB'' $\geq |\phi_6-\phi_v| = 90+\eta_2$; which is true in this case.

From Equations 2.20

$$\left(\frac{P_6-P'_v}{2k}\right)_{max} = \frac{1}{2}\sin 2\eta_2;\ \left(\frac{P_6-P'_v}{2k}\right)_{min} = -\frac{1}{2}\sin 2\eta_2 - 2\eta_2$$

Here, at the vertex, $\frac{P_6-P'_v}{2k} = \frac{1}{2}\sin 2\eta_2$. Hence, the vertex does not yield for any η_2.

Vertex HPB, angle HPV=$90-\eta_2$

Both shear stresses are directed towards the vertex. So, with

$$\phi_8 = \frac{1}{2}\sin^{-1}\frac{s_8}{k} = 45,\ \phi_v = \frac{1}{2}\sin^{-1}\frac{s'_v}{k} = -(45-\eta_2).$$

It is necessary that, angle HPV $\geq |\phi_8-\phi_v| = 90-\eta_2$; which is true in this case.

Using equations 2.20, it can be shown that

$$\left(\frac{P_8-P'_v}{2k}\right)_{max} = \frac{1}{2}\sin 2\eta_2;\ \left(\frac{P_8-P'_v}{2k}\right) = \frac{1}{2}\sin 2\eta_2.$$ But, at the vertex $\frac{P_8-P'_v}{2k} = \frac{1}{2}\sin 2\eta_2$. So, the vertex does not yield for any η_2.

Vertex BPC, angle CPV=Δ

The shear stresses s'_T and s_{14} are directed away from the vertex. So, with $\phi_v = \frac{1}{2}\sin^{-1}\frac{s'_T}{k} = -(45-\eta_2)$ and $\phi_{14} = \frac{1}{2}\sin^{-1}\frac{s_{14}}{k} = 45-\eta_3$, it is necessary that, angle CPV $\geq |\phi_{14}-\phi_v| = 90-\eta_3-\eta_2$.

At this vertex $\frac{P'_v-P_{13}}{2k} = \frac{1}{2}(2\phi + \sin 2\eta_3 - \sin 2\eta_2)$ must be within the following limits:

$$\left(\frac{P_v'-P_{13}}{2k}\right)_{max} = \frac{1}{2}\left(\cos(90-2\eta_3) + \cos(2\eta_2-90)\right) + (\Delta-45+\eta_2+45-\eta_3-\pi/2)$$

$$= \frac{1}{2}\left(\sin 2\eta_3 + \sin 2\eta_2\right) + (\Delta+\eta_2-\eta_3-\pi/2), \text{ for } \Delta+\phi_v+\phi_{13} \geq \pi/2$$

Similarly

$$\left(\frac{P_v'-P_{13}}{2k}\right)_{max} = \frac{1}{2}\left(\sin 2\eta_3 + \sin 2\eta_2\right) - \cos(\Delta+\eta_2-\eta_3), \text{ for } \Delta-\phi_v-\phi_{13} \leq \pi/2$$

$$\left(\frac{P_v'-P_{13}}{2k}\right)_{min} = -\frac{1}{2}\left(\sin 2\eta_3 + \sin 2\eta_2\right) + \cos(\Delta+\eta_3-\eta_2), \text{ for } \Delta-\phi_v-\phi_{13} \leq \pi/2$$

$$\left(\frac{P_v'-P_{13}}{2k}\right)_{min} = -\frac{1}{2}\left(\sin 2\eta_3 + \sin 2\eta_2\right) - (\Delta+\eta_3-\eta_2-\pi/2), \text{ for}$$

$$\Delta-\phi_v-\phi_{13} \geq \pi/2$$

and

$$\Delta \geq 90-\eta_3-\eta_2$$

THIS BOOK CONTAINS NUMEROUS PAGES THAT WERE BOUND WITHOUT PAGE NUMBERS.

THIS IS AS RECEIVED FROM CUSTOMER.

APPENDIX III

Computer Program

```
$JOB
C *** PROGRAM TO DETERMINE THE GEOMETRY OF THE SLIP-LINE FIELD,
C *** THE DIMENSIONLESS STRESS DISTRIBUTION AND THE DIMENSIONLESS
C *** FORCES EXERTED BY THE TOOL.THE NOMENCLATURE USED IN
C *** THE PROGRAM IS SIMILAR TO THE ONE USED IN THE THESIS.
   10 FORMAT(10X,'ALPHAD',10X,'DELTAD',12X,'PHID',11X,'TETAD',11X,
     1'ETA1D',11X,'ETA2D',11X,'ETA3D',14X,'HQ'/13X,'FVD',13X,'FHD',
     113X,'FTD',13X,'SBC',14X,'S3',13X,'SVA',13X,'S13',15X,'D'/
     113X,'PBC',14X,'P3',13X,'PVA',13X,'P13',12X,'CHTD',12X,'PMOK',
     113X,'VOH',14X,'ACMC'//)
   15 FORMAT(8F16.8)
   20 FORMAT(5X,'ADHESION COEFFICIENT=ACM')
      WRITE(6,20)
      ACM=0.5
      WRITE(6,15) ACM
      WRITE(6,10)
C *** ALPHAD=RAKE ANGLE IN DEGREES
      ALPHAD=60.0
      PI=22.0/7.0
      RAD=PI/180.0
      ALPHAR=ALPHAD*RAD
      DEL=1.0*RAD
      RHO=ARCOS(ACM)/2.0
      SN=SQRT(2.0)*(1.0+PI/2.0+2.0*RHO+SIN(2.0*RHO))/
     1(2.0*SQRT(2.0)+4.0*SIN(RHO))
      ARLIM=1.0-0.52*(1.0-ACM)**0.325
      FA=ACM*ARLIM/SN/2.0
      B2=ARLIM/(1.0-ARLIM)/SN
      B1=(1.0-ARLIM)*EXP(B2*SN)
   89 FORMAT('_',10X,'DID NOT CONVERGE')
      EPSS=0.00001
      EPS=0.0001
C *** LOOP FOR VARYING ADHESION COEFFICIENT
C *** ITERATION FOR ETA 1
      DE1=10.0*RAD
      TETA1=PI/2.0
      IITER=0
  310 ITER=0
  311 P3=1.0+SIN(TETA1)
      IF(P3/2.0.GT.SN) GO TO 312
      E1TEST=FA*(1.0+SIN(TETA1))-COS(TETA1)
      GO TO 313
  312 E1TEST=ACM*(1.0-B1*EXP(-B2*P3))-COS(TETA1)
  313 IF(E1TEST.LT.0.0) GO TO 322
      TE1SAV=TETA1
      TETA1=TETA1-DE1
      ITER=ITER+1
      IF (ITER.GT.12) GO TO 370
      GO TO 311
  322 IITER=IITER+1
      IF (IITER.GT.19) GO TO 900
      DIFF=TE1SAV-TETA1
      IF (ABS(E1TEST).LT.EPS) GO TO 900
      DE1=DIFF*0.1
      TETA1=TE1SAV
      GO TO 310
  370 WRITE(6,89)
  900 ETA1R=TETA1*0.5
      ETA1D=ETA1R/RAD
      DO 100 I=1,3
```

```
C *** ITERATION FOR ETA 2
C *** GUESS FOR TETAD=TETGD
      TETGD=20.0
      TETG=TETGD*RAD
      TETA2=PI/2.0
      TETA3=PI/2.0
      PHIR=60.0*RAD
      DO 200 J=1,90
      PHID=PHIR/RAD
      JITER=0
  209 IITER=0
      DE2=10.0*RAD
  210 ITER=0
  211 PV=0.5*(1.0+TETG+SIN(TETA2))
      IF(PV.GT.SN) GO TO 212
      E2TEST=FA*PV*2.0-COS(TETA2)
      GO TO 213
  212 E2TEST=ACM*(1.0-B1*EXP(-B2*PV))-COS(TETA2)
  213 IF(E2TEST.LE.0.0) GO TO 222
      TE2SAV=TETA2
      TETA2=TETA2-DE2
      ITER=ITER+1
      IF(ITER.GT.12) GO TO 77
      GO TO 211
  222 IITER=IITER+1
      IF(IITER.GT.19) GO TO 277
      DIFF=TE2SAV-TETA2
      IF(ABS(E2TEST).LT.EPS) GO TO 277
      DE2=DIFF*0.1
      TETA2=TE2SAV
      GO TO 210
   77 WRITE(6,89)
  277 ETA2R=TETA2*0.5
      ETA2D=ETA2R/RAD
      SV=COS(2.0*ETA2R)
C *** ITERATION FOR ETA 3
      DE3=10.0*RAD
      IITER=0
  412 ITER=0
  411 P13K=1.0+2.0*TETG+2.0*PHIR+SIN(TETA3)
      IF(P13K/2.0.GT.SN) GO TO 413
      E3TEST=FA*P13K-COS(TETA3)
      GO TO 414
  413 E3TEST=ACM*(1.0-B1*EXP(-B2*P13K/2.0))-COS(TETA3)
  414 IF(E3TEST.LE.0.0) GO TO 422
      TE3SAV=TETA3
      TETA3=TETA3-DE3
      ITER=ITER+1
      IF(ITER.GT.20) GO TO 477
      GO TO 411
  422 IITER=IITER+1
      IF(IITER.GT.19) GO TO 430
      DIFF=TE3SAV-TETA3
      IF(ABS(E3TEST).LT.EPS) GO TO 430
      DE3=DIFF*0.1
      TETA3=TE3SAV
      GO TO 412
  477 WRITE (6,89)
  430 ETA3R=TETA3*0.5
      ETA3D=ETA3R/RAD
```

```
      ALPHAR=ALPHAD*RAD
      DELTAD=90.0+ETA3D-PHID+ETA2D
      DELTAR=DELTAD*RAD
      TETAR=ATAN((SIN(PI-ETA3R)*SIN(PI/4.0-ETA1R+ALPHAR)-
     1SIN(3.0*PI/4.0)*SIN(ETA1R+DELTAR-ETA2R-ALPHAR-PI/2.0))/
     1(SIN(PI-ETA3R)*COS(PI/4.0-ETA1R+ALPHAR)+SIN(3.0*PI/4.0)*
     1COS(ETA1R+DELTAR-ETA2R-ALPHAR-PI/2.0)))
      TETAD=TETAR/RAD
C *** CHECKING THE GUESSED VALUE OF TETAD
      TETD=TETAR-TETG
      IF(ABS(TETD).LT.EPSS) GO TO 600
      TETG=TETAR
      GO TO 209
  600 R=1.0
C *** CHECK IF VERTEX BPC IS NOT OVER STRESSED
      PD=(PHIR*2.0+SIN(2.0*ETA3R)-SIN(2.0*ETA2R))/2.0
      A1=DELTAD-45.0+ETA2D+45.0-ETA3D
      IF(A1.LT.90.0) GO TO 800
      PMAX=0.5*(SIN(2.0*ETA3R)+SIN(2.0*ETA2R))+
     1(DELTAR+ETA2R-ETA3R-PI/2.0)
      GO TO 801
  800 PMAX=0.5*(SIN(2.0*ETA3R)+SIN(2.0*ETA2R))
     1-COS(DELTAR+ETA2R-ETA3R)
  801 IF(PD.GT.PMAX) GO TO 700
      A2=DELTAD+45.0-ETA2D-45.0+ETA3D
      IF(A2.GT.90.0) GO TO 850
      PMIN=-0.5*(SIN(2.0*ETA3R)+SIN(2.0*ETA2R))+
     1COS(DELTAR+ETA3R-ETA2R)
      GO TO 851
  850 PMIN=-0.5*(SIN(2.0*ETA3R)+SIN(2.0*ETA2R))-
     1(DELTAR+ETA3R-ETA2R-PI/2.0)
  851 IF(PD.LT.PMIN) GO TO 700
      TETAR=ATAN((SIN(PI-ETA3R)*SIN(PI/4.0-ETA1R+ALPHAR)-
     1SIN(3.0*PI/4.0)*SIN(ETA1R+DELTAR-ETA2R-ALPHAR-PI/2.0))/
     1(SIN(PI-ETA3R)*COS(PI/4.0-ETA1R+ALPHAR)+SIN(3.0*PI/4.0)*
     1COS(ETA1R+DELTAR-ETA2R-ALPHAR-PI/2.0)))
      TETAD=TETAR/RAD
      IF(TETAD.LE.0.0) GO TO 700
      BCP=180.0-ETA1D-TETAD-DELTAD+ETA2D
      IF(BCP.LE.0.0) GO TO 700
C *** GEOMETRICAL PROPERTIES,REFER FIG.4.1.
C *** LENGTHS
C *** R=FAN RADIUS
      R=1.0
      PD=R
      PC=PD/SIN(ETA3R)
      DC=PC*COS(ETA3R)
      PB=PC*SIN(PI-ETA1R-TETAR-DELTAR+ETA2R)/
     1SIN(ETA1R-ETA2R+TETAR/2.0)
      BC=PC*SIN(DELTAR+TETAR/2.0)/SIN(ETA1R-ETA2R+TETAR/2.0)
      HB=PB*SIN(PI/2.0-TETAR/2.0-ETA2R)/SIN(TETAR)
      HP=PB*SIN(PI/2.0-TETAR/2.0+ETA2R)/SIN(TETAR)
      OB=PB*SIN(PI/2.0-TETAR/2.0)/SIN(TETAR)
      OP=OB
C *** HQ=DEPTH OF CUT
      HQ=HP*SIN(ETA1R+TETAR-ALPHAR)
      IF(HQ.LT.0.0) GO TO 700
      AB=HB*SIN(PI/4.0)/SIN(PI/4.0+ETA1R)
      HA=HB*SIN(PI/2.0-ETA1R)/SIN(PI/4.0+ETA2R)
C *** CHTD=CHIP THICKNESS
```

```
      CHTD=HA*COS(PI/4.0-ETA1R)/HQ
      TB=OB*SIN(ETA1R-ETA2R)
      OT=OB*COS(ETA1R-ETA2R)
      OZ=OP*COS(ETA2R+ETA3R-PHIR)
      PZ=OP*SIN(ETA2R+ETA3R-PHIR)
      FP=PC/SIN(PI/4.0)
      QL=FP*SIN(PI/4.0-ETA1R-TETAR+ALPHAR)
      ZM=PC/2.0
      OM=OZ+ZM
      TC=TB+BC
C *** HL=HEIGHT OF CHIP FORMATION
      HL=HQ+QL
      AC=AB+BC
      D=HQ/HL
C *** DIMENSIONLESS STRESS DISTRIBUTIONS,REFER TO FIG.4.4.
C *** S=SHEAR STRESS K
      S=1.0
      P3=S*(1.0+SIN(2.0*ETA1R))
      S3=S*COS(2.0*ETA1R)
      SV=S*COS(2.0*ETA2R)
      PV=S*(1.0+TETAR+SIN(2.0*ETA2R))
      P13=S*(1.0+2.0*TETAR+2.0*PHIR+SIN(2.0*ETA3R))
      S13=S*COS(2.0*ETA3R)
C *** CONDITIONS OF EQUILIBRIUM ON THE DEAD ZONE,REFER FIG.4.4.
C *** FORCE ON DEAD ZONE PARALLEL TO THE TOOL FACE.  'RX'
      S13T=S13*PC
      P13T=P13*PC
      S13TX=S13T*COS(PI-ETA1R-TETAR-DELTAR+ETA2R)
      P13TX=P13T*SIN(PI-ETA1R-TETAR-DELTAR+ETA2R)
      PVTX=S*OB*(COS(ETA1R-ETA2R)-COS(ETA1R-ETA2R+TETAR)+2.0*
     1(SIN(ETA1R-ETA2R+TETAR)-TETAR*COS(ETA1R-ETA2R+TETAR)-
     1SIN(ETA1R-ETA2R))-SIN(2.0*ETA2R)*(COS(ETA1R-ETA2R+TETAR)-
     1COS(ETA1R-ETA2R)))
      SVTX=S*OB*COS(2.0*ETA2R)*(COS(PI/2.0-ETA1R+ETA2R-TETAR)-
     1COS(PI/2.0-ETA1R+ETA2R))
      RX=SVTX+P13TX-S13TX-PVTX
C *** SHEAR STRESS ON 'BC'
      SBC=RX/BC
      IF(SBC.GT.1.0) GO TO 700
C *** FORCE ON DEAD ZONE NORMAL TO TOOL FACE. 'RY'
      P13TY=P13T*COS(PI-ETA1R-TETAR-DELTAR+ETA2R)
      S13TY=S13T*SIN(PI-ETA1R-TETAR-DELTAR+ETA2R)
      PVTY=S*OB*(SIN(ETA1R-ETA2R+TETAR)-SIN(ETA1R-ETA2R)+2.0*
     1(COS(ETA1R-ETA2R+TETAR)+TETAR*SIN(ETA1R-ETA2R+TETAR)-
     1COS(ETA1R-ETA2R))-SIN(2.0*ETA2R)*(SIN(ETA1R-ETA2R+TETAR)-
     1SIN(ETA1R-ETA2R)))
      SVTY=S*OB*COS(2.0*ETA2R)*(SIN(PI/2.0-ETA1R+ETA2R)-
     1SIN(PI/2.0-ETA1R+ETA2R-TETAR))
      RY=S13TY+P13TY+PVTY+SVTY
      PBC=RY/BC
      PBC2=PBC/2.0
C *** LOCATION OF THE RESULTANT FORCE ON THE DEAD ZONE.  'TR'
      SVTO=S*OB*OB*COS(2.0*ETA2R)*TETAR
      RYTR=P13T*OM-S13T*PZ+SVTO-RX*OT
      TR=RYTR/RY
      IF(TR.LT.TB) GO TO 700
      IF(TR.GT.TC) GO TO 700
C *** ADHESION COEFFICIENT BETWEEN DEAD ZONE AND TOOL FACE
C *** ACMC=AVERAGE ADHESION COEFFICIENT ON TOOL FACE BC.
      ACMC=0.5
```

```
      IT=0
  980 RC=0.5*ARCOS(ACMC)
      SNC=SQRT(2.0)*(1.0+PI/2.0+2.0*RC+SIN(2.0*RC))/
     1(2.0*SQRT(2.0)+4.0*SIN(RC))
      ARLC=1.0-0.52*(1.0-ACMC)**0.325
      B2C=ARLC/(1.0-ARLC)/SNC
      B1C=(1.0-ARLC)*EXP(B2C*SNC)
      ARC=1.0-B1C*EXP(-B2C*PBC2)
      ACMCC=ABS(SBC)/ARC
      DMC=ACMCC-ACMC
      IF(ABS(DMC).LE.EPS) GO TO 982
      ACMC=ACMCC
      IF(ABS(ACMC).GT.1.0) ACMC=0.98
      IT=IT+1
      IF(IT.GE.20) GO TO 982
      GO TO 980
  982 DM=ACMC-ACM
      IF(PBC2.LE.SN) GO TO 970
      FC=ACM*B1*B2*EXP(-B2*PBC2)/2.0
      GO TO 983
  970 FC=ACM*ARLIM/2.0/SN
  983 IF(PBC2.LE.SNC) GO TO 981
      FCC=ACMC*B1C*B2C*EXP(-B2C*PBC2)/2.0
      GO TO 971
  981 FCC=ACMC*ARLC/2.0/SNC
  971 DFC=FCC-FC
C *** TOTAL HORIZONTAL AND VERTICAL FORCES ON THE TOOL. 'FH&FV'
 1000 P3Y=P3*AB
      S3X=S3*AB
      FT=S3X+RX
      FTD=FT/HQ
      FH=COS(ALPHAR)*(RY+P3Y)-SIN(ALPHAR)*(RX+S3X)
      FV=SIN(ALPHAR)*(P3Y+RY)+COS(ALPHAR)*(S3X+RX)
C *** AVERAGE NORMAL COMPRESSION STRESS ON TOOL
      PMOK=FV/AC/S
C *** RATIO OF VERTICAL FORCE TO HORIZONTAL FORCE
      VOH=FV/FH
C *** DIMENSIONLESS TOTAL HORIZONTAL AND VERTICAL FORCES ON TOOL
      FHD=FH/HQ
      FVD=FV/HQ
      SVA=SV
      PVA=PV
      WRITE(6,15) ALPHAD,DELTAD,PHID,TETAD,ETA1D,ETA2D,ETA3D,HQ,
     1FVD,FHD,FTD,SBC,S3,SVA,S13,D,
     1PBC,P3,PVA,P13,CHTD,PMOK,VOH,ACMC
  700 PHIR=PHIR-DEL
      IF(PHIR.LE.0.0) GO TO 710
  200 CONTINUE
  710 ALPHAD=ALPHAD+5.0
  100 CONTINUE
      STOP
      END
```

APPENDIX IV

Numerical Results

Table 1. Geometry of Slip-Line Field.

m	α	Δ	φ	θ	η_1	η_2	η_3	D	D/d_o	d/D
0.1	50	155.97	20	16.49	43.88	43.41	42.55	0.62	0.34	3.04
	55	147.94	28	25.62	43.88	43.41	42.53	0.33	0.24	1.86
	60	139.91	36.0	34.74	43.88	43.41	42.50	0.21	0.18	1.22
	65	130.85	45.0	44.37	43.88	43.37	42.48	0.15	0.16	0.81
	70	121.79	54.0	54.0	43.88	43.33	42.46	0.11	0.16	0.54
	75	112.72	63.0	63.61	43.88	43.29	42.43	0.09	0.16	0.35
	76	110.71	65.0	65.64	43.88	43.28	42.43	0.08	0.17	0.32
	77	110.69	65.0	66.64	43.88	43.27	42.42	0.06	0.12	0.31
	78	110.68	65.0	67.64	43.88	43.26	42.42	0.03	0.06	0.30
	79	110.67	65.0	68.64	43.88	43.26	42.42	0.001	0.004	0.28
0.3	50	140.12	27.0	23.61	41.45	39.93	37.19	1.04	0.47	2.03
	55	129.12	38.0	34.63	41.45	39.93	37.18	0.76	0.45	1.22
	60	120.94	46.00	44.01	41.45	39.81	37.13	0.56	0.42	0.87
	65	112.76	54.00	53.37	41.45	39.70	37.06	0.44	0.42	0.62
	70	104.55	62.00	62.73	41.45	39.55	37.00	0.36	0.45	0.44
	75	101.37	65.0	69.38	41.45	39.43	37.00	0.21	0.36	0.35
	80	101.20	65.0	74.41	41.45	39.30	36.89	0.06	0.14	0.30
	81	101.17	65.0	75.41	41.45	39.28	36.88	0.03	0.08	0.29
	82	101.13	65.0	76.42	41.45	39.26	36.78	0.007	0.02	0.28

Table 1 - continued

m	α	Δ	φ	θ	η_1	η_2	η_3	D	D/d_o	d/D
0.5	50	122.96	36.5	32.89	38.63	36.79	32.66	1.41	.58	1.36
	55	112.58	45.5	43.34	38.63	36.20	31.87	1.09	.57	.95
	60	104.09	53.0	52.90	38.63	35.72	31.37	.87	.58	.71
	65	96.29	60.0	62.10	38.63	35.27	31.01	.71	.62	.54
	70	94.92	61.0	67.73	38.63	35.02	30.90	.47	.54	.49
	75	94.62	61.0	72.77	38.63	34.80	30.82	.29	.41	.43
	80	94.34	61.0	77.80	38.63	34.60	30.74	.17	.22	.38
	81	94.28	61.0	78.81	38.63	34.55	30.73	.08	.17	.37
	82	94.23	61.0	79.82	38.63	34.51	30.71	.05	.11	.36
	83	94.18	61.0	80.82	38.63	34.47	30.70	.02	.06	.35
0.7	45	117.49	30.0	27.90	35.22	30.67	23.82	2.49	0.61	1.99
	50	99.97	44.0	43.98	35.22	30.27	23.70	1.97	0.67	1.06
	55	91.48	52.0	54.16	35.22	29.89	23.59	1.57	0.71	0.81
	60	89.02	54.0	60.49	35.22	29.52	23.50	1.20	0.68	0.72
	65	89.60	53.0	64.89	35.22	29.18	23.42	0.85	0.58	0.69
	70	89.19	53.0	69.96	35.22	28.85	23.34	0.58	0.49	0.65
	75	89.81	52.0	74.32	35.22	28.53	23.28	0.34	0.34	0.62
	80	89.46	52.0	79.35	35.22	28.23	23.23	0.15	0.18	0.57
	81	89.39	52.0	80.35	35.22	28.17	23.21	0.11	0.14	0.56
	82	89.39	52.0	81.35	35.22	28.17	23.21	0.07	0.10	0.55
	83	89.39	52.0	82.35	35.22	28.17	23.22	0.04	0.06	0.54
	84	89.39	52.0	83.35	35.22	28.17	23.21	0.007	0.01	0.53

Table 1 - continued

m	α	Δ	ϕ	θ	η_1	η_2	η_3	D	D/d_o	d/D
0.9	40	83.99	45.0	43.86	30.51	24.65	14.33	5.09	0.82	1.08
	45	83.01	45.0	49.00	30.51	23.93	14.08	3.95	0.79	1.05
	50	83.26	44.0	53.32	30.51	23.32	13.95	3.05	0.73	1.04
	55	83.55	43.0	57.64	30.51	22.73	13.82	2.23	0.66	1.03
	60	83.89	42.0	61.94	30.51	22.18	13.72	1.74	0.57	1.02
	65	84.26	41.0	66.24	30.51	21.65	13.62	1.26	0.47	1.02
	70	84.65	40.0	70.53	30.51	21.14	13.54	0.85	0.37	1.00
	75	85.12	39.0	74.81	30.51	20.66	13.46	0.52	0.25	1.00
	80	85.59	38.0	79.08	30.51	20.20	13.39	0.24	0.13	0.99
	81	85.25	38.0	80.11	30.51	19.93	13.32	.19	0.10	0.99
	82	85.25	38.0	81.11	30.51	19.93	13.32	.14	0.08	0.98
	83	85.20	38.0	82.11	30.51	19.89	13.32	.09	0.05	0.97
	84	85.10	38.0	83.11	30.51	19.79	13.32	.05	0.03	0.96
0.999	35	77.58	28.0	38.44	23.82	14.33	1.25	74.22	0.78	1.86
	40	77.58	28.0	43.44	23.82	14.33	1.25	44.42	0.69	1.77
	45	78.75	26.0	46.49	23.82	13.50	1.25	33.72	0.61	1.90
	50	79.05	25.0	50.52	23.82	12.81	1.25	25.64	0.53	1.97
	60	82.38	18.0	53.70	23.82	9.12	1.25	12.01	0.29	2.97
	65	82.38	18.0	58.70	23.82	9.12	1.25	8.95	0.23	2.92
	70	82.38	18.0	63.70	23.82	9.12	1.25	6.44	0.18	2.86
	75	83.36	16.0	66.75	23.82	8.1	1.25	3.92	0.11	3.29
	80	84.34	14.0	69.80	23.82	7.18	1.25	2.06	0.06	3.84
	85	84.78	13.0	73.83	23.82	6.53	1.25	0.80	0.02	4.19
	86	85.46	12.0	73.85	23.82	6.21	1.25	0.55	0.02	4.59
	87	85.44	12.0	74.85	23.82	6.19	1.25	0.36	0.01	4.58
	88	86.12	11.0	74.87	23.82	5.87	1.25	0.17	0.005	5.06
	89	86.11	11.0	75.87	23.82	5.86	1.25	0.009	0.003	5.05

Table 2. Stresses in Slip-Line Field

m	α	s_3^D	s_{va}^D	s_B^D	s_{Bc}^D	p_3^D	p_{va}^D	p_{13}^D	p_{Bc}^D
0.1	50	0.04	0.06	0.08	0.04	2.00	2.29	3.27	1.95
	55	0.04	0.06	0.09	0.05	2.00	2.45	3.89	2.84
	60	0.04	0.06	0.09	0.06	2.00	2.61	4.47	3.67
	65	0.04	0.06	0.09	0.07	2.00	2.77	5.12	4.47
	70	0.04	0.06	0.09	0.07	2.00	2.94	5.77	5.25
	75	0.04	0.06	0.09	0.07	2.00	3.11	6.42	6.01
	76	0.04	0.06	0.09	0.07	2.00	3.14	6.56	6.16
	77	0.04	0.06	0.09	0.02	2.00	3.16	6.59	6.33
	78	0.04	0.06	0.09	-0.03	2.00	3.18	6.63	6.50
	79	0.04	0.06	0.09	-0.09	2.00	3.20	6.62	6.67
0.3	50	0.12	0.18	0.27	0.12	2.00	2.39	3.73	2.05
	55	0.12	0.18	0.27	0.18	2.00	2.59	4.50	2.87
	60	0.12	0.18	0.27	0.22	2.00	2.75	5.11	3.64
	65	0.12	0.18	0.27	0.27	2.00	2.92	5.76	4.41
	70	0.12	0.19	0.28	0.26	2.00	3.08	6.32	5.19
	75	0.12	0.19	0.28	0.13	2.00	3.19	6.65	5.90
	80	0.12	0.20	0.28	-0,14	2.00	3.28	6.83	6.59
	81	0.12	0.20	0.28	-0.20	2.00	3.30	6.86	6.74
	82	0.12	0.20	0.28	-0.26	2.00	3.31	6.90	6.88

Table 2 - continued

m	α	s_3^D	s_{va}^D	s_B^D	s_{Bc}^D	p_3^D	p_{va}^D	p_{13}^D	p_{Bc}^D
0.5	50	.22	.28	.42	.27	1.98	2.53	4.33	2.38
	55	.22	.30	.44	.34	1.98	2.71	5.00	3.17
	60	.22	.32	.46	.39	1.98	2.87	5.59	3.91
	65	.22	.33	.47	.42	1.98	3.03	6.15	4.66
	70	.22	.34	.47	.27	1.98	3.12	6.38	5.25
	75	.22	.35	.48	.05	1.98	3.21	6.55	5.82
	80	.22	.36	.48	-.23	1.98	3.29	6.73	6.41
	81	.22	.36	.48	-.29	1.98	3.31	6.76	6.53
	82	.22	.36	.48	-.35	1.98	3.33	6.80	6.64
	83	.22	.36	.48	-.42	1.98	3.35	6.83	6.78
0.7	45	0.33	0.48	0.67	0.31	1.94	2.37	3.66	1.96
	50	0.33	0.49	0.68	0.50	1.94	2.63	4.81	2.98
	55	0.33	0.50	0.68	0.58	1.94	2.81	5.44	3.71
	60	0.33	0.51	0.68	0.51	1.94	2.91	5.73	4.25
	65	0.33	0.52	0.68	0.32	1.94	2.99	5.85	4.69
	70	0.33	0.53	0.69	0.12	1.94	3.07	6.02	5.16
	75	0.33	0.54	0.69	-0.14	1.94	3.13	6.14	5.60
	80	0.33	0.55	0.69	-0.42	1.94	3.22	6.31	6.07
	81	0.33	0.55	0.69	-0.48	1.94	3.24	6.35	6.17
	82	0.33	0.55	0.69	-0.54	1.94	3.25	6.38	6.26
	83	0.33	0.55	0.69	-0.61	1.94	3.27	6.42	6.35
	84	0.33	0.55	0.69	-0.68	1.94	3.29	6.45	6.45

Table 2 - continued

m	α	s_3^D	s_{va}^D	s_{13}^D	s_{Bc}^D	p_3^D	p_{va}^D	p_{13}^D	p_{Bc}^D
0.9	40	.48	.65	.88	.80	1.88	2.52	4.58	2.71
	45	.48	.67	.88	.74	1.88	2.60	4.76	3.10
	50	.48	.69	.88	.63	1.88	2.66	4.87	3.46
	55	.48	.70	.89	.50	1.88	2.72	4.98	3.80
	60	.48	.72	.89	.34	1.88	2.78	5.09	4.14
	65	.48	.73	.89	.15	1.88	2.84	5.20	4.47
	70	.48	.74	.89	-0.07	1.88	2.90	5.32	4.79
	75	.48	.75	.89	-0.32	1.88	2.97	5.43	5.10
	80	.48	.76	.89	-0.60	1.88	3.03	5.54	5.39
	81	.48	.77	.89	-0.65	1.88	3.04	5.57	5.46
	82	.48	.77	.89	-0.71	1.88	3.06	5.61	5.52
	83	.48	.77	.89	-0.77	1.88	3.07	5.64	5.59
	84	.48	.77	.89	-0.83	1.88	3.09	5.68	5.65
0.999	35	0.67	0.88	0.999	0.77	1.74	2.15	3.36	2.51
	40	0.67	0.88	0.999	0.69	1.74	2.24	3.54	2.76
	45	0.67	0.89	0.999	0.58	1.74	2.27	3.58	2.96
	50	0.67	0.90	0.999	0.47	1.74	2.31	3.68	3.19
	60	0.67	0.95	0.999	0.14	1.74	2.25	3.55	3.42
	65	0.67	0.95	0.999	-0.01	1.74	2.34	3.72	3.63
	70	0.67	0.95	0.999	-0.18	1.74	2.43	3.90	3.83
	75	0.67	0.96	0.999	-0.38	1.74	2.45	3.93	3.93
	80	0.67	0.97	0.999	-0.59	1.74	2.47	3.97	3.99
	85	0.67	0.97	0.999	-0.81	1.74	2.52	4.08	4.10
	86	0.67	0.98	0.999	-0.86	1.74	2.50	4.04	4.06
	87	0.67	0.98	0.999	-0.90	1.74	2.52	4.08	4.09
	88	0.67	0.98	0.999	-0.95	1.74	2.51	4.04	4.05
	89	0.67	0.98	0.999	-0.997	1.74	2.53	4.08	4.08

Table 3. Dimensionless Forces

m	α	FHD	FVD	FTD	PMOk	VOH
0.1	50	8.95	11.12	0.28	1.54	1.24
	55	12.08	17.95	0.39	2.20	1.49
	60	17.24	31.00	0.55	3.03	1.80
	65	21.72	48.57	0.82	3.94	2.24
	70	25.47	73.26	1.09	4.85	2.88
	75	27.45	107.72	1.30	5.75	3.92
	76	26.60	112.68	1.39	5.93	4.24
	77	38.67	170.85	0.66	6.12	4.42
	78	73.37	338.53	-1.57	6.32	4.61
	79	1253.23	6047.25	-79.76	6.53	4.83
0.3	50	6.23	8.38	0.61	1.63	1.35
	55	6.77	11.10	0.82	2.28	1.64
	60	7.91	15.83	1.06	3.03	2.00
	65	8.84	22.13	1.33	3.88	2.50
	70	9.26	30.20	1.61	4.77	3.26
	75	12.49	51.32	1.19	5.59	4.11
	80	35.53	180.30	-3.78	6.42	5.08
	81	61.75	328.44	-9.80	6.60	5.32
	82	287.21	1604.08	-62.11	6.77	5.59
0.5	50	4.96	7.47	1.00	1.89	1.50
	55	5.46	9.96	1.23	2.55	1.82
	60	6.02	13.41	1.49	3.31	2.23
	65	6.40	17.85	1.73	4.12	2.79
	70	8.07	26.54	1.49	4.78	3.29
	75	11.71	45.55	.46	5.47	3.89
	80	24.08	113.65	-4.04	6.19	4.72
	81	31.64	155.83	-6.97	6.34	4.93
	82	47.31	243.48	-13.10	6.50	5.15
	83	99.81	537.80	-33.84	6.65	5.39
0.7	45	4.70	6.53	1.29	1.61	1.39
	50	4.51	7.70	1.49	2.36	1.70
	55	4.88	10.02	1.74	3.04	2.05
	60	5.65	13.35	1.77	3.59	2.36
	65	7.07	18.70	1.49	4.06	2.65
	70	9.11	27.57	0.89	4.62	3.03
	75	13.65	47.18	-1.00	5.18	3.46
	80	27.25	111.06	-7.61	5.81	4.08
	81	34.93	147.52	-11.51	5.94	4.22
	82	49.49	216.83	-18.96	6.07	4.38
	83	87.93	400.01	-38.76	6.20	4.55
	84	481.08	2275.41	-241.97	6.34	4.73

Table 3 - continued

m	α	FHD	FVD	FTD	BMOk	VOH
0.9	40	3.55	5.24	1.73	2.08	1.48
	45	4.05	6.65	1.84	2.40	1.64
	50	4.68	8.48	1.86	2.70	1.81
	55	5.50	10.99	1.79	3.03	2.00
	60	6.58	14.55	1.57	3.39	2.21
	65	8.13	19.95	1.06	3.76	2.46
	70	10.60	29.04	-0.04	4.18	2.74
	75	15.40	47.42	-2.63	4.62	3.08
	80	29.75	103.81	-11.33	5.08	3.49
	81	36.34	130.67	-15.53	5.18	3.60
	82	47.36	175.39	-22.59	5.30	3.70
	83	69.08	263.73	-36.58	5.40	3.82
	84	131.77	518.95	-77.11	5.51	3.93
0.999	35	4.12	5.59	2.22	1.84	1.34
	40	4.49	6.73	2.27	2.03	1.50
	45	5.12	8.47	2.37	2.20	1.65
	50	5.84	10.64	2.36	2.41	1.82
	60	9.22	20.43	2.22	2.70	2.21
	65	10.81	26.38	1.34	2.95	2.44
	70	13.14	35.47	-0.23	3.23	2.70
	75	18.57	55.26	-3.67	3.43	2.98
	80	30.47	99.50	-12.78	3.63	3.27
	85	8.56	247.16	-46.91	3.91	3.60
	86	96.65	351.32	-72.13	3.91	3.63
	87	141.50	525.60	-114.12	3.98	3.71
	88	297.04	1109.80	-258.82	3.99	3.74
	89	5185.11	19788.11	-4851.38	4.06	3.81

ACKNOWLEDGEMENTS

I wish to express my sincere appreciation to Prof. Dr. F. C. Appl for his direction and consultation. Also, I would like to thank the African-American Institute, the Mechancial Engineering Department of Kansas State University, Christensen, Inc., and the Ethiopian Government for their financial support while I am working on this project.

VITA

MINASSE ABEBE

Candidate for the Degree

Master of Science

THESIS: SLIP-LINE FIELD SOLUTION WITH DEAD ZONE FOR LARGE NEGATIVE RAKE CUTTING

MAJOR FIELD: Mechanical Engineering

BIOGRAPHICAL:

Personal Data: Born November 16, 1949 at Addis Abeba, Ethiopia, the son of Abebe Techane and Aynalem Mulatu.

Education: Graduated from Entotto Comprehensive High School, Addis Abeba, Ethiopia in 1966; received a B.S. degree in Mechanical Engineering from Addis Abeba University in June 1972, completed requirements for the M.S. degree in May 1980.

Experience: July, 1972 to June, 1974 served as an Engineer of Thermal Plants in Ethiopian Electric Light and Power Authority; July, 1974 to August, 1978 worked as Assistant Technical Manager in the Ethiopian Beverage Corporation.

SLIP-LINE FIELD SOLUTION WITH DEAD ZONE FOR LARGE NEGATIVE RAKE CUTTING

by

MINASSE ABEBE

B.S., Addis Abeba University, 1972

AN ABSTRACT OF A MASTER'S THESIS

submitted in partial fulfillment of the
requirements for the degree

MASTER OF SCIENCE

Department of Mechancial Engineering

Kansas State University
Manhattan, Kansas

1980

ABSTRACT

A slip-line field which leads to an upper bound solution to a problem of metal cutting with large negative rakes is developed based on experimental observations. The slip-line field consists of a prow and a dead zone which are formed in front of the tool. The prow is the material of the workpiece which is in the state of leaving the workpiece material and becoming a chip. The dead zone is the stagnant region ahead of the tool which separates the flow of workpiece metal that becomes a chip and that which rejoins the workpiece material as the machined surface.

The slip-line field can be used to calculate the cutting forces required to cut a material whose physical properties and friction conditions can be estimated. This slip-line field accounts for the experimental fact that the tangential force on the tool face becomes zero for a certain high negative rake. Also, it accounts for the experimental facts that: there is a certain negative rake angle at which the tool does not cut; the vertical component of the cutting force is larger in magnitude than the horizontal component; and the cutting force components increase as the rake angle becomes more negative. The slip-line solution presented explains why friction is necessary in cutting with large negative rake tools.